Thesis entitled

'MULTI-POINT FIBER OPTIC GAS SENSOR SYSTEMS'

Submitted by HO HOI LUT

for the degree of Doctor of Philosophy in Engineering

at The Hong Kong Polytechnic University in October 2002

ACKNOWLEDGEMENTS

I would like to express sincere gratitude to my chief supervisor, Dr. Wei Jin for his valuable support, suggestions and constructive criticism. I am also very grateful to my co-supervisor, Prof. M. S. Demokan for his useful advice and encouragement throughout this project.

I wish also to take this opportunity to thank Mr. H. B. Yu in Electronic Engineering Department of Tsinghua University, China for his invaluable discussion and technical support.

In addition, I would like to thank my parents, my friends and colleagues for their continuous support and helpful advice.

Finally, I greatly appreciate the generous funding of the entire project from the Department of Electrical Engineering of HKPU through the Research Grant (G-V 591).

ABSTRACT

Multiplexing is a very important issue for fiber optic sensors. It enhances the system utilization and the competitiveness of fiber sensors against conventional technologies. Although, multiplexing techniques for optical fiber sensors have been proposed and theoretically studied over the last 20 years, implementations in chemical (gas) sensors context are rarely reported experimentally. It is believed that an increasing attention will focus in this area in the coming years. The main objective of this project is to develop and investigate multi-point gas detection systems for quantitative measurement. Two different multiplexing systems for fiber optic gas sensors, one named time-division-multiplexed (TDM) system, the other frequency modulated continuous wave (FMCW) system, are investigated theoretically and experimentally in this project.

In our systems, quantitative measurement of gas concentration based on wavelength modulation spectroscopy (WMS) and second-harmonic detection are demonstrated by applying low-frequency wavelength modulation to an external-cavity tunable diode laser. The tunable laser operating at 1.53 μm region is used to detect acetylene (C_2H_2) based on direct absorption through the use of micro-optic cells. A time-division multiplexed three-sensor system with a forward-coupled ladder topology have been implemented and experimentally tested. The experimental system using micro-optic cells of length 25mm have demonstrated sensitivity of 81 ppm/$\sqrt{Hz}$. The crosstalk between the sensors was found to be -30 dB. Power budget analysis shows that a sensor network consisting of 90 sensors could be realized with the same multiplexing topology. The performance of such a networked system has been examined in terms of shot noise limit, inter-channel crosstalk and detection sensitivity.

Apart from the TDM techniques, we also applied a frequency modulated continuous

wave (FMCW) technique for multiplexing optical fiber gas sensors. The sensor network is again of a ladder topology and is interrogated by the same tunable laser. For the FMCW system, the optical delays of each channel are carefully designed in order to satisfy the basic requirements that will be discussed in the following chapters. The system performance in terms of detection sensitivity and crosstalk between sensors was investigated and found limited by the coherent mixing between signals from different channels. The system performance can be improved significantly by use of appropriate wavelength modulation/scanning coupled with low pass filtering. Computer simulation shows that an array of 37 acetylene sensors with a detection accuracy of 2000ppm for each sensor may be realized. A three-sensor network of ladder topology is experimentally demonstrated for the detection of acetylene gas. A minimum detectable concentration of 270 ppm/$\sqrt{Hz}$ is obtained with 25mm gas cells under atmospheric pressure which corresponds to a minimum detectable absorbance of 1.48×10^{-4} /$\sqrt{Hz}$. The crosstalk between the sensors is below -20 dB.

With the theoretical and experimental justifications, the relative advantages and disadvantages of the TDM and FMCW systems can be summarized as follows. TDM system works with a simple concept where simple circuitries are employed for either encoding or decoding. It shows excellent system tolerance compared with the FMCW system. For the TDM system, the performance is mainly affected by the extinction ratio of the optical switch that can be simply improved by using a double M-Z type modulator or switch. In contrast, the performance of the FMCW system is heavily influenced by a number of factors such as the biases of the fiber delays, the settings of the triangular chirped carrier and the linearity of the VCO. Deviations from the optimized values of the above parameters would cause a raise in inter-channel crosstalk and unwanted interferometric signals (noise). If a highly coherent light source is used and no noise

suppression techniques are implemented, the sensitivity and the crosstalk of the FMCW system are definitely worse than that of the TDM system. However, these unwanted interferometric signals can be effectively suppressed by using a low coherent source and specified signal processing techniques, therefore the FMCW system would have superior performance because of its better optical power utilization where a continuous optical signal is fed into the network instead of the optical pulses used in the TDM system. Better signal-to-noise ratio would be obtained with the FMCW system since the detected signal would be greatly enhanced compared with the optical-power-related noise (shot noise). The FMCW system is shown to have a better sensitivity when the performance of the system is shot-noise ("quantum") limited.

CONTENTS

ACKNOWLEDGEMENTS i

ABSTRACT ii

1. Introduction

1.1 *Project Motivation and Contributions* 1
1.2 Thesis Outline 3
1.3 Publications 4

2. Background Review

2.1 Introduction 7

2.2 Molecular Absorption Spectroscopy 7
2.2.1 Absorption spectra 8
2.2.2 Spectra linewidth broadening 10
2.2.3 Measures of absorption strength 11
2.2.4 Detection Sensitivity 13
2.2.5 Gas species with absorption in near-infrared region 15
2.2.6 Absorption spectrum of acetylene (C_2H_2) at 1.53μm 15

2.3 Classifying Fiber Optic Sensors for Chemical (Gas) Sensing 17
2.3.1 Open path absorption sensors 17
2.3.2 Fiber optrodes 19
2.3.3 Evanescent wave sensors 19
2.3.4 Multi-pass absorption cell 21
2.3.5 Advantages of fiber optic chemical sensors 21

2.4 Sensitive Modulation/Detection Techniques for Optical Absorption Sensors 22
2.4.1 Wavelength modulation spectroscopy 23
2.4.2 Frequency modulation spectroscopy 23
2.4.3 Two-tone frequency modulation spectroscopy 24

2.5 Multiplexing Techniques and Network Topologies 24

2.5.1 Spatial division multiplexing (SDM) 25
2.5.2 Time division multiplexing (TDM) 26
2.5.3 Frequency modulated continuous wave technique 29
2.6 Chapter Summary 29
References 30

3. Single-sensor Gas Detection System

3.1 Introduction 34
3.2 Wavelength Modulation Spectroscopy and Second Harmonic Detection 35
3.2.1 Modulation amplitude optimization 35
3.3 Experimental Setup and Results 38
3.3.1 Tunable external-cavity diode laser 39
3.3.2 Micro-optic gas cell 40
3.3.3 System arrangement 40
3.3.4 Optical fringes elimination 42
3.3.5 Performance of the single sensor system 43
3.4 System Sensitivity Limitation 45
3.4.1 Shot-noise-limited sensitivity 46
3.4.2 Flicker noise 47
3.4.3 Sensitivity limit due by unwanted interferometric signals44 48
3.5 Chapter Summary and Conclusions 54
References 55

4. Performance Analysis of TDM System

4.1 Introduction 56
4.2 General Description for the TDM Gas Sensor System 57
4.3 Shot-noise-limited Sensitivity 59
4.4 Crosstalk and Noise Analysis 61
4.4.1 Incoherent crosstalk 65

4.4.2 First order coherent crosstalk 67
4.4.3 Second order coherent crosstalk 72

4.5 Other Considerations on System Performance 73
4.5.1 Low-pass filtering 74
4.5.2 Polarization effect 74
4.5.3 Coherence of light source 75

4.6 Chapter Summary 75

References 76

5. Experimental Implementation of TDM Gas Sensor System

5.1 Introduction 78

5.2 Experimental Setup 78
5.2.1 Problem found with the use of AC-coupled photodetector 82
5.2.2 Drift of transfer function of the intensity modulator 84

5.3 Performance of the Experimental TDM System 86

5.4 Multiplexing Capacity 88

5.5 Chapter Summary 89

References 90

6. FMCW Multiplexing of Gas Sensors

6.1 Introduction 91

6.2 FMCW Principle 92
6.2.1 Mathematical formulation of the beat note 93
6.2.2 Simulated beat note spectrum 97

6.3 FMCW Multiplexed Gas Sensor System 99

6.4 Shot-noise-limited Sensitivity for the FMCW system 105

6.5 Unwanted Interferometric Signals in FMCW System 106

6.6 Minimization of the Unwanted Interferometric Signals 110
6.6.1 Wavelength modulation technique 110
6.6.2 Low-pass filtering technique 113
6.7 Crosstalk resulting from the sidelines 116
6.8 Chapter Summary 119
References 119

7. Experimental Studies on FMCW System

7.1 Introduction 121
7.2 System Configuration and Output Signals 121
7.3 SNR Enhancement by Using Wavelength Modulation 126
7.4 Performance Evaluation 128
7.4.1 System sensitivity 128
7.4.2 Inter-channel crosstalk 129
7.4.3 Multiplexing capacity 131
7.5 Chapter Summary 131
References 131

8. Research Summary and Future Work

8.1 Research Summary 133
8.2 Future Work 135

CHAPTER 1 INTRODUCTION

1.1 Project Motivation and Contributions

The increasing global concern over the environment has become a vital part of most Governments' policy. A number of nations have passed legislation to deal with environmental hazards and control. In 1997, Kyoto Protocol was issued which is an international agreement struck by 159 nations attending the Third Conference of Parties (COP-3) to the United Nations Framework Convention on Climate Change (held in December 1997 in Kyoto, Japan) for reducing worldwide emissions of greenhouse gases. These emissions primarily result from electricity use, transportation, industrial processes and deforestation. To perform this task, exhausted gas monitoring is indispensable. Gas sensors, especially optical sensors, are likely to play a key role here. According to a 1997 report from Frost and Sullivan (Mountain View, CA) entitled World Fiber-Optic Sensor Markets, world market for fiber-optic chemical sensors, mainly the gas types, totaled $34 million in 1995 and is expected to grow to $109 million by 2002. Demand will be driven by environmental monitoring devices, leak detectors, and medical equipment, particularly blood/gas analyzers.

So far, most fibre optic chemical sensor systems are single point sensors and hence their competitiveness is lowered due to the high cost of the optical system. Apparently, the cost-per-sensing-point can be reduced by multiplexing a number of point sensors in a quasi-distributed manner where expensive optical components such as light source can be shared. However, the realization of a multi point system requires technical advances in several aspects such as network design and optimization, novel signal processing schemes for signal demultiplexing and demodulation. This project addresses these issues and concentrates on developing novel techniques for signal processing and optical and electronic

system design and implementation. The project focuses on a particular type of gas sensors, i.e., acetylene sensors. The basic principle may however be applied for other absorption based sensors or chemical sensors in general.

The successful completion of this project would contribute to the sensing technologies for chemical (gas) analysis which are important for either environmental monitoring or industrial control process. The multiplexed system would allow significant reduction of cost of the optical sensor system in terms of cost-per-point and would allow the optical fibre sensors to compete with conventional catalytic sensors with additional benefits such as improved safety, remote and passive sensing, and selective sensing as it can be tuned to the spectroscopic properties of the sample gas.

For this research, the main contributions may be summarized as follows:

1. A time-division multiplexed (TDM) sensor system with a forward-coupled ladder topology has been investigated for which quantitative measurement of gas concentration based on wavelength modulation spectroscopy (WMS) and second-harmonic detection is performed. Theoretical analysis shows that the minimum detectable gas concentration is mainly limited by the direct interferometric effect of the first order coherent crosstalk. It sets the limit of around 1800ppm with the time delay of 300ns for α_e^2 = -30 dB and N = 100. The minimum detectable gas concentration of 50 ppm may be achieved by using a double Mach-Zhender intensity modulator (α_e^2 = -60 dB). By using proper filtering techniques, the unwanted interferometric signals can be further reduced to 1.8 ppm for α_e^2 = -30 dB and N = 100.

2. The sensor system uses single path 25mm absorption cells and has demonstrated sensitivity of 81 ppm/$\sqrt{Hz}$. The crosstalk between the sensors was found to be -30 dB.

Power budget analysis shows that a sensor network consisting of 90 sensors could be realized with the same multiplexing topology.

3. Frequency modulated continuous wave (FMCW) technique has been applied for the first time on multiplexing optical fiber gas sensors. Theoretical analysis of the system performance in terms of detection sensitivity and crosstalk between sensors was investigated and found limited by the coherent mixing between signals from different channels. Simulation results showed that the system performance can be significantly improved by use of appropriate wavelength modulation/scanning coupled with low pass filtering. It is theoretically possible to realize a 37-sensor array with detection accuracy of better than 2000 ppm.

4. A three-sensor network in ladder topology by the use of frequency-modulated continuous wave and wavelength modulation spectroscopy techniques is experimentally demonstrated for the detection of acetylene gas. A minimum detectable concentration of 270ppm/√Hz is obtained with 25mm gas cells under atmospheric pressure which corresponds to a minimum detectable absorbance of 1.48×10^{-4}. The crosstalk between the sensors is below -20 dB.

1.2 Thesis Outline

This thesis documents the research program that was performed during the investigation of fiber optic multiplexed systems for gas concentration measurements, and describes the various phases of the experimental work, in addition to reviewing relevant literature that was acquired during the course of the study. This thesis is organized as follows:

In chapter 2, an overview of the background on fiber optic gas sensors is given. Several

demodulation techniques, multiplexing schemes and network topologies are discussed.

In chapter 3, the experimental work on a single sensor system is described. Also, optimization of the modulation index for wavelength modulation technique is presented mathematically and this is shown to be correct by way of experiment.

In chapter 4, a multi-sensor system with time-division multiplexing is theoretically studied. Investigation with computer simulations on the system performance in terms of shot-noise limit, detection sensitivity and crosstalk are reported.

Chapter 5 discusses the experimental arrangement of the three-sensor TDM system. The results of the experimental study on that system are presented.

Chapter 6 describes theoretical aspects and practical design considerations of the FMCW gas sensor system. Basic principle and performance analysis of the system are presented.

Chapter 7 presents the experimental work for the realization of a three-sensor system with the FMCW approach. The system performance in terms of sensitivity and crosstalk are discussed.

Chapter 8 gives general conclusions and several recommendations for the further work.

1.3 Publications

The publications arose within the period of research study for the degree of Ph.D:

Journal Publications:

(1) H.L. Ho, W. Jin, and M.S. Demokan, "Sensitive, multipoint gas detection using TDM and wavelength modulation spectroscopy," *Electronics Letters*, Vol.36, No.14, pp.1191-1193, 2000.

(2) H.L. Ho, W. Jin, H.B. Yu, K.C. Chan and M.S. Demokan, "Experimental demonstration of a fibre-optic gas sensor network addressed by FMCW," *IEEE Photonics Technology Letters*, Vol.12, No.11, pp.1546-1548, 2000.

(3) H.B. Yu, W. Jin, H.L. Ho, K.C. Chan and et al., "Multiplexing of optical fibre gas sensors with an FMCW technique," *Applied Optics*, Vol.40, No.7, pp.1011-1020, 2001.

(4) C.C. Chan, W. Jin, H.L. Ho, D.N. Wang and Y. Wang, "Improvement of measurement accuracy of FBG sensor systems by use of gas absorption lines as multi-wavelength references", *Electronics Letters*, Vol.37, No.12, pp.742-743, 2001.

(5) C.C. Chan, Y.J. Gao, K.T. Lau, H.L. Ho, L.M. Zhou and W. Jin, "Characterization of crosstalk of a TDM FBG sensor array using a laser source", *Optics and Laser Technology*, Vol.33, No.5, pp.299-304, 2001.

(6) C.C. Chan, W. Jin, H.L. Ho, and M.S. Demokan, "Performance Analysis of a Time-Division-Multiplexed Fiber Bragg Grating Sensor Array by Use of a Tunable Laser Source," *IEEE Journal of Selected Topics in Quantum Electronics*, Vol. 6, No.5, pp.741-749, Sept 2000.

(7) H.L. Ho, A.B. Rad, C.C. Chan and Y.K. Wong, "Comparative studies of three adaptive controllers," ISA Transactions, 38, pp.43-53, 1999.

(8) H.L. Ho, W. Jin , C.C. Chan, Y. Zhou and X.W. Wang, "A fiber Bragg grating sensor for static and dynamic measurands", *Sensors and Actuators A (Physical)*, Vol. 96, No.1, pp.21-24, 2002.

(9) Y.L. Hoo, W. Jin, H.L. Ho, D.N. Wang, "Evanescent wave gas sensing using microstructure fiber," *Optical Engineering*, Vol. 41, No.1, pp.8-9, 2002.

Conference Papers:

(10) H.L. Ho, W. Jin, H.B. Yu, K.C. Chan and M.S. Demokan, " Sensitive, multi-point gas detection using FMCW and WMS," OFS2000, 14th International Conference on Optical Fiber Sensors, pp.420-423, 2000

(11) H.L. Ho, W. Jin and M.S. Demokan, "Time division multiplexed gas sensing system with a forward-coupled ladder topology," ICSC2000/ SPIE Vol.4077, pp.7-10, 2000.

(12) H.L. Ho, W. Jin and M.S. Demokan, "Quantitative measurement of acetylene by using external cavity tunable diode laser," SPIE Vol.3852, pp.124-133, 1999.

(13) H.B. Yu, H.L. Ho, W. Jin, Y.B. Liao and Y.H. Li, "Remote multipoint fiber optic gas sensors using a FMCW technique and a tunable laser," SPIE Vol.4220, pp.44-53, 2000.

(14) W. Jin, H.L. Ho, C.C. Chan and K.C. Chan, "Effect of interferometric noise in fiber Bragg grating sensors using tunable laser sources," SPIE Vol.3330, pp.272-283, 1998.

CHAPTER 2 BACKGROUND REVIEW

2.1 Introduction

Optical techniques in absorption spectroscopy are widely used in conventional chemical (gas) analysis by employing bulk-optical systems [1]. Due to the rapid development of optical fiber technology, optical fiber sensors based on these techniques have attracted significant attention in the past ten years [2-5] because of their importance in applications such as environmental monitoring, biomedical sensing, and industrial process control. As mentioned by many other authors, these sensors or systems offer a number of notable features and advantages in chemical/gas sensing. They include remote detection capability, safety in hazardous environments, immunity to electromagnetic interference and so forth. A number of important gases around NIR region, including methane, acetylene, carbon dioxide, carbon monoxide, hydrogen sulfide, ammonia, etc, have been detected and excellent detection sensitivities have been obtained [6]. In this chapter, the foundations of absorption spectroscopy, such as the origin of absorption spectra, the lineshapes and absorption strength determination, will be reviewed. In addition, classification of fiber optic gas sensors and possible demodulation and multiplexing techniques suitable for fiber optic gas sensors will be summarized.

2.2 Molecular Absorption Spectroscopy

Optical methods for the identification of chemical species are well known [1] and were widely used long before advent of modern fiber optics. Most of these techniques are based on measurement of the absorption of radiation by the chemical species. This approach permits the identification and quantitative measurement of different compound by their specific molecular structure and absorption strength.

2.2.1 Absorption spectra

The experiments in the early part of this century by Planck, Bohr and Einstein showed that the energy of a microscopic system such as an atom or a molecule is quantized [7]. In a certain approximation, we may resolve the total energy of a molecule into the sum of electronic, vibrational, and rotational energy [8]. These three major forms of energy may be summarized in a single energy level diagram as shown in Fig. 2.1(a).

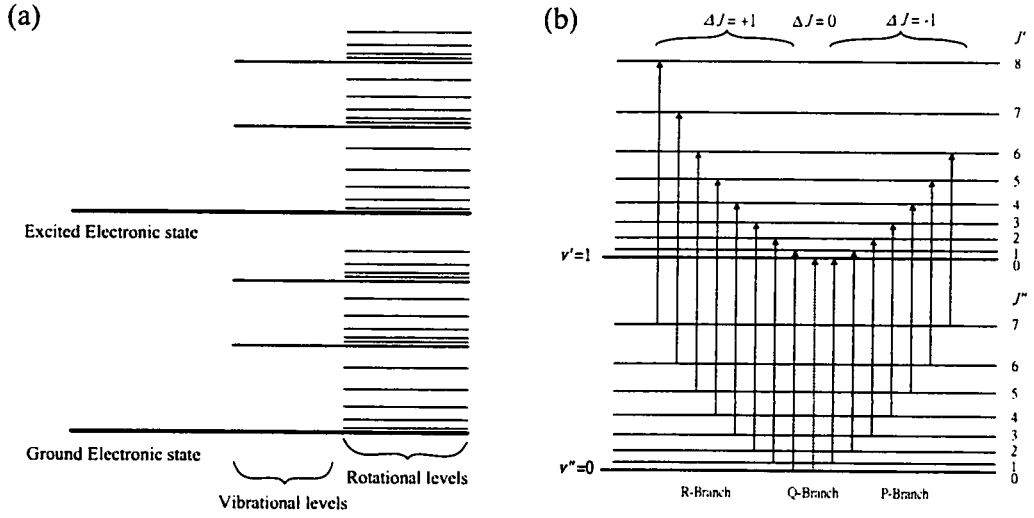

Fig. 2.1 (a) Schematic view of the manifold of energy levels: electronic, vibrational and rotational; (b) Vibrational-rotational energy transitions.

Transitions between different energy levels can take place by either energy absorption or emission. Corresponding to different type of transitions, the molecule absorption spectra can be classified into four categories[9]: rotational spectra, vibrational spectra, vibrational-rotational spectra and electronic spectra. Gas molecules have a number of absorption lines corresponding to electronic transitions as well as vibrational-rotational transitions. However, almost all electronic transitions of molecules are located in the visible and ultra-violet wavelength regions, therefore the wavelengths involved are too short for gas detection with the use of silica optical fiber. Hence, we would be interested in gas absorption

at near-IR region, i.e., 0.8-1.8 μm, the low loss region of the silica fiber, where vibrational or vibrational-rotational spectra could be dominant. Fig 2.1 (b) shows a typical energy level diagram for the fine structure of vibrational-rotational energy transition. In most cases, vibrational and rotational energy levels are indicated by the quantum numbers v and J respectively. The energy state prior to the absorption of radiation is described by double-primed, v'' and J''; the energy state after absorption will be designated by the single-primed symbols $v'$and J'. The fundamental vibrational energy change is a transition from $v''= 0$ to $v'=1$, so $\Delta v = v' - v'' = +1$, which corresponds to the fundamental vibrational absorption band. Absorption spectra due to transitions from $v = 0$ to higher states ($v' = 2, 3, \ldots$), called overtones, may also exist and located approximately at the multiples of the fundamental frequency.

When a molecule changes its vibrational state, it may also change its rotational energy, and therefore a series of absorption lines due to rotational transitions are superimposed. The changes in rotational quantum number, J, associated with these rotational transitions can be presented as

$$\Delta J = J' - J'' \tag{2.1}$$

Energy transitions for which $\Delta J = 0$ are called Q-branch transitions. The transitions where $\Delta J = +1$ are R-branch and those where $\Delta J = -1$ are P-branch transitions. However, for polyatomic molecules, the molecular absorption spectra is frequently more complicated and guided by different selection rules for the transitions in different radiation regions. Further details are given by reference [10].

2.2.2 Spectra linewidth broadening

The linewidth of the absorption lines acts as an important consideration in gas concentration measurements especially for the system using wavelength modulation technique. The ratio between the amplitude of wavelength modulation and the linewidth of the absorption line should be optimized, and, this will be presented in section 3.3.1.

In general, absorption of electromagnetic radiation by a chemical species takes place at well-defined wavelengths (λ) or frequencies (f) defined by:

$$E_2 - E_1 = \frac{hc}{\lambda} = hf \tag{2.2}$$

where E_2-E_1, is the difference in energy levels of an energy transition, hf is the photon energy required to induce the transition, h is Planck's constant and c is the free space velocity of light. In practice, a range of frequencies will be effective in producing a spectral transition. The frequency range defines the linewidth (or absorption width) and is affected by several contributions and also experimental conditions. Amongst the main contributors are the natural linewidth, Doppler broadening and collisional broadening [7]:

- Natural linewidth: According to Heisenberg's uncertainly principle[11], the energy of a state is only precisely defined if the lifetime of that state is infinite. If the lifetime is finite, then there will be a corresponding uncertainty in its energy. The lifetime of a ground state may well be essentially infinite, but that of an excited state will depend on the Einstein A coefficient of spontaneous emission. This limitation, which is not dependent on the experimental conditions of temperature, pressure, etc., represents the irreducible minimum linewidth of any spectroscopic transition. But, in fact, the natural linewidth makes a negligible contribution under most experimental conditions.

- Doppler broadening: The Doppler effect [12] produces a shift in observed frequency of a

wave motion when the source and the observer are in relative motion. In the gas phase, there will be a distribution of molecular velocities, in different directions. These velocities produce small shifts in the observed frequency of a spectral line, and hence line broadening. At pressure below about 10 torr, the line shape and width are essentially defined by Doppler broadening arising from random thermal motion of the gas molecules. The absorption lines usually have Gaussian shapes, with typical tens to hundreds of *MHz* linewidth.

- Collisional or pressure broadening: Collisions have the effect of reducing the lifetimes of excited states (quenching) and can thus make a contribution to the measured absorption spectra linewidth. For quantitative measurement, the pressure in the gas cell is definitely important in high sensitivity detection especially for pressure above 100 torr. The absorption lines, in that case, are defined by the Lorentzian function. This applies to gas samples under atmospheric pressure. The pressure broadening linewidths are typically around several *GHz* at ambient pressure, which are about two orders larger in magnitude than pure Doppler broadening linewidth.

2.2.3 Measures of absorption strength

Thus far we have concentrated on the frequencies and the lineshapes (linewidths) of atomic and molecular transitions. Besides having characteristic absorption spectrum, the strength of the gas absorption lines can serve as an additional aid to perform quantitative measurement of gas concentration. Absorption is characterized by the Beer-Lambert law [8,13]. For light of intensity I_o incident on a cell of length l containing a chemical species which has an absorption line or band at specific frequencies, the output intensity I is given by:

$$I = I_O 10^{-\varepsilon lN} \tag{2.3}$$

where N is the concentration of the sample gas in molecules cm^{-3}, l (cm) is the cell length and ε is the molar extinction coefficient (or sometimes referred to as the peak absorption cross-section). Some spectroscopists prefer to use the equivalent expression:

$$I = I_O \exp[-\alpha_m lN] \tag{2.4}$$

where α_m is the (molar) absorption coefficient of the absorbing material. In practical gas measurements, gas concentration is often expressed in terms of the fraction (percentage or parts per million) of the gas within a fixed volume. Assume that N_0 is the total number of molecules per cm^3, the concentrations of the sample gas in *ppm* (C) and in molecules cm^{-3} (N) are related by

$$C = \left(\frac{N}{N_0}\right) \tag{2.5}$$

For pure gas at atmospheric pressure N=N_0, C=100% or 10^6ppm.

The Beer-Lambert law may be re-written as

$$I = I_O \exp[-2\alpha_0 lC] \tag{2.6}$$

where $\alpha_0 = \alpha_m N_0 / 2$ is called amplitude absorption coefficient of the sample gas. The value of α_0 depends on the type of gas (through N_0 and α_m) and the specific absorption line (through α_m) chosen to perform the measurement. In this thesis, Eq.(2.6) will be used. The absorbance of the sample is given by

$$A = \log\left(\frac{I_0}{I}\right) = \varepsilon lN = 0.434\alpha_m lN = 0.868\alpha_0 lC \tag{2.7}$$

The most important practical consequence of this equation is that when I and I_o are known,

the calculated absorbance A is directly proportional to the concentration C *or* N, thereby yielding a linear calibration.

It is important to point out, however, that there are practical limitations to the applicability of the Beer-Lambert (BL) law, or, in particular, the linear dependence of absorbance on concentration:

1. The bandwidth $\Delta\lambda$ of the incident beam should be very narrow, ideally approximating monochromatic radiation. Deviations from perfect BL behavior increase as $\Delta\lambda$ increases, but are particularly severe when $\Delta\lambda$ is greater than the spectral width of the absorption band of the absorbing species. Such deviations result in a nonlinear calibration for the sensor, which, although acceptable in some instances, results in a sensitivity that falls off with concentration and a consequent reduction in the useful measurement range.

2. Deviations from perfect BL behavior are also observed in highly absorbing or highly scattering media. Both of these effects yield a very limited linear range for the absorbance-concentration relationship. Furthermore, high concentrations of the absorbing species can also result in measurement problems due to reactions or complexation taking place. In such circumstances the optical characteristics of the absorbing material will differ significantly from those observed at low concentrations.

2.2.4 Detection sensitivity

In general, the sensitivity of a system for absorption measurement is defined in terms of the minimum detectable absorbance A_{min}, corresponding to (absorption) signal power (proportional to the square of the signal amplitude) equal to the noise power within the detection bandwidth (signal to noise ratio =1). As the noise power increases with detection bandwidth, the value of A_{min} also increases with detection bandwidth. In many cases, the system noise can be regarded as white within the frequency range of interest, and the noise

power is proportional to the detection bandwidth (B). The minimum detectable absorbance A_{min} is thus proportional to the square root of B. For the purpose of comparison, the sensitivity of the system is often expressed in terms of a normalized minimum detectable absorbance $A_{min}/\sqrt{B}$ with unit $1/\sqrt{Hz}$. The parameter $A_{min}/\sqrt{B}$ is independent of the detection bandwidth, the interaction length and absorption coefficient (determined by the type and the specific absorption line of the gas being measured).

For a particular gas, the sensitivity is often expressed in terms of the fraction (*ppm*) of the gas (C) within a fixed volume. They are related through Eq.(2.7), i.e.,

$$C_{min}/\sqrt{Hz} = \left(\frac{1}{0.868\alpha_0 l}\right) A_{min}/\sqrt{Hz} \tag{2.8}$$

For ease of comparison, in some literatures, the detection sensitivity is also expressed in terms of minimum detectable concentration for a unit interaction length (1 cm):

$$C^*_{min}/\sqrt{Hz} = C_{min} l/\sqrt{Hz} = \left(\frac{1}{0.868\,\alpha_0}\right) A_{min}/\sqrt{Hz} \tag{2.9}$$

For a particular absorption line of acetylene gas (the line at 1330.37nm), the value of α_0 is estimated to be $0.252cm^{-1}$ (see section 2.2.5). The relations between $C_{min}/\sqrt{Hz}$, $C^*_{min}/\sqrt{Hz}$ and $A_{min}/\sqrt{Hz}$ are

$$C_{min}/\sqrt{Hz} = \frac{1}{l} C^*_{min}/\sqrt{Hz} = \frac{4.572}{l} A_{min}/\sqrt{Hz} \tag{2.10}$$

It should be mentioned that in some cases, the noise may not be regarded as white within the detection bandwidth, and the detection sensitivity would not be proportional to the square root of bandwidth anymore. However, Eq.(2.9) and Eq.(2.10) will still hold but with $C_{min}/\sqrt{Hz}$, $C^*_{min}/\sqrt{Hz}$ and $A_{min}/\sqrt{Hz}$, replaced, respectively, by C_{min}, C^*_{min} and A_{min}.

2.2.5 Gas species with absorption in near-infrared region

Near-infrared spectroscopy (NIRS) [10] is the measurement of the wavelength and intensity of the absorption of near-infrared light with a sample. NIR light spans approximately the 800 - 2500 nm (12,500 - 4000 cm^{-1}) range and is energetic enough to excite overtones and combinations of molecular vibrations to higher energy levels. This is especially true for compounds containing N-H, C-H and O-H groups. For optical fiber chemical (gas) sensors, molecular species with absorption band around the NIR region [14,15] and falling within the transmission window [16] of optical fiber are listed in Table 2.1.

Molecule		Absorption Wavelength (μm)	Descriptions
Oxygen	O_2	0.761	Strong oxidizer, supports and vigorously accelerates combustion
Nitrogen dioxide	NO_2	0.800	Greenhouse gas
Hydrogen Fluoride	HF	1.330	Toxic, colorless, extremely corrosive
Hydrogen Bromide	HBr	1.341	Highly toxic, colorless
Water Vapor	H_2O	1.365	-
Acetylene	C_2H_2	1.530	Extremely flammable
Hydrogen iodide	HI	1.541	Highly toxic, colorless
Ammonia	NH_3	1.544	Toxic, irritating and destructive to tissues
Carbon Monoxide	CO	1.567	Combustion product, toxic, colorless
Carbon Dioxide	CO_2	1.573	Main greenhouse gas
Hydrogen Sulfide	H_2S	1.578	Toxic, colorless, flammable
Methane	CH_4	1.651	Flammable, greenhouse gas
Hydrogen Chloride	HCl	1.747	Toxic, colorless, extremely irritating

Table 2.1 Molecular species with absorption around NIR

2.2.6 Absorption spectrum of acetylene (C_2H_2) at 1.53μm

Acetylene is chosen as the gas sample in our measurements because of its wide

applications and suitable absorption wavelength (within the tuning range of the laser we use). It is a colorless, non-toxic but narcotic gas, and is highly flammable. Basically, it acts as the fuel gas and provides a high flame temperature in the oxygen enriched environment. It is widely used in the welding industries. Apart from the explosive and flammable concern in the industrial application, it is also an engine exhaust gas and a gaseous discharge from the electrical power transformer oil. More recently, the instrument grade acetylene is used as the optical wavelength reference in various optical instruments. Figure.2.2 shows acetylene absorption spectrum taken by using a tunable laser source and a photodetector with wavelength range of 1518nm to 1545 nm. It was measured with a 2.5 cm long C_2H_2 gas cell filled to a pressure of 760 torr (atmospheric pressure).

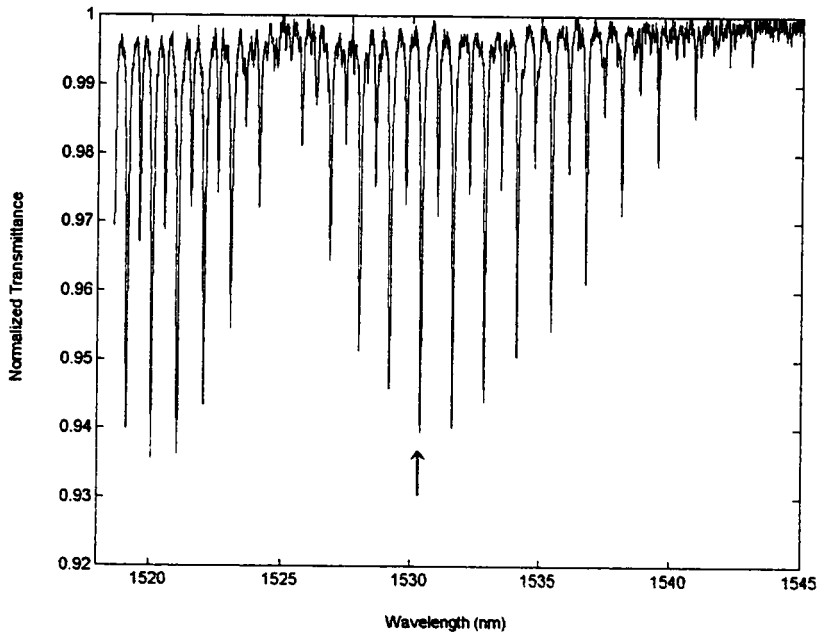

Figure 2.2. Absorption spectrum of acetylene (5% concentration or C=0.05) in the wavelength range from 1518 to 1545 nm measured with the tunable laser of resolution = 0.01nm for a 2.5cm long C_2H_2 gas cell at atmospheric pressure.

These regular absorption lines can be attributed to the first overtone of vibrational-rotational absorption of H-C≡C-H molecules [15]. The group of absorption lines in the shorter wavelength region at around 1.52 μm belongs to the P branch of the vibrational-rotational modes and the group of absorption lines in the longer wavelength region at around 1.53 μm belongs to the R branch.

In this thesis, we use the absorption line of acetylene at 1530.37nm (the marked line in Fig,2.2). The absorbance of this line for 5% concentration and for 2.5cm interaction length can be obtained as 0.0274 from Fig.2.2, giving a value of $\alpha_0 = \frac{A}{0.868lC} = 0.252\ cm^{-1}$.

2.3 Classifying Fiber Optic Sensors for Chemical (Gas) Sensing

Optical techniques for chemical analysis are well established. For spectroscopic applications or gas concentration measurement, it is necessary to use an absorption cell (sensor) which allows an optical path to be attained through the gas species. In addition, the terms extrinsic and intrinsic are sometimes applied to fiber optic gas sensors. Extrinsic sensors are those in which the optical fiber merely acts as a light guiding link between the measurement point and the interrogating and display electronics; intrinsic sensors are where the fiber, probably in some modified form, is the sensing transducer such as evanescent wave sensors that will be discussed in Section 2.3.3.

As far as sensor construction is concerned, the fiber optic sensors used in environmental monitoring can broadly be divided into three categories: open path absorption sensors, fiber optrodes and evanescent field sensors.

2.3.1 Open path absorption sensors

Open path sensors are where the fiber performs a purely passive role in transferring light to and from an absorption cell. The fiber provides a convenient way to access the cell in

remote or multiplexing systems, but plays no part in chemical sensing. Fig 2.3 illustrations the typical construction of the open path sensors. In Fig 2.3(a), a lens is used to collimate the output light from the fiber and, and after passing through the cell, a second lens focuses the light into the output fiber. The cell may typically be 10-50 cm in length. Using this type of construction, Tai *et al.* [17] demonstrated a sensor for both methane and acetylene with a sensitivity of 5ppm/$\sqrt{Hz}$ and 3ppm/$\sqrt{Hz}$, respectively. Fig 2.3(b) shows how the path length can be doubled by placing the cell at the end of the fiber and using a reflective coating to return the light back along the same path. The combination of fiber optics and bulky-optics in the cells as described is undesirable. The cells are relatively bulky, and care must be taken to ensure accurate alignment between the lenses. Improvement can be gained through the use of micro-optic cells, as illustrated in Fig 2.3(c). In the micro-optic cell, the bulk lenses are replaced by miniature gradient-index rod lenses (GRIN lens) and the cell is made compatible with fiber optic connector technology.

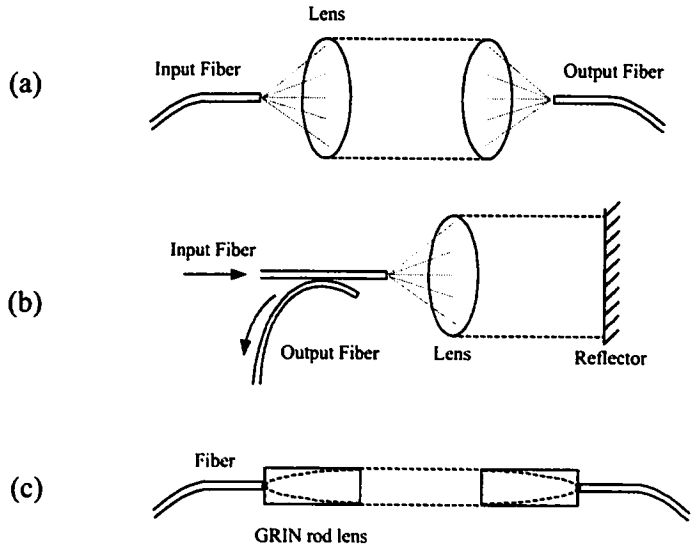

Fig 2.3 Open path absorption sensors

2.3.2 Fiber optrodes

Fiber optrodes (or optodes) are where the working sensor chemistry (involving, for example, absorbing or fluorescent dyes) is formed directly at or on the fiber tip. These sensors are particularly suitable for sensors based on indicator dye systems (either absorption or fluorescence) and optrodes have been developed for pH [18], carbon dioxide, oxygen [19], etc. Fig 2.4(a) shows a typical construction for an optrode for use in environmental monitoring to sense acidic or basic gases such as carbon dioxide. A gas-permeable membrane is used to contain the working chemistry at the end of the fiber, which consists of a pH-sensitive dye in a bicarbonate solution. Another form of a fiber optrode is illustrated in Fig 2.4(b), where the indicator dye is covalently immobilized in a polymer film, porous glass bead or ion-exchange membrane that is attached to the end of the fiber.

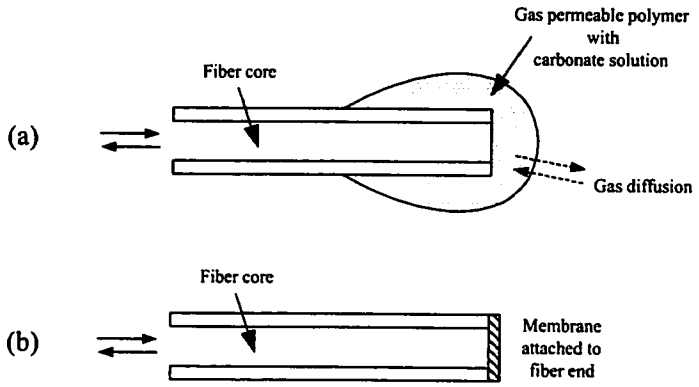

Fig 2.4 Fiber optrodes

2.3.3 Evanescent wave sensors

Evanescent wave sensors [20] are where interaction with the chemical occurs within the evanescent field region of the optical fiber. In this case, the fiber plays the most direct role in the sensing process. Typical examples of fiber construction for evanescent field sensors are shown in Fig. 2.5. The simplest and cheapest is the plastic-clad silica (PCS) multimode fiber (Fig. 2.5(a)). The plastic cladding can easily be removed over a suitable fiber length

exposing the core and allowing access to the evanescent field. PCS fibers are commonly used in the sensors based on indicator dyes, such as pH sensors. However, the disadvantage of this sensor type is that the sensitivity is dependent on the mode distribution and hence on launching condition and external disturbances. Using single mode fibers may over come this problem. But, single-mode fibers have core diameters of only a few microns surrounded by a relatively thick cladding, and so removal of the cladding to gain access to the evanescent field results in a very fragile filament. For this reason, two possible protocols may be used. In Fig 2.5(b), the single-mode fiber is first mounted in a curved slot cut in a quartz block and the top surface is then polished to remove the cladding region on one side of the fiber. The disadvantages here are the procedure is time consuming and only short length of fiber can be treated. In Fig. 2.5(c), the fiber is made from a conventional preform but half the cladding region removed. Hence, the fibers pulled from the preform with a D-shaped cross section, allowing continuous access to the evanescent field. Again the disadvantages are the limited commercial availability of D-fiber [20,21] and the problems associated with splicing and connecting.

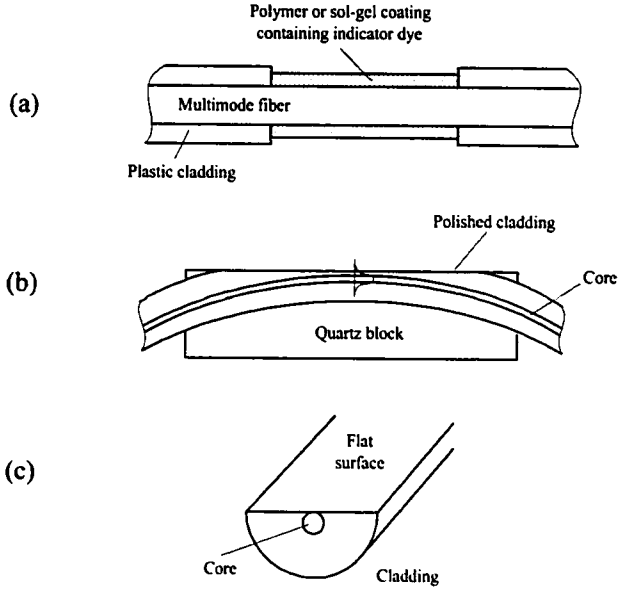

Fig 2.5 Evanescent field sensors

2.3.4 Multi-pass absorption cell

When absorption coefficients are low or enhancement on detection sensitivity is required, multi-pass cells may need to be used. Two basic designs of multi-pass absorption cells are commonly used in absorption spectroscopy: White cells [22] and Herriott cells [23].

White cell, as the name implies, was originally designed by White, and is most commonly used in laser absorption spectroscopy instruments. The mirror arrangement and beam paths are shown in Fig. 2.6(a). A "standard" Herriott cell is shown in Fig. 2.6(b), which consists of two identical spherical mirrors with the same focal length whose curved surfaces face each other with a common optical axis. The optical beam is injected through a hole in one mirror and is reflected back and forth a number of times before exiting from the same hole. The spacing between the mirrors determines the actual number of passes. Unlike the White cell the beam remains essentially collimated throughout its traversal of the cell.

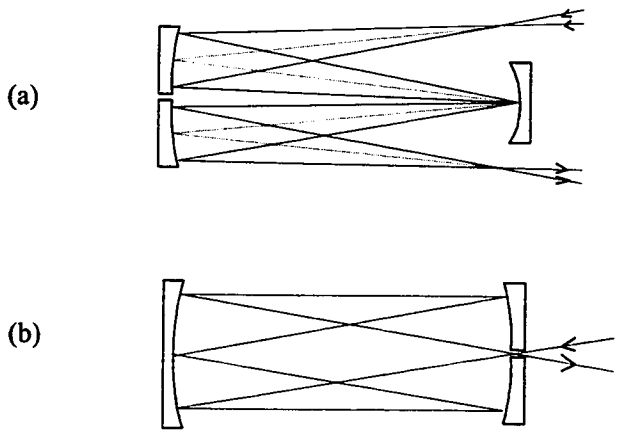

Fig 2.6 Multi-pass absorption cells: (a) White cell; (b) Herriott cell.

Most multi-pass cells were developed for use in laboratories and hence, for field applications, multi-pass cells have shown that they can become unstable and mechanical stability control becomes extremely important.

2.3.5 Advantages of fiber optic chemical sensors

The advantages of fiber optic chemical sensors are freedom from electromagnetic interference, having wide bandwidth, being compact, having geometric versatility and offering economy. In general, the fiber optic sensor is characterized by high sensitivity when compared to other types of sensors. It is also passive in nature due to the dielectric construction. Specially prepared fibers can withstand high temperature and other harsh environments. In telemetry and remote sensing applications it is possible to use a segment of the fiber as a sensor while a long length of the same or another fiber can convey the sensed information to a remote station. Deployment of distributed and array sensors covering extensive structures and geographical locations is also feasible. Many signal processing devices (splitter, combiner, multiplexer, filter, delay line etc.) can also be made of fiber elements thus enabling the realization of an all-fiber measuring system. Recently a photonic circuit [24-26] has been proposed where integrated optics components or signal processing elements were used to achieve miniaturization, batch production, economy and enhanced capabilities.

2.4 Sensitive Modulation and Detection Techniques for Optical Absorption Sensors

Routine absorption measurement can be made by measuring the change in intensity of the laser power transmitted through the gas as the laser wavelength is tuned across the absorption feature of interest. This direct detection method is the most basic technique and is useful at high concentrations of gas. Here we summarize some of the various techniques for sensitive absorption measurement. For most of these techniques, either wavelength or frequency modulation is implemented and the modulation frequency would be up to hundreds Megahertz.

In the laboratory, these modulation techniques have made it possible to detect absorbance below $10^{-7}/\sqrt{Hz}$. This sensitivity, when combined with path lengths through an absorbing sample of several tens of meters, translates into parts-per-million to parts-per-billion detections for many molecular species.

2.4.1 Wavelength modulation spectroscopy

The first method, wavelength-modulation spectroscopy (WMS) [27,28], has been used with tunable diode-laser sources since the late 1960s. In WMS with diode lasers, the injection current is sinusoidally modulated as the laser wavelength is tuned through an absorption line. In general, only the first- and second-harmonic signals are recorded, and they are proportional to the first and second derivatives of the absorption line shape. For weak absorptions, the signals are also proportional to the concentration of the absorbing molecular species. Modulation frequencies in the kilohertz or lower region have traditionally been used for sensitive spectroscopic detection, and absorbance, A, as weak as $10^{-5}/\sqrt{Hz}$ have been measured in field [29,30]. The detail of this method will be discussed in section 3.3.

2.4.2 Frequency modulation spectroscopy

In the early 1980s, a related spectroscopic method - frequency modulation spectroscopy (FMS) - was developed [31,32]. The differences between FMS and WMS are slight, they actually are two limiting cases of the same technique. In FMS, the laser is modulated at much higher frequencies than normally used in WMS, typically in the radio-frequency (RF) region. Modulation and detection are performed up to hundreds *MHz* or several *GHz* because the laser excess-noise at this frequency range is negligible, so that better signal-to-noise ratios can be achieved. In controlled laboratory experiments using short optical paths the high frequency techniques have been shown to be capable of quantum limited sensitivities of

around 1 x $10^{-7}/\sqrt{Hz}$ [33]. The high frequency modulation schemes are more complex and costly than WMS. They are more demanding of laser performance and pose problems with coupling of modulation power into the laser and with avoidance of RF pickup.

2.4.3 Two-tone frequency modulation spectroscopy

A third method of diode-laser modulation spectroscopy is a simple variation of FMS: two-tone frequency modulation spectroscopy [34,35]. TTFMS requires diode-laser modulation at two distinct radio frequencies with detection at the difference between the two applied frequencies. This method offers the advantage that arbitrarily large modulation frequencies can be applied to the laser, detection at the lower-beat frequency allows for the use of relatively low-bandwidth detectors and demodulation circuitry.

2.5 Multiplexing Techniques and Network Topologies

From the point of view of cost, a single optical gas sensor system is not really attractive due to the high cost even though its sensitivity is practically better than other conventional sensors. Hence, sensor multiplexing must be implemented in order to reduce the cost-per-sensing-point. Multiplexed and distributed optical-fiber gas sensing systems offer an extra level of information gathering over a large area. The potential of applications in environmental monitoring such as petrochemical engineering is immense.

Multiplexing techniques [36] may be performed in space, time or frequency domain and these methods are referred to respectively as Spatial Division Multiplexing (SDM), Time Division Multiplexing (TDM) and Frequency Division Multiplexing (FDM). FDM has a number of variations. One of its variations, Frequency Modulated Continuous Wave (FMCW) technique is discussed here because it is more suitable for gas sensor multiplexing and has been experimentally demonstrated in this project. Furthermore, Wavelength Division

Multiplexing (WDM) is omitted since gas absorption measurement is wavelength-dependent and light sources with specific wavelengths are required for different gases.

In general, multiplexing involves the concept of network topology. The topology of a fiber optic sensor network is strongly determined by the desired method of sensor modulation and interrogation. Three major network topologies will be discussed in combination with TDM systems due to their universality and their applicability to multiplex gas absorption sensors.

2.5.1 Spatial division multiplexing (SDM)

A number of fiber optic sensors, each with its individual input and return fiber links, may be combined into simple network by operating these sensors with a common light source and a multiple detector array. This way of addressing sensors via separate fiber links is termed Spatial Division Multiplexing (SDM) and is shown schematically in Fig. 2.7. This configuration offers the advantage that the signal returned from each sensor is analyzed separately so that sensor crosstalk is not an issue. Placing each sensor on a different fiber also minimizes the risk of system failure due to a break in the fiber network and improves the overall system reliability. A SDM system employing micro-optic cell has been used to measure the concentration of methane and has been reported by G. Stewart [37].

Alternatively, instead of multiple-source or detector arrangements, a single source or detector in combination with fiber switches or one-to-*N* and *N*-to-one couplers may be used. Synchronous fiber switching, that is, successively connecting a single source and single detector to individual sensors, is also conceivable. The use of switching functions on a time-sharing basis adds a time-division multiplexing feature to the system. The disadvantage of the SDM system is that it is considerably more expensive than other multiplexing systems because it uses more couplers and detectors/switches.

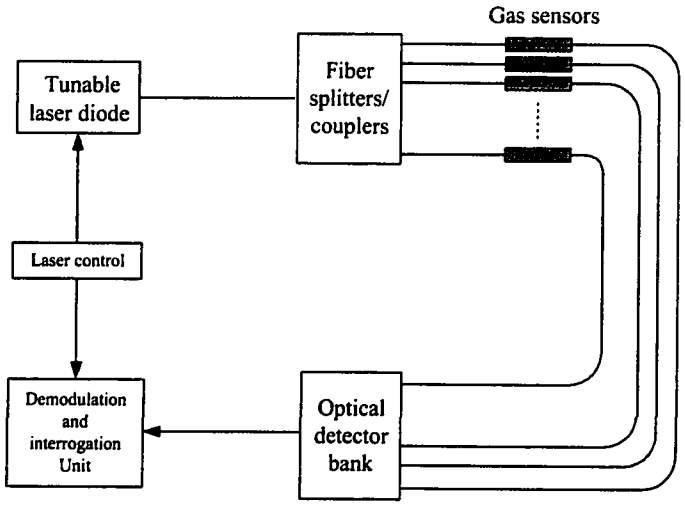

Fig 2.7 Spatial-division-multiplexing system for fiber optic gas sensors

2.5.2 Time division multiplexing (TDM)

One of the most straightforward techniques for multiplexing of fiber sensors, and indeed, the first passive discrete-sensor network proposed by Nelson et al [38] uses time division multiplexing to address a number of fiber sensors arranged in a network with different delays from the source and detector. In such a system, a short-duration pulse of light input to the network produces a series of distinct pulses at the output. These pulses represent time samples of the sensor outputs interleaved in time sequence, as depicted in Fig 2.8, which shows three different sensor topologies, i.e., normal ladder, forward ladder, and star [39]. The required duration of the input pulse is determined by the effective differential optical delay (τ) between the fiber paths to the sensor elements, and repetitive pulsing of the system allows each sensor to be addressed by simple time-selective gating of the detector.

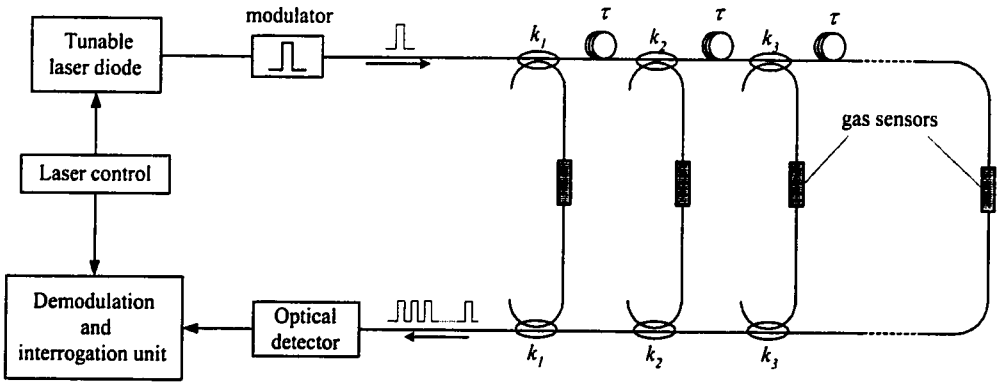

(a)

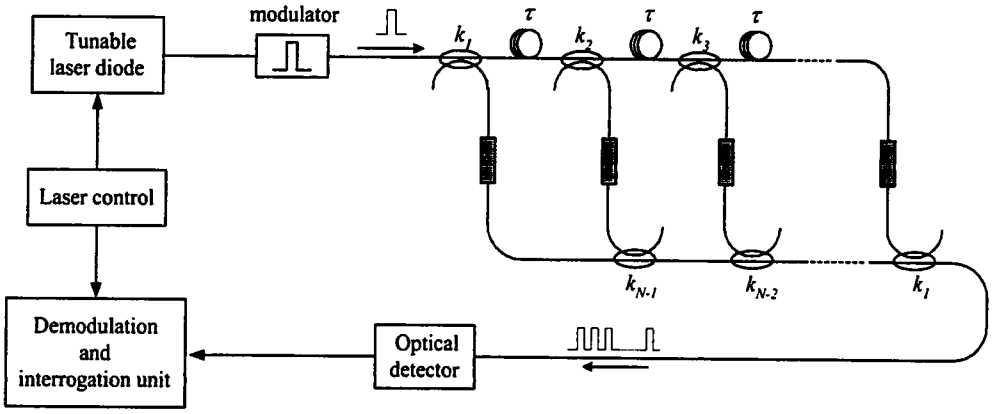

(b)

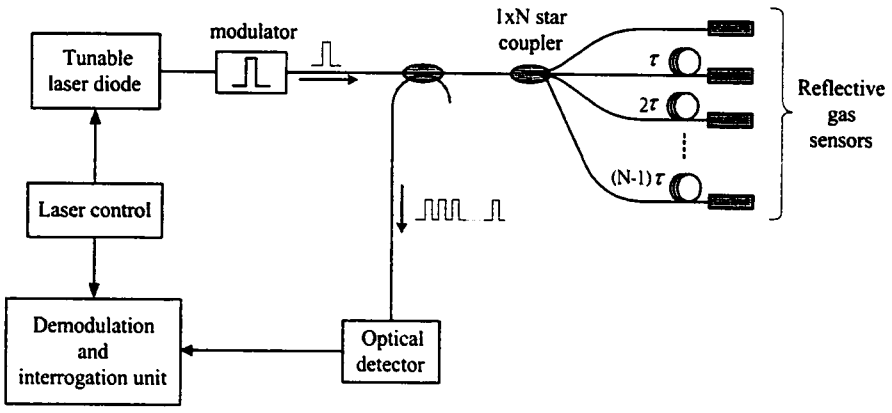

(c)

Fig. 2.8 Time-division-multiplexing gas sensor systems using (a) return coupled ladder topology, (b) forward coupled ladder array and (c) reflective star topology.

One consideration in these types of array topologies is the balancing of the optical power returned for each sensor in the system. In a return coupled ladder array configuration, as shown in Fig. 2.8(a), pulsed light from a laser is coupled to an input fiber bus, which feeds light to each sensor element in the array. In order to couple an equal power level to and from each sensor the input distribution and recombination coupler splitting ratios have to be set to a certain predetermined value. These coupling values are trivial to determine for a system without excess loss, and are given by (for the j-th coupler in the ladder) [40]:

$$k_j = \frac{1}{N - j + 1} \tag{2.11}$$

where N is the total number of sensors in the system.

Additional losses due to splices and couplers leads to the need to skew the distribution in coupling ratios to compensate these effects. This type of compensation works well for small numbers of sensors (i.e. <10), larger arrays become problematic due to the very small coupling ratios required, and the tolerances to within which the coupling ratios have to be set. To overcome this, a sensor array configuration based on a forward-coupled array topology have been implemented. In this system, illustrated in Fig. 2.8(b), the array is configured such that all the sensor signals pass through the length of the array in either the input or output bus. Consequently each sensor channel experiences a similar loss, and improved uniformity in the sensor signals produced is attained using the standard coupling ratios defined in the above equation. For the reflective star arrangement (Fig. 2.8(c)), adequate power branching can be accomplished by setting the splitting ratio of the 1:N splitter at $1/N$ for all output ports. The forward ladder TDM network was investigated in this project, and a detailed theoretical analysis and experimental study are given in Chapter 4 and Chapter 5, respectively.

2.5.3 Frequency modulated continuous wave technique

The concept of frequency-modulated continuous-wave (FMCW) technique originally developed for microwave frequency radar, [41], has been applied to laser diode light sources coupled to fiber-optic interferometers, as illustrated by earlier work [42]. The basic principle of FMCW technique is the mixing of two signals originating from the same linearly chirped source, one signal following a sensing path, while the other acting as a reference. The two signals are then mixed. The time delay between the signal from the sensing path and the reference signal gives rise to a beat frequency at the mixer output. The beat frequency is proportional to the time delay when the frequency excursion of the signals is fixed. The amplitude of the signal at the beat frequency is proportional to the corresponding measurand. If different delay lines are added into the sensing channels, the signals from these channels can thus be separated in the frequency domain.

In addition, FMCW technique is characterized by its way of signal detection - coherent or incoherent - and by the characteristics of the modulation of light. Coherent systems modulate the frequency of the light; the light from the sensor is superimposed with the reference light wave and then detected by a photo detector. Incoherent systems modulate the intensity of light. The light from the sensing channel is detected by a photodetector and then electronically mixed with the reference signal. Incoherent FMCW technique has been used in our system for gas sensor multiplexing. A more detailed description is given in Chapter 6 and the experimental work is presented in Chapter 7.

2.6 Chapter Summary

In this chapter, a systematic overview of fiber optic gas sensor systems has been presented. It is obvious that fiber optic sensors for chemical analysis offers a number of notable features and advantages compared with conventional sensing methods. Although

excellent performances of single sensor systems using sensitive detection techniques given in section 2.4 have been reported by many authors, articles about the integration of these techniques into multi-sensor systems are rarely published. Furthermore, multiplexing is a very important issue in order to enhance the applicability and competitiveness of fiber sensors. Hence, in the following chapters of this thesis, our work on system multiplexing will be described.

REFERENCES

1. D.L. Andrews, "An introduction to laser spectroscopy," New York : Plenum Press, 1995.
2. J.P. Dakin, C.A. Wade, D. Pinchbeck and J. S. Wykes, "A novel optical fibre methane sensor," *Journal of Optical Sensors*, Vol.2, pp.261-267, 1987.
3. K. Uehara and H. Tai, "Remote detection of methane using a 1.66 μm diode laser," Applied Optics, Vol.31, pp.809-814, 1992.
4. V. Weldon, P. Phelan and J. Hegarty, "Methane and carbon dioxide sensing using a DFB laser diode operating at 1.64 μm," *Electronics Letters*, Vol.29, pp.560-561, 1993.
5. Y. Shimose, T. Okamoto, A. Maruyama, M. Aizawa, and H. Nagai, "Remote sensing of methane gas by differential absorption measurement using a wavelength-tunable DFB LD," *IEEE Photonic Technology Letters*, Vol.3, pp.86-87, 1991.
6. D.E. Cooper and R.U. Martinelli, "Near-infrared diode lasers monitor molecular species," *Laser Focus World*, pp.133-146, Nov. 1992.
7. C.N. Banwell and E.M. McCash, "Fundamentals of molecular spectroscopy: Introduction," Chapter 1, McGraw-Hill Book Company, 1994.
8. P.F. Bernath, "Spectra of atoms and molecules," Oxford University Press, New York, 1995.
9. S. Svanberg, "Atomic and molecular Spectroscopy: Basic aspects and practical applications", Chapter 4, Springer-Verlag 1992, 1992.

10. C.N. Banwell and E.M. McCash, "Fundamentals of molecular spectroscopy: Infra-red spectroscopy," Chapter 3, McGraw-Hill Book Company, 1994.

11. J. Barrett, "Structure and bonding: A Brief Summary of Atomic Theory," Chapter 1, Cambridge : Royal Society of Chemistry, 2001.

12. T.P. Gill, "The doppler effect : an introduction to the theory of the effect," London : Logos Pr., 1965.

13. J.R. Edisbury, "Practical hints on absorption spectrometry," London : A. Hilger, 1966.

14. L.S. Rothman, "The HTTRAN molecular database: editions of 1991 and 1992," *J. Quant Spectrosc. Radiat. Trans.*, Vol. 48, pp.469 – 507, 1992.

15. W.J. Moore, "Phyiscal Chemistry," 3rd Edition, Prentice Hall, 1962.

16. G. Keiser, "Optical fiber communications," New York : McGraw-Hill, 2000.

17. H. Tai, K. Yamamoto, M. Uchida, et al, "Long distance simultaneous detection of methane and acetylene by using diode lasers coupled with optical fibers," *IEEE Photonics Technology Letters*, Vol.4, No.7, pp.804-807, 1992.

18. J.I. Peterson, S.R. Goldstein, R.V. Fitzgerald and D.K. Buckhold, "Fiber optic pH probe for physiological use," *Analytical Chemistry*, Vol.52, pp.864-869, 1980.

19. J.I. Peterson, R.V. Fitzgerald and D.K. Buckhold, "Fiber optic probe for in-vivo measurement of oxygen partial pressure," *Analytical Chemistry*, Vol.56, 66, 1984.

20. R.B. Dyott, "Elliptical fiber waveguides," Artech House, 1995.

21. F.A. Muhammad, H.S. Al-Raweshidy and J.M. Senior, "Polarimetric optical D-fiber sensor for chemical applications," *Microwave and Optical Technology Letters*, Vol.19, No.5, pp.318-321,1998.

22. J. U. White, "Very long optical paths of large aperature," *J. Optical Soc. Am.*, Vol.66, pp.411-416, 1976.

23. D. Herriott and H. J. Schulte, "Folded optical delay lines," *Applied Optics*, Vol.4, pp.883-889, 1965.

24. G.A. Ozin, M. Y. San, "The race for the photonic chip: colloidal crystal assembly in silicon wafers," *Advanced Functional Materials*, Vol. 11, No.2, pp.95-104, 2001.

25. F. Coppinger,S. Yegnanarayanan, P.D. Trinh, B. Jalali, "All-optical incoherent negative taps for photonic signal processing," *Electronics Letters*, Vol.33, No.11, p.973-975, 1997.

26. N. Dagli, "Hybrid integration of polymers and semiconductors for photonic integrated circuits," *Technical Digest. CLEO/Pacific Rim '99*, Vol.2, pp.258-259, 1999.

27. J. Reid and Labrie, "2nd harmonic detection with tunable diode lasers - comparison of experiment and theory," *Applied Physics B,* Vol. 26, pp. 203 - 210 1981.

28. Q. Nguyen, R. W. Dibble and T. Day, "High-resolution oxygen absorption spectrum obtained with an external-cavity continuously tunable diode laser," *Optics Letters*, Vol.19, No.24, pp.2134-2136, 1994.

29. B. F. Ventrudo and D. T. Cassidy, "Operating characteristics of a tunable diode laser absorption spectrometer using short-external-cavity and DFB laser diodes," *Applied Optics*, Vol.29, pp.5007-5013, 1990.

30. D. M. Bruce and D. T. Cassidy, "Detection of oxygen using short external cavity GaAs semiconductor diode lasers," *Applied Optics*, Vol.29, pp.1327-1332, 1990.

31. J. A. Silver, "Frequency-modulation spectroscopy for trace species detection: theory and comparison among experimental methods," *Applied Optics*, Vol.31, pp.707-717, 1992.

32. D. S. Bomse, A. C. Stanton, and J. A. Silver, "Frequency-modulation and wavelength modulation spectroscopies: comparison of experimental methods using a lead-salt diode laser," *Applied Optics*, Vol.31, pp.718-731, 1992.

33. P. Werle, F. Slemr, M. Gehrtz and C. Brauchle, "Quantum-limited FM-spectroscopy with a lead-salt diode laser," *Applied Physics B*, Vol.49, pp.99-108, 1989.

34. G.R. Janik, C.B. Carlisle and T.F. Gallagher, "Two-tone frequency-modulation spectroscopy," *J. Optical Soc. Am. B*, Vol.3, No.8, pp.1070-1074, 1986.

35. D.E. Cooper and R.E. Warren, "Two-tone optical heterodyne spectroscopy with diode lasers: theory of line shapes and experimental results," *J. Optical Soc. Am. B*, Vol.4, No.4, pp.470-480, 1987.

36. J.P. Dakin, "Review article: Multiplexed and distributed optical fiber sensor system," J. Phys. E: Sci. Instrum., Vol.20, pp.954-967, 1987.

37. G. Stewart,C. Tandy, D. Moodie, M.A. Morante, F. Dong, "Design of a fibre optic multi-point sensor for gas detection," *Sensors and Actuators B*, Vol.B51, pp227-232, 1998.

38. A.R. Nelson, D.H. McMahon and H. Van de Vaart, "Multiplexing system for fibre optic sensors using pulse compression techniques," *Electronics Letters*, Vol.17, pp.263-264, 1981.

39. A.D. Kersey, "Fiber optic sensor multiplexing techniques," Fiber Optic Smart Structures: Chapter 15, John Wiley & Sons, Inc.,1995.

40. A.D. Kersey, A.D. Dandridge, et al., "64-element time-division multiplexed interferometric sensor array with EDFA telemetry," *OFC '96 Technical Digest*, pp.270-271, 1996.

41. A. J. Hymans and J. Lait, "Analysis of a frequency-modulated continuous-wave ranging system", *Proc. IEE*, Vol. 107B, pp.365-372, 1960.

42. D. Uttam and B. Culshaw, "Precision time domain reflectometry in optical fiber systems using a frequency modulated continuous wave ranging technique", *Journal of Lightwave Technology*, Vol. LT-3, No.5, pp.971-977, 1985.

CHAPTER 3 SINGLE-SENSOR GAS DETECTION SYSTEM

3.1 Introduction

A prior task to actualize multiplexing techniques onto fiber optic gas sensor is to examine the system performance and the sensitivity of a single-sensor system. For gas concentration analysis, an exploration of the limits on the detection of small changes in the light intensity is of fundamental and practice importance. As discussed in Section 2.4, a variety of sensitive modulation and detection techniques have been used in absorption spectroscopy, but they are really variations of the same technique with the differences arising from the detection frequencies, the depth of modulation and the number of modulation tones. Although one- or two-tone FM techniques at *MHz* frequencies have been used to achieve the sensitivity equivalent to an absorbance of the order of $10^{-7}/\sqrt{Hz}$, WMS is used here. As the project motivation stated in Chapter 1, the intentions of sensor multiplexing are cost reduction per sensing point and information gathering over a large area, mostly, for environmental monitoring or leakage detection. Hence, we try to strike a proper balance between the sensitivity and the cost. WMS is preferred because of its robustness and simplicity compared with the high frequency modulation schemes that are more complex and costly than WMS. Actually, WMS with minimum detectable absorbance of $10^{-5}/\sqrt{Hz}$ is sufficient for most real-world applications. In the following sections, a mathematical derivation of WMS and optimization of the modulation factor are presented (Section 3.2). Under such a scheme, a single-sensor system is constructed and experimentally tested (Section 3.3). Further, in Section 3.4, noise analysis for our system is presented. Finally, a chapter summary will be given.

3.2 Wavelength Modulation Spectroscopy and Second Harmonic Detection

For WMS, harmonic detection is employed which produces a second derivative signal of the gas absorption line and results in a significant improvement in signal-to-noise ratio (SNR) since the noise at frequencies other than that of reference are rejected and do not affect the measurement. For this application, a sinusoidal modulation is impressed on the optical wavelength of a tunable diode laser while the center wavelength is slowly ramped over the absorption line of interest (as illustrated in Fig.3.1).

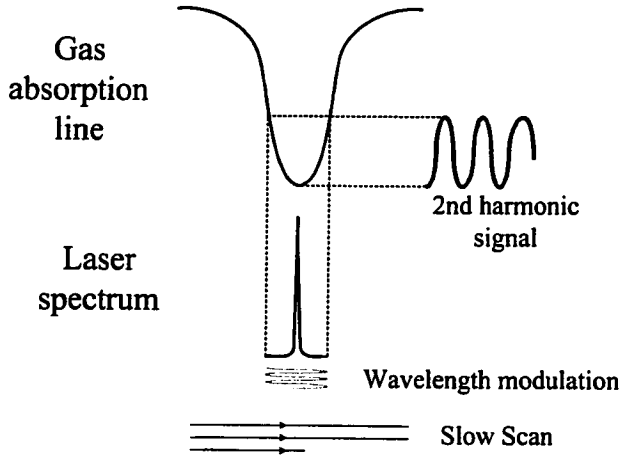

Fig. 3.1 Wavelength modulation spectroscopy (WMS)

The signal output is processed by, in general, a lock-in amplifier referenced to the modulation frequency. The absorption strength is related to amplitude of the second harmonic signal and can be recovered from the second harmonic amplitude.

3.2.1 Modulation Amplitude Optimization

Consider a tunable laser source whose linewidth is much narrower than the linewidth of the gas absorption line. Assume that the wavelength (frequency) of the laser is modulated sinusoidally, i.e.,

$$\nu = \nu_{LO} + \nu_{Lm} \sin \omega t \tag{3.1}$$

Modulation of laser wavelength is usually accompanied with a residual intensity modulation, the intensity of the output light from the laser may be expressed as

$$I_i(t) = I_o[1 + \eta \sin \omega t] \tag{3.2}$$

where I_o and ν_{LO} represent, respectively, the average laser output intensity and the average laser frequency. ν_{Lm} is the amplitude of the frequency modulation and η is an intensity modulation index. ω is the angular frequency of the modulation.

When the modulated laser light is passing through the transmission-type gas cell with the interaction length of L and with a gas sample of the concentration C, the output light intensity obeys the Beer-Lambert law as stated in Section 2.2.3 and may be written as

$$I(t) = I_o[1 + \eta \sin \omega t] \exp[-2\alpha(\nu_{LO} + \nu_{Lm} \sin \omega t)CL] \tag{3.3}$$

where the absorption coefficient of the gas will also vary with the frequency of laser light.

In practical applications, we are mostly interested in the measurement of small gas concentrations, and residual intensity is usually very small. Considering these facts, we may assume that $-2\alpha(\nu)CL \ll 1$ and $\eta \ll 1$. $I(t)$ may then be approximated as

$$I(t) \approx I_o[1 + \eta \sin \omega t - 2\alpha(\nu_{LO} + \nu_{Lm} \sin \omega t)CL] \tag{3.4}$$

where the approximation of $\exp[-2\alpha(\nu)CL] \approx 1 - 2\alpha(\nu)CL$ has been used and the higher-order terms have been neglected.

Normally, most of our measurements are under atmospheric pressure, which ensures that the gas absorption line is collision broadened and the line shape is given by the Lorentzian distribution, i.e.,

$$\alpha(\nu)=\frac{\alpha_o}{1+\left(\frac{\nu-\nu_g}{\delta\nu}\right)^2} \tag{3.5}$$

where α_o is the absorption coefficient for pure gas at the center of the absorption line, and ν_g and $\delta\nu$ are respectively the center frequency and the half-width of the absorption line. Equation (3.4) can be rewritten as

$$I(t)\approx I_o\left[1+\eta\sin\omega t-\frac{2\alpha_o CL}{1+\left(\frac{\nu_{LO}-\nu_g+\nu_{Lm}\sin\omega t}{\delta\nu}\right)^2}\right] \tag{3.6}$$

In the case of the average wavelength of the laser corresponding to the center of the absorption line, (i.e., $\nu_{LO}=\nu_g$), $I(t)$ can be rewritten as

$$I(t)\approx I_o\left[1+\eta\sin\omega t-\frac{2\alpha_o CL}{1+x^2\sin^2\omega t}\right] \tag{3.7}$$

where $x=\nu_{Lm}/\delta\nu$.

$I(t)$, as expressed in Equation (3.7), can be expanded into a Fouries series with the magnitudes of the first and second harmonic of

$$I_1=I_o\eta, \tag{3.8}$$

$$I_2=2k\alpha_o CLI_o \tag{3.9}$$

with

$$k=\frac{2\left[2+x^2-2\sqrt{(1+x^2)}\right]}{x^2\sqrt{(1+x^2)}}=\frac{2\left[\sqrt{(1+x^2)}-1\right]^2}{x^2\sqrt{(1+x^2)}} \tag{3.10}$$

It should be noted that the amplitude of the second harmonic signal contains information about C, the gas concentration we are trying to measure; that is why we are

interested in the second harmonic of $I(t)$.

In order to maximize the second harmonic signal (i.e. the k value), x should be adjusted to a value of 2.2 for which the modulation amplitude is 2.2 times half of the linewidth of the gas absorption line. A comparison between the calculated value and the experiment results is conducted by using the experiment setup presented in the next section and is shown as Fig.3.2.

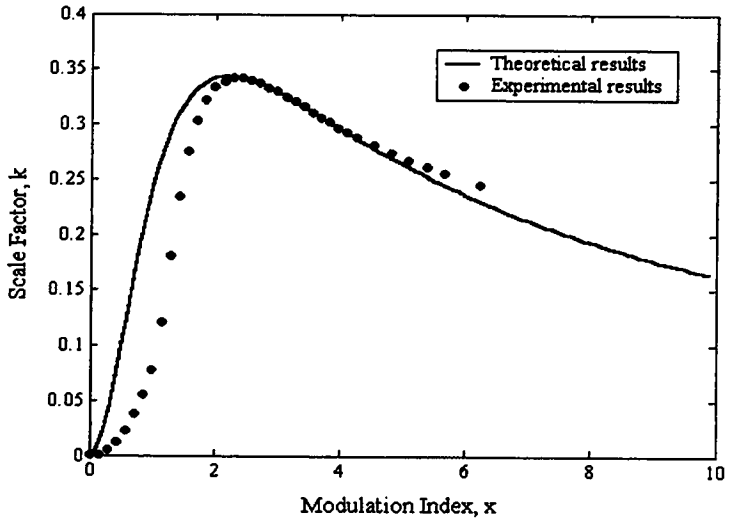

Fig. 3.2 Proportionality factor, k, versus modulation index, x.

3.3 Experimental Setup and Results

The generic fiber optic sensor system consists principally of a light source, a photodetector, the sensing element, control electronics and output signal processing unit. The most critical component is the laser to be used as the light source.

3.3.1 Tunable laser

Widely tunable laser sources are desirable for spectroscopy as well as other applications. The ideal tunable laser sources should provide high stability, high power, low frequency

noise and tunability through the entire gain bandwidth without mode hops. There are several tuning approaches that can be considered. DFB/DBR lasers provide compact narrow linewidth operation, but are only available at limited wavelengths and have limited tuning range. Solid state and dye lasers produce large tuning ranges at high power but are typically large frame lasers that can be difficult to use. External-cavity diode lasers (ECDL) are one of the most suitable lasers to use in our system because they can provide a variety of wavelengths with a moderate tuning range, very narrow linewidth, and high frequency stability in which the wavelength selection and tuning functions are external to the semi-conductor structure. The maximum tuning range of ECDL can be up to 240 nm [1,2].

A New Focus (Model 6262) ECDL [3] is used as light source in our systems where a diode laser is placed in an external cavity with a grating in a Littman configuration [4]. The wavelength of the laser can be tuned between 1518nm to 1580nm with a linewidth of 300 kHz. The grating serves as the wavelength-selective output coupler. The narrow linewidth is a result of the highly dispersive nature of the grating, which forces the laser to oscillate in a single longitudinal mode at any given setting. Adjusting the angle of a feedback mirror with respect to the grating tunes the output wavelength. There are two methods of doing this: a DC motor provides rapid (>10 nm/s) coarse tuning over the entire tuning range of greater than 60 nm. Fine wavelength adjustment is achieved with a stack of piezoelectric crystals. This piezo stack provides the user with the ability to modulate the output wavelength with frequencies as high as 2 kHz with a wavelength modulation range of ± 30 GHz.

3.3.2 Micro-optic gas cell

Fig. 3.3 shows a single-pass gas cell designed for the gas detection systems. The cell consists of two pigtailed Gradient-Index (GRIN) lenses aligned with each other and glued on a mechanical holder and the distance between the lenses is 25 mm. The insertion loss is

below 1dB (typically 0.7dB). For intensity-based measurement systems, back reflection is an important factor that may cause degradation in system sensitivity. The back-reflection of the GRIN lens used here is around -40 dB. In fact, GRIN lenses or collimators with back reflection as low as -65 dB are commercially available for which angle-polished facets and advanced anti-reflection coating are employed.

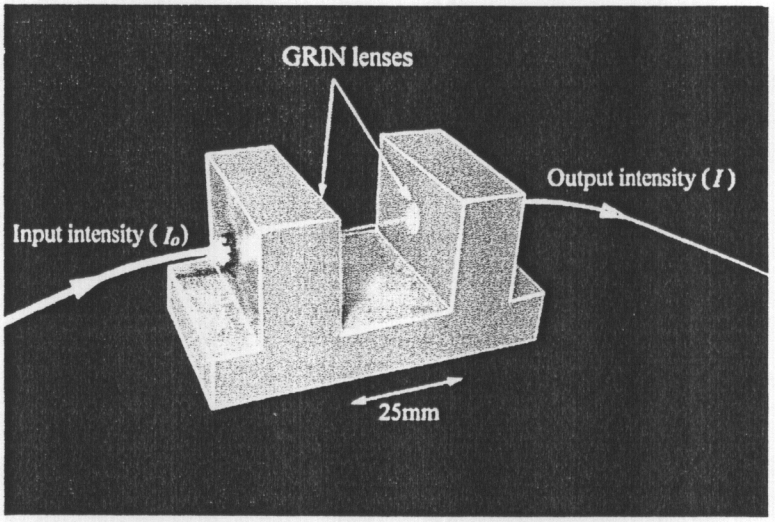

Fig.3.3 Photo of a gas cell

3.3.3 System arrangement

The single-sensor system for detecting acetylene concentration is illustrated in Fig 3.4. The tunable laser was operated under a stable temperature of 18 °C and a constant injection current of 70mA. The laser wavelength was coarsely tuned to an absorption line around 1530.37nm (6534.4 cm^{-1}) and modulated sinusoidally to apply the WMS technique with second harmonic ($2f$) detection.

Light from the laser was guided to the gas cell through a single mode optical fiber. Light passes through the gas cell containing acetylene at atmosphere pressure and was received by a photodetector. The detector output was lock-in detected at $2f$ with a DSP lock-in amplifier (Standford Research System SR830) which was connected to a personal

computer through GPIB interface for data acquisition. The time constant and the filter slope of the lock-in amplifier were set to 300ms and 12dB/oct respectively. The output would be more steady if a longer time constant is used. A high resolution sawtooth function was generated by the AD/DA card in the computer and was scanned from -2.5V to +2.5V with each step of about 1.2 mV. This sawtooth signal was combined with a sinusoidal signal and applied to the low frequency modulation input port of the tunable laser to provide wavelength sweeping and modulation. The wavelength tuning/modulation are achieved by using a piezoelectric transducer (PZT, which is included in the ECTL package) that makes adjustments in the tuning mirror angle. The maximum laser modulation frequency is limited by the movement of the mechanical parts in the tuning mechanism and is specified to be 2 kHz by the manufacturer. However, the modulation efficiency would reduce when the modulation frequency is increased. In our experiment, the modulation (sinusoidal) signal was set to an amplitude of 2.4 V_{pp} with a frequency f = 200 Hz which corresponds to a ± 14.3GHz variation of the laser frequency.

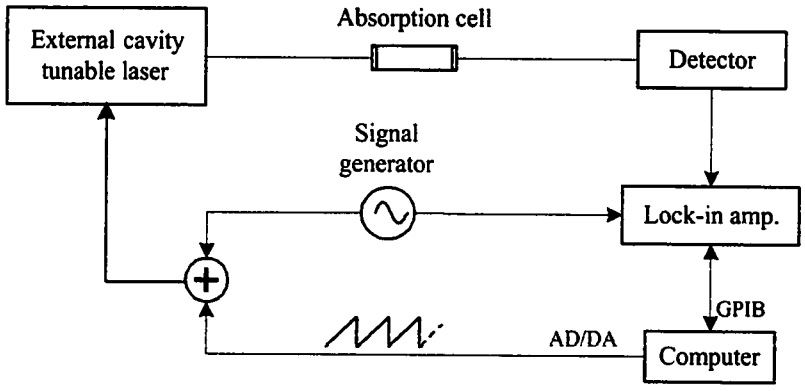

Fig. 3.4 Experimental setup of the single sensor system with WMS.

3.3.4 Optical fringe elimination

In most tunable diode laser absorption spectroscopy systems (TDLAS), optical fringes are superimposed on the measured spectrum. These result from unwanted etalons formed by reflections and scattering in the optical system. The external-cavity diode laser used in our systems is the main troublemaker for the output power oscillation. The wavelength tuning curve of Newfocus ECDL is shown in Fig. 3.5 where the output power oscillate sinusoidally up to 20% with a fringe spacing of about 0.34 nm. These fringes may be reduced by careful optical design and adjustment, but it is usually difficult to reduce the fringe amplitude to a level much below that equivalent to an absorbance of $10^{-4}/\sqrt{Hz}$. Other methods for fringe reduction must be found. These techniques can be categorized as follows: (i) mechanical modulation or dithering of the etalon spacing [5] (ii) modified modulation schemes [6] and (iii) background subtraction. The first two techniques are effective only at removing fringes with a period less than the absorption linewidth since the modulation amplitude needed to remove longer period fringes would also smear the absorption lineshape and reduce its peak height. For a stable system, a background spectrum would display the same etalon fringes that can act as a base line for measurements. Subtraction of this base line would then remove the fringes. Real systems however are subject to thermal drift, so that in the time between taking the sample spectrum and the background spectrum the fringes will have drifted and cancellation will not be perfect. Thus the success of background subtraction depends on the thermal and mechanical stability of the system. For real-time detection, an electronic noise-canceling circuit [7] can be implemented to reduce these background signals as well as other noises.

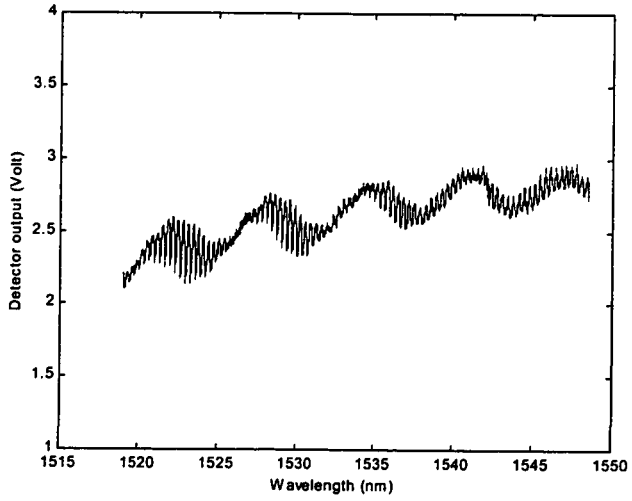

Fig. 3.5 Wavelength tuning curve of New Focus Model 6262 ECDL

3.3.5 Performance of the single sensor system

For the purpose of testing the system performance and comparing with the sensitivity achieved by WMS, we have performed a routine absorption measurement made by measuring the change in intensity of the laser power transmitted through the gas as the laser wavelength is directly tuned across the absorption line without modulation around 1530.37nm of 9344ppm acetylene. Fig 3.6 shows the normalized differential output with fine scanning and off-line background subtraction where the SNR is estimated to be ~ 4. The minimum detectable gas concentration corresponding to SNR=1 is 2336ppm, equivalent to an absorbance of 1.2×10^{-3}. By this method, it is apparently difficult to achieve the sensitivity equivalent to an absorbance of $10^{-4}/\sqrt{Hz}$. Hence, the single-sensor system with WMS technique as stated in Section 3.3.3 is implemented here.

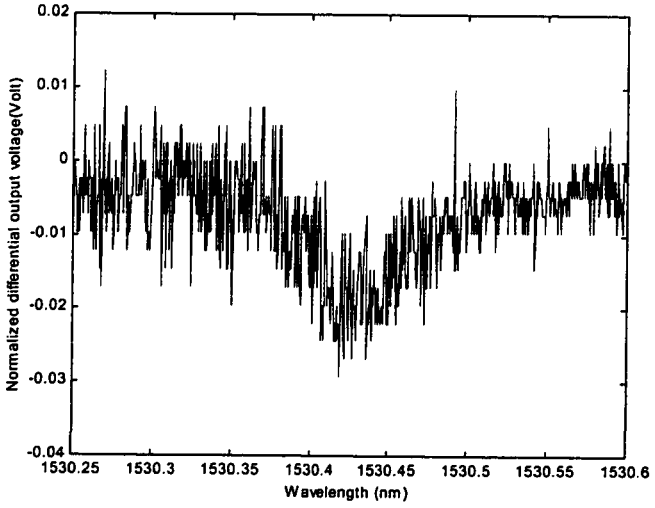

Fig. 3.6 Absorption spectrum of acetylene (9344ppm) around 1530.37nm with background signals suppression.

For the gas detection system with wavelength modulation, the background signals were also suppressed by using off-line data subtraction with the personal computer. Fig. 3.7 (a) and (b) show respectively the lock-in detected f and $2f$ signal around 1530.37 nm when the gas cell is filled with 9344 ppm C_2H_2. The signal-to-noise ratio is measured from the second harmonic signal to be 125. This SNR was obtained by repeatedly measuring the peak amplitude of the second harmonic signal for 100 times and was equal to the ratio between the mean and the standard deviation of the measured peak amplitude. It is obvious that a much higher sensitivity can be achieved compared with the routine method. The minimum detectable concentration was calculated to be 9344ppm/125 = 75ppm/$\sqrt{Hz}$ with the 25mm-long gas cell, or 1.9ppm.m. The sensitivity in terms of the minimum detectable absorbance per $\sqrt{Hz}$ was calculated to be $4.1\times10^{-5}/\sqrt{Hz}$.

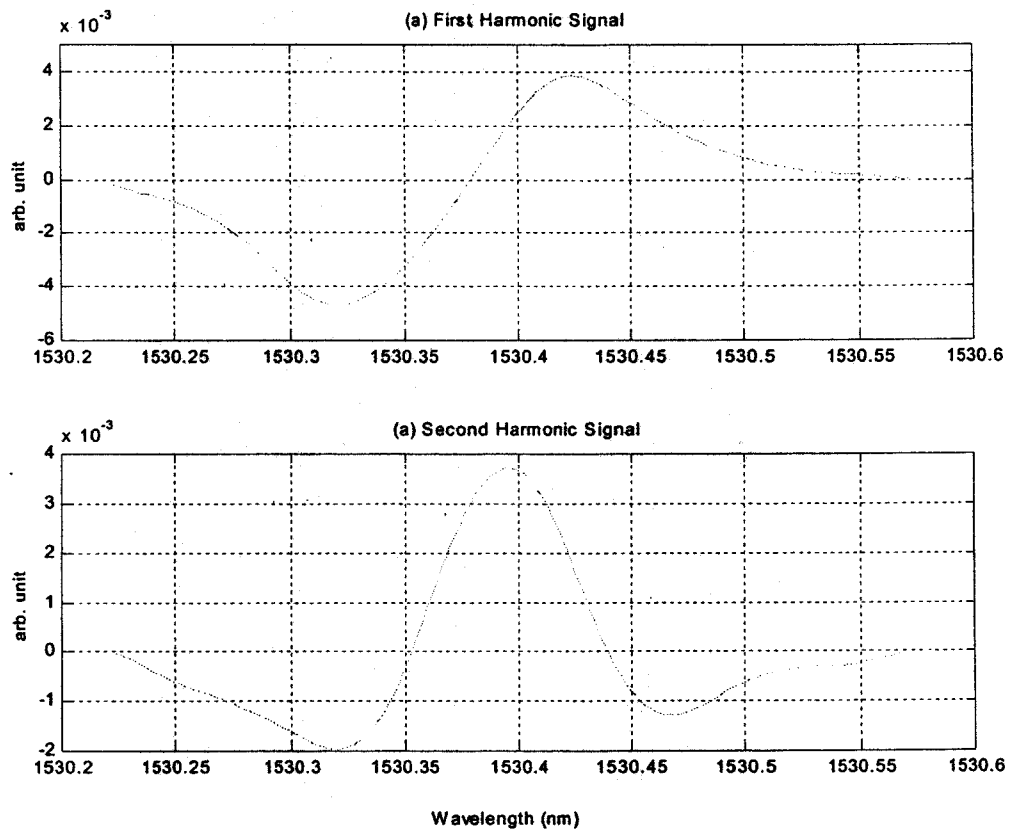

Fig.3.7 Absorption signals of acetylene detected with a 25mm gas cell and background suppressed. (a) Lock-in detected fundamental signal; (b) Lock-in detected second harmonic signal.

3.4 System Sensitivity Limitation

In WMS the output signal is directly proportional to the laser power, incident on the detector. The sensitivity of the system depends on the achievable signal-to-noise ratio. Basically, the main contributions to noise are the laser excess noise, the detector shot noise and the thermal noise. The laser excess noise decreases with increasing frequency and because of this dependence it is often referred to as $1/f$ noise. In contrast, the shot noise and the thermal noise do not depend on frequency and are said to have a white noise spectrum. Thermal noise arises from the random velocity fluctuations of the charge carriers in the load resistor of the photodetector and it is often referred to as Johnson noise. Shot

noise is caused by the random generation of electrons by the photodetector due to the random arrival of photons. For most fiber sensor systems, thermal noise is found to be much lower (~10dB) than the shot noise [9]. Also, the relative importance of these noise components depends on the operating frequency and on the laser power. For WMS using second-harmonic detection laser excess-noise may dominate. Hence, shot noise and $1/f$ noise would be considered in turn. Furthermore, the unwanted interferometric signals may also exist due to the reflections along the path of transmission. It may set the limit to the minimum detectable gas concentration of our system. The sensitivity limit due to various noise sources will be calculated with a detailed mathematical analysis.

3.4.1 Shot-noise-limited sensitivity

The minimum detectable concentration limited by the shot noise may be calculated as follows. When the wavelength of the tunable laser is tuned to the specific absorption line, the second harmonic signal current may be written, from Eq. (3.9), as

$$i_{2\omega} = 2k\alpha_o CLRP \tag{3.11}$$

where P is the optical power at the photodetector and R is the responsivity of the photodetector. The *rms* shot noise current with the detection bandwidth B is conventionally expressed as

$$i_s = \sqrt{2qBRP} \tag{3.12}$$

where q is the charge of an electron.

The shot noise equivalent gas concentration using the second harmonic detection technique can be obtained by setting the second harmonic signal given by Eq. (3.11) to be equal to the shot noise contribution (Eq. 3.12) and can be expressed as

$$\frac{C}{\sqrt{B}} = \frac{1}{k\alpha_o L}\sqrt{\frac{q}{2RP}} \tag{3.13}$$

For calculating the shot-noise limit, the parameters of our system are k =0.34 (from Fig. 3.2), α_o=0.252 cm^{-1}(for that line of acetylene at 1530.37nm), L=2.5cm, P=0.05mW, and R=1 A/W. In such a case, the detection sensitivity in terms of minimum detectable absorbance limited by the shot noise is about $1.02\times10^{-7}/\sqrt{Hz}$ (equivalent to 0.2 ppm $/\sqrt{Hz}$). In fact, the experimental result for our single sensor system is 2 to 3 orders of magnitude worse than the shot-noise-limited sensitivity. Hence, it is evident that the system is not limited by the shot noise.

3.4.2 Flicker noise

It is well-known that substantial improvements of detection limits were obtained by introducing high-frequency modulation for laser absorption spectroscopy. A number of literatures [8] suggest the frequency related noises are responsible for the limited sensitivity of the systems with wavelength modulation performed at the frequency less than 100 kHz.

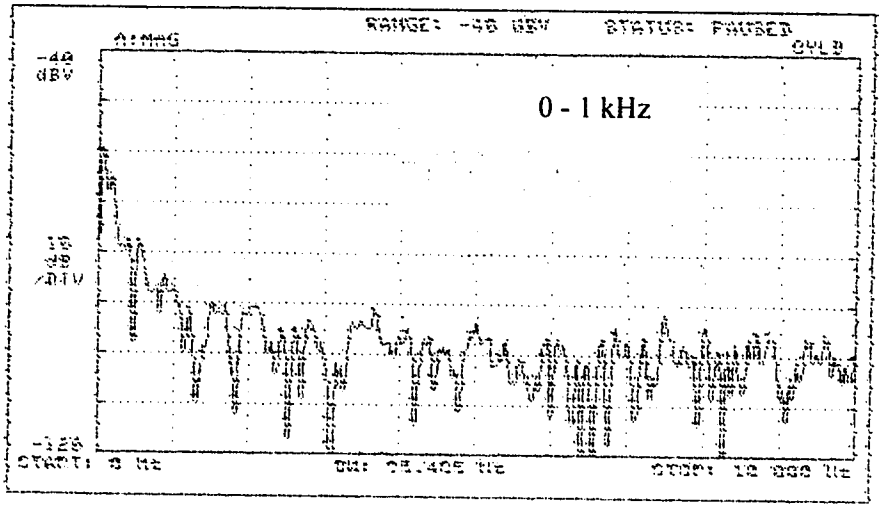

Fig. 3.8 Noise spectrum at frequency <10 kHz

The power spectrum of this noise falls off rapidly with frequency and is thus called "*1/f* noise". Flicker noise may include the laser excess noise, noise due to a lack of an ohmic contact at the detector electrodes,etc. A noise spectrum obtained with a simple system where the Newfocus tunable laser is directly connected to the photodetector without any wavelength modulation is shown in Fig. 3.8. It is seen that the *1/f* noise becomes predominant at low frequency. The empirical expression for the noise current is [9]

$$i_f = RP\sqrt{\sigma_{ex}{}^2 \frac{B}{f}} \tag{3.14}$$

where P is the optical power, R is the responsivity of the photodetector, σ_{ex} is a system dependent constant defined as the excess noise at 1-Hz bandwidth and 1-Hz frequency, B is the detection bandwidth and f is the detection frequency. Similar to the calculation in Section 3.4.1, the *1/f*-noise limited sensitivity can be determined by setting the second harmonic signal current given by Eq. (3.11) to be equal to i_f (Eq. 3.14) with $\sigma_{ex}{}^2 = 1\times10^{-10}$, $f = 200$ Hz. The sensitivity in terms of minimum detectable absorbance is calculated as $9.04\times10^{-7}/\sqrt{Hz}$ ($\approx$ 1.65 ppm/$\sqrt{Hz}$) which is about 10 dB larger than the shot-noise limitation.

3.4.3 Sensitivity limit due by unwanted interferometric signals

The use of tunable ECDL, which provides high power within narrow spectral width and a large tuning range, would basically enhance the sensitivity and the selectivity for the gas detection system. However, the highly coherent nature does introduce problems such as the interferometric signals arising from coherent reflections. Reflections can occur at fiber connectors, fiber-cell joints (cell surfaces), and so forth and which would interfere with the signal wave. These unwanted interferometric signals could be larger than the source and

detector noises and might set a limit on the sensor performance. As shown in Fig. 3.9, the first-order reflections are directly fed back into the source, thus we may assume they have no effect on system performance when a proper isolator is used at the laser output port. The second-order reflection (reflection caused by a pair of reflective points along the fiber), however, can reach the photo detector and will affect the system performance. In the light output of the system, in addition to a primary beam, many second-order waves resulting from second-order reflections may exist. The second-order reflections can be divided into two different categories: (1) reflection pairs across the cell, (2) reflection pairs before or after the cell. We have consider only the first case. The second category can be considered in the same way and similar results can be obtained [10].

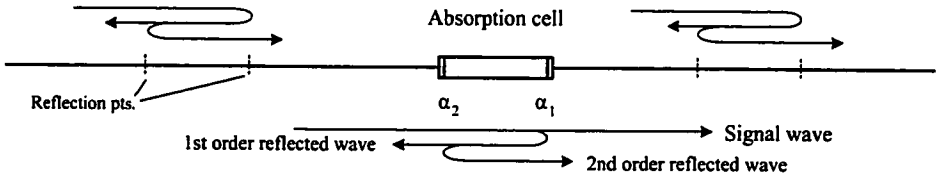

Fig. 3.9 Second-order reflection pairs in a single-sensor system

To study these interferometric signals, the laser light output can be represented with its electric field as

$$E_o(t) = [I_o(1+\eta \sin \omega t)]^{1/2} \exp\left[j2\pi\left(\nu_{LO} t + \nu_{Lm} \int_0^t \sin \omega u du \right)\right] \tag{3.15}$$

When passing through the gas cell, the signal wave at the detector may be expressed as

$$\begin{aligned} E_s(t) = {} & [I_o(1+\eta \sin \omega t)]^{1/2} \times \exp[-\alpha(\nu_{LO} + \nu_{Lm} \sin \omega t) CL] \\ & \times \exp\left[j2\pi\left(\nu_{LO} t + \nu_{Lm} \int_0^t \sin \omega u du \right)\right] \end{aligned} \tag{3.16}$$

where we have neglected the phase modulation term $\phi(\nu)$ resulting from changes of

refractive index of the gas sample because it is very small for low gas concentrations. The magnitude of $\phi(\nu)$ increases with gas concentration and interaction length. The signal intensity can be calculated with $I(t)=\left\langle |E(t)|^2 \right\rangle$ and is given by Eq. (3.3). For the case (1), reflection pairs across the cell, the reflected wave may be written as,

$$\begin{aligned} E_r(t) = r_1\, r_2\, [I_o(1+\eta\sin\omega(t-\tau))]^{1/2} \times \exp[-3\alpha(\nu_{LO}+\nu_{Lm}\sin\omega(t-\tau))CL] \\ \times \exp\left\{ j2\pi\left[\nu_{LO}(t-\tau)+\nu_{Lm}\int_0^{t-\tau}\sin\omega u du \right]\right\} \end{aligned} \tag{3.17}$$

where r_1 and r_2 are the reflection coefficients of the two reflection points and τ is the time delay between the signal wave and the reflected wave. The total light intensity may be written as

$$I(t)=\left\langle |E_s(t)+E_r(t)|^2 \right\rangle \tag{3.18}$$

The total light intensity at the output detector, $I(t)$, may be divided into three parts: intensity of the signal wave $\left\langle |E_s(t)|^2 \right\rangle$, intensity of the reflected wave, $\left\langle |E_r(t)|^2 \right\rangle$, the mixing term between the signal wave and the reflected wave. The intensity of the reflected wave is of a smaller magnitude compared with the other two terms and may be neglected. We consider only two terms: signal term and the mixing term (unwanted interferometric signals), which induces errors in the measurement. The signal intensity is given by Eq. (3.16) and the intensity of the interferometric signal may be expressed as

$$\begin{aligned} I_n(t) &= 2\,\mathrm{Re}\left\langle E_s(t)E_r^*(t)\right\rangle \\ &= 2r_1\, r_2\, I_o[1+\eta\sin\omega(t-\tau)]^{1/2}[1+\eta\sin\omega t]^{1/2} \\ &\quad \times \exp\{-[3\alpha(\nu_{LO}+\nu_{Lm}\sin\omega(t-\tau))+\alpha(\nu_{LO}+\nu_{Lm}\sin\omega t)]CL\} \\ &\quad \times \cos\left\{2\pi\left[\nu_{LO}\tau+\nu_{Lm}\int_{t-\tau}^{t}\sin\omega u du\right]\right\} \end{aligned} \tag{3.19}$$

For low modulation frequency such as that used in our experiment (200 Hz) and the limited time delay between the signal wave and the reflected wave, we may use the approximation

$$[1+\eta\sin\omega(t-\tau)]^{1/2}[1+\eta\sin\omega t]^{1/2}\approx 1+\eta\sin\omega t \tag{3.20}$$

and for small gas concentration, i.e., $\alpha(\nu)CL << 1$, we may assume

$$\exp\{-[3\alpha(\nu_{LO}+\nu_{Lm}\sin\omega(t-\tau))+\alpha(\nu_{LO}+\nu_{Lm}\sin\omega t)]CL\}\approx 1 \tag{3.21}$$

Hence, $I_n(t)$ may be approximated as

$$I_n(t)\approx 2r_1r_2I_o(1+\eta\sin\omega t)\cos[\psi+\zeta\sin\omega t] \tag{3.22}$$

where $\psi=2\pi\nu_{LO}\tau$ and $\zeta=2\pi\nu_{Lm}\tau$.

In the derivation of Eq. (3.22), we assumed that $\sin\left(\frac{\omega\tau}{2}\right)\approx\frac{\omega\tau}{2}$ and $\omega\left(t-\frac{\tau}{2}\right)\approx\omega t$ for $\omega\tau<<1$ and thus,

$$\begin{aligned}2\pi\nu_{Lm}\int_{-\tau}\sin\omega u\,du &= \frac{4\pi\nu_{LM}}{\omega}\sin\left(\frac{\omega\tau}{2}\right)\sin\omega\left(t-\frac{\tau}{2}\right) \\ &\approx \frac{4\pi\nu_{LM}}{\omega}\left(\frac{\omega\tau}{2}\right)\sin\omega t \\ &= \zeta\sin\omega t\end{aligned} \tag{3.23}$$

By using Bessel functions, $\cos[\psi+\zeta\sin\omega t]$ in Eq. (3.22) can be expressed as

$$\begin{aligned}\cos[\psi+\zeta\sin\omega t] = \cos\psi[J_0(\zeta)+2J_2(\zeta)\cos 2\omega t+2J_4(\zeta)\cos 4\omega t+\cdots] \\ -\sin\psi[2J_1(\zeta)\sin\omega t+2J_3(\zeta)\sin 3\omega t+2J_5(\zeta)\sin 5\omega t+\cdots]\end{aligned} \tag{3.24}$$

According to the above expansion, the second harmonic of $I_n(t)$ can be found as

$$I_{n(2\omega)}(t)=2r_1r_2I_0[2\cos\psi J_2(\zeta)\cos 2\omega t-2\eta\sin\psi J_1(\zeta)\sin 2\omega t] \tag{3.25}$$

For simplicity, we assume $r_1 = r_2 = r$. Considering the fact that $\eta << 1$ (as the Newfocus 6262 tunable laser with wavelength modulation of ±14.3GHz, η is about 0.023), the second term may be neglected. The relative measurement error δ_{coh} due to unwanted interferometric signal can be found by dividing $I_{n(2\omega)}(t)$ by I_2 by as given in Eq.(3.9) and expressed as

$$\delta_{coh} = \frac{I_{n(2\omega)}(t)}{I_2} = 2r^2 \left| \frac{\cos\psi J_2(\zeta)}{k\alpha_0 CL} \right| \tag{3.26}$$

To determine the system sensitivity, the relative measurement error is set to be equal to 1. We can obtain the minimum detectable concentration as:

$$|C_{\min}|_{rms} = \frac{\sqrt{2}r^2}{k\alpha_o L} |J_2(\zeta)| \tag{3.27}$$

where we have used the *rms* value of cos ψ as $\frac{1}{\sqrt{2}}$. For the case of reflection pairs before or after the cell, the above solution of minimum detectable concentration is valid based on the stated assumptions during the derivation.

Fig.3.10 shows the calculated minimum detectable concentration $|C_{\min}|_{rms}$ limited by the unwanted interferometric signal as functions of the overall reflection coefficients r^2 and the amplitude of wavelength modulation ν_{Lm} where reflections occur at the surfaces of the GRIN lenses within the gas cell with α_o=0.252cm^{-1}, L=2.5cm, τ=1.67×10^{-10}sec, k and ζ are the functions of the amplitude of wavelength modulation as stated in Eqs (3.10) and (3.22) respectively. Fig. 3.11 shows the calculated minimum detectable concentration as the function of the wavelength modulation amplitude ν_{Lm} only with the reflection coefficient of -40 dB. Examination of Eq. (3.27) and Fig.3.11 shows that the magnitude of the interferometric signals depends on the Bessel function $J_2(\zeta)$. Hence, it may be possible in

principle to eliminate the interference effects by choosing an appropriate amplitude of the wavelength modulation. In practice, there might be multiple reflection points in the systems that will reduce the possibility to set $J_2(\zeta)$=0. From the simulation results in Fig.3.11, the $|C_{\min}|_{rms}$ is around 60ppm with $\nu_{Lm} \approx$ 14.3 GHz. This simulated sensitivity is in good agreement with our experimental result (75ppm) as presented in Section 3.3.5. This good agreement indicates that the sensitivity of our system is limited by the unwanted interferometric signals due to reflections occurring at the gas cell. $|C_{\min}|_{rms}$ can also be reduced by increasing the modulation amplitude. This result may help to reduce the measurement error in systems within multiple pair of reflection points.

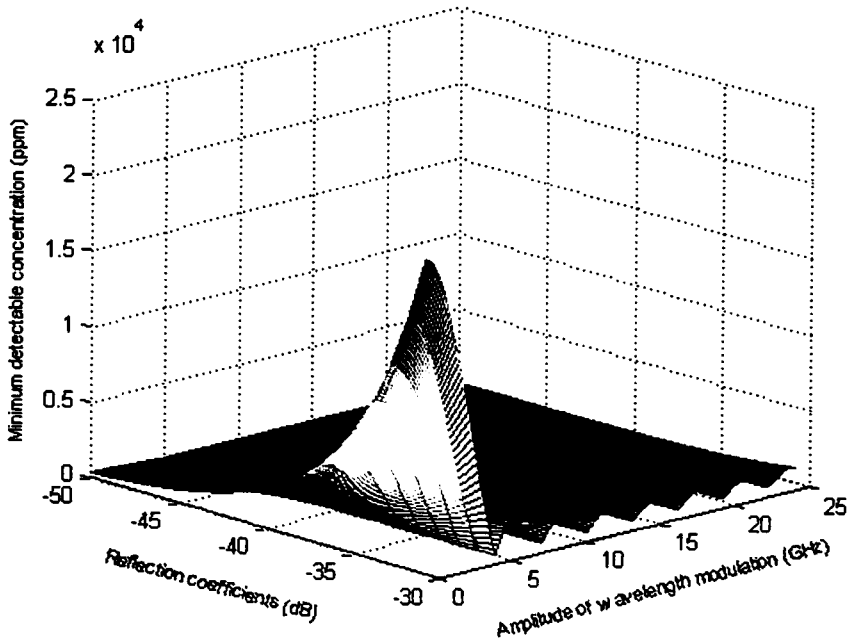

Fig. 3.10 The calculated minimum detectable concentration limited by the second-order coherent reflection as functions of the overall reflection coefficients r^2 and the amplitude of wavelength modulation ν_{Lm}.

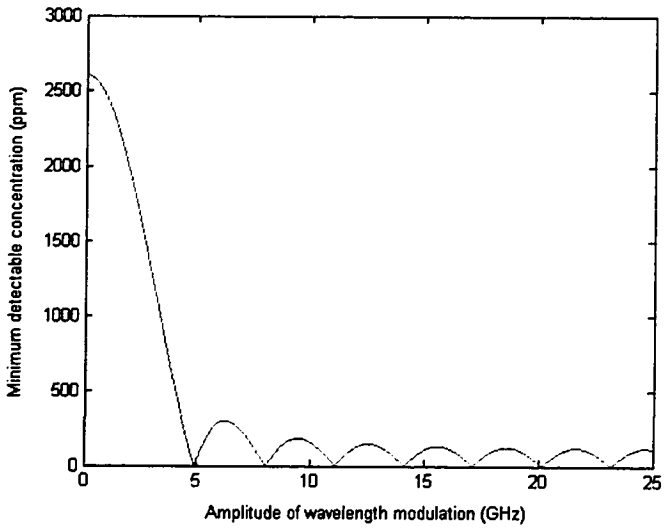

Fig. 3.11 The calculated minimum detectable concentration as the function of the wavelength modulation amplitude ν_{Lm} with the reflection coefficient of -40 dB.

3.5 Chapter Summary and Conclusions

In this chapter, gas detection using WMS technique with second-harmonic detection is presented theoretically and experimentally. A single-sensor system is experimentally tested and a sensitivity in terms of minimum detectable absorbance of $4.1\times10^{-5}/\sqrt{Hz}$ is obtained. The sensitivity limitations due to various noise sources are considered. Shot noise, thermal noise, *1/f* flicker noise and unwanted interferometric signals due to coherent reflections are examined. We found that, for our system, the measurement error in gas concentration is mainly due to the unwanted interferometric signals and set the limit to the system sensitivity. In contrast, the sensitivity limitations due to the *1/f* noise, thermal noise and shot noise are 2 and 3 orders of magnitude lower than that of the unwanted interferometric signals. The performance of the system may be improved by using anti-reflecting optical components such as angled connectors and GRIN lenses with AR-coating. The signal-to-noise ratio can

be further enhanced by using a longer time-constant (smaller detection bandwidth) lock-in detection and digital signal processing[11].

REFERENCES

1. M. Bagley, R. Wyatt, D.J. Elton, et al, "242 nm continuous tuning from a GRIN-SC-MQW-BH InGaAsP laser in an extended cavity," *Electronics Letters*, Vol.26, pp.267-269, 1990.
2. H. Tabuchi, H. Ishikawa, "External grating tunable MQW laser with wide tuning range of 240 nm," *Electronics Letters*, Vol.26, pp.742-743, 1990.
3. User manual of Newfocus external cavity diode laser (Model 6262), *Newfocus*.
4. K.C. Harvey, C.J. Myatt, "External-cavity diode laser using a grazing-incidence diffraction grating," *Optics Letters*, Vol.16, No.12, pp.910-912, 1991.
5. J.A. Silver, A.C. Stanton, "Optical interference fringe reduction in laser absorption experiments", *Applied Optics*, Vol.27, No.10, pp.1914-1916, 1988.
6. D.T. Cassidy, J. Reid, "Harmonic detection with tunable diode lasers-two-tone modulation", *Applied Physics B*, Vol.29, pp.279-285, 1982.
7. X. Zhu and D. T. Cassidy, "Electronic subtracter for trace-gas detection with InGaAsP diode laser," *Applied Optics*, Vol.34, No.36, pp.8303-8308, 1995.
8. D. S. Bomse, A. C. Stanton, and J. A. Silver, "Frequency-modulation and wavelength modulation spectroscopies: comparison of experimental methods using a lead-salt diode laser," *Applied Optics*, Vol.31, pp.718-731, 1992.
9. E. L. Dereniak, D.G.Crowe, "Noise sources," Section 2.3, pp.36-43, *Optical Radiation Detectors*, John Wiley & Sons, 1984.
10. W. Jin, Y.Z. Xu, M.S. Demokan and G. Stewart, "Investigation of interferometic noise in fiber-optic gas sensors with the use of wavelength modulation spectroscopy," *Applied Optics*, Vol.36, No.28, pp.7239-7246, 1997.
11. H. Riris, C.B. Carlisle, R.E. Warren and et al, "Signal-to-noise ratio enhancement in frequency-modulation spectrometers by digital signal processing," *Optics Letters*, Vol.19, No.2, pp.144-146, 1994.

CHAPTER 4 PERFORMANCE ANALYSIS OF TDM SYSTEM

4.1 Introduction

Gas sensors based on wavelength modulation spectroscopy technique has demonstrated practical absorption sensitivity of 10^{-5} in 1-Hz bandwidth. However, the commercial acceptance of these sensors was poor due to complexity and high cost. The commercial viability of this technique may therefore be enhanced if a number of sensors in an optical fiber network can share the expensive components which dominates the costs. Correspondingly, lower operational and maintenance costs per sensing point may be achieved. For sensor multiplexing three important aspects should be considered: the sensor principle, the network configuration and the sensor addressing technique. In practice, not all configurations or techniques can be implemented for addressing certain type of sensors. The feasibility of the systems may greatly depend on the principle of measurement. For example, wavelength division multiplexing [1] is difficult to be applied on gas sensors based on absorption spectroscopy due to the wavelength dependence of the gas absorption. In various techniques of multiplexing, time-division is the most popular and straightforward technique that can be used for the interrogation of gas sensors. In this chapter, a multi-sensor system with time-division multiplexing is studied. The results of a theoretical investigation on the performance of the system are reported in this chapter. An analysis of the performance as limited by shot noise is presented in Section 4.2. Crosstalk caused by incoherent and coherent effects due to the finite extinction ratio of the optical intensity modulator (switch) is discussed in Section 4.3. Formulas that relate the crosstalk level to the extinction ratio of the switch, the modulation parameters and the optical path difference between sensing channels are derived. With real system parameters, the predicted performance of our experimental system in terms of detection sensitivity and crosstalk are also given.

4.2 General Description for the TDM Gas Sensor System

Fig 4.1 shows the simplified block diagram of a multiplexed gas sensor system. The system uses time-division addressing and a forward-coupled ladder topology. For optical pulse generation, light from the tunable laser source is modulated in intensity, through the use of an external intensity modulator. The period and the pulse width can be adjusted by changing the settings of the electrical pulse generator. Pulsed light is then coupled to the input fiber bus and evenly diverted to the N gas sensors in the forward-coupled ladder array. The splitting ratios of the distribution and recombination couplers are predetermined and are given by [2]:

$$k_j = \frac{1}{N-j+1} \tag{4.1}$$

where k_j represents the coupling ratio of the j-th coupler as indicated in Eq.(4.1), for j=1,2,...,N-1.

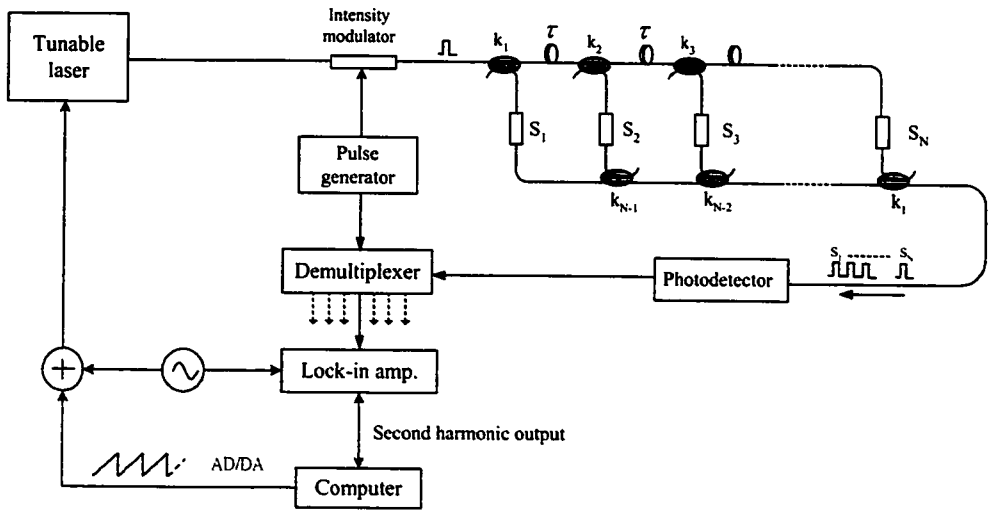

Fig. 4.1 TDM gas sensor system

Here, the forward-coupled topology is preferred over the normal ladder array configuration as it is more tolerant to the coupling ratios of the couplers required for

balancing the sensor performance [2]. With this topology, all the sensor signals pass through the length of the array, and each sensor channel, consequently, experiences a similar loss. In our system, it is assumed that the optical path differences between adjacent channels are the same. τ is the time-delay difference between adjacent sensors. If the period (T_p) and width (ΔT) of the input optical pulse satisfy the conditions

$$\tau \geq \Delta T \qquad T_p \geq N \cdot \tau \tag{4.2}$$

then the pulses from different channels can be distinguished in the time domain when they arrive at the photodetector and can be separated by electronic switching after photodetection (as shown in Fig. 4.2).

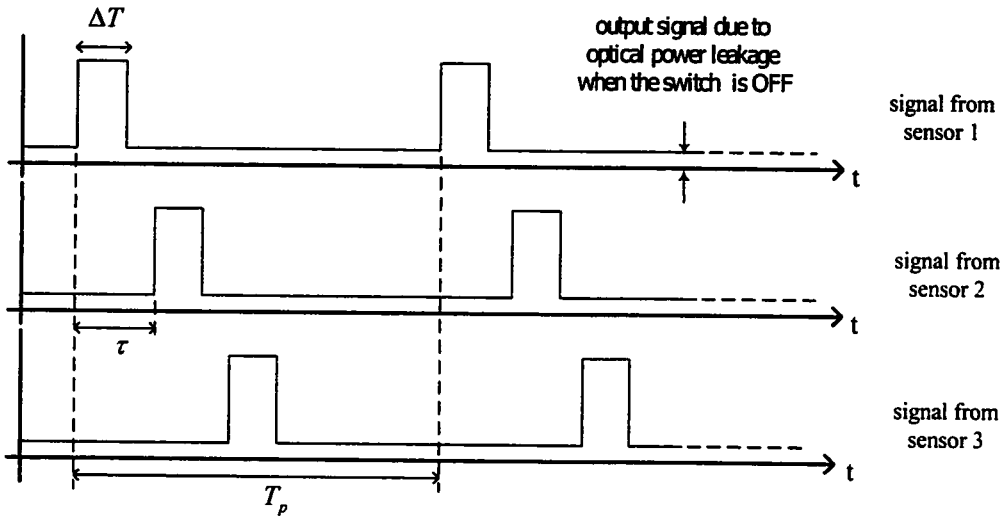

Fig. 4.2 Pulse trains from different channels after photodetection.

With the implementation of the wavelength modulation technique, the pulse train from a selected channel acts as an information carrier where the modulation signal as well as the information on gas concentration is carried by the envelope. The useful signal can then be extracted by lock-in detection of the pulse train at the second harmonic of the modulation frequency with a lock-in amplifier.

4.3 Shot-noise-limited Sensitivity

In this section, the detection sensitivity of the TDM system limited by the shot noise is determined. We assume that the peak power of the input pulses is P_o and the power loss associated with each individual sensor channel is the same and equals to α_l^2. The peak power of each received pulse will be $\alpha_l^2 P_o / N^2$. The average optical power for each sensing channel and the total average optical power at the receiver will then be $\frac{\alpha_l^2 P_o}{N^2}\frac{\Delta T}{T_p}$ and $\frac{\alpha_l^2 P_o}{N}\frac{\Delta T}{T_p}$. respectively. The shot noise current at the detector output is proportional to the square root of the total average optical power at the photodetector. Assuming that an ideal electric switch is used as the demultiplexer and that the electric switch is synchronized with the optical switch, the root-mean-square (*rms*) amplitude of the shot-noise current, after switching (demultiplexing), for each individual sensing channel may be expressed as [3]

$$i_{shot,rms} = \sqrt{\frac{2qRB\alpha_l^2 P_o}{N^2}\frac{\Delta T}{T_p}} \tag{4.3}$$

where R is the responsivity of the photodetector, q is the electron charge and B is the detection bandwidth. Consider a gas sensing system that uses wavelength modulation where the laser wavelength is aligned to the center of the gas absorption and the second harmonic signal is used as a measure of gas concentration, the *rms* value of the second-harmonic signal current for an individual sensor may be written, using Eq.(3.11), as

$$i_{2\omega,rms} = \sqrt{2}\, R k \alpha_o C L \frac{\alpha_l^2 P_o}{N^2}\frac{\Delta T}{T_p} \tag{4.4}$$

where C is the gas concentration, L is the interaction length (the length of the gas cell), and k is a constant as defined in Eq.(3.10) in Chapter 3. The gas absorption line is assumed to be collision broadened with a Lorentzian shape and α_o is the absorption coefficient for pure gas at the center of the absorption line. The shot-noise-limited detection sensitivity using the second harmonic detection technique can be obtained by setting the second harmonic signal given by Eq.(4.4) to be equal to the shot noise contribution given by Eq.(4.3) and can be expressed as

$$\frac{\alpha_o CL}{\sqrt{B}} = \frac{N}{k}\sqrt{\frac{q}{R}\frac{1}{\alpha_l^{\,2} P_o}\frac{T_p}{\Delta T}} \tag{4.5}$$

The optimal result is obtained when $\Delta T = \tau$ and $N\Delta T = N \cdot \tau = T_p$, and the shot-noise-limited detection sensitivity can then be written as

$$\frac{\alpha_o CL}{\sqrt{B}} = \frac{1}{k}\sqrt{\frac{q}{R}\frac{N^3}{\alpha_l^{\,2} P_o}} \tag{4.6}$$

Fig. 4.3 shows the simulation result of the shot-noise-limited performance as a function of sensor number where the real parameters used in our system are substituted into Eq. (4.6). The parameters are P_o=1 mW, $\alpha_l^{\,2}$=0.8, q=1.6×10^{-19}C, R=1 A/W, α_o=0.252cm^{-1}, L=2.5cm. For a sensor array with as many as 50 sensors, the detection limit is below 8 ppm/$\sqrt{Hz}$. It is clear that the sensitivity of the sensor array decreases as the number of sensors increases but it is still within an acceptable limit for relatively large values of N. Of course, we will again show that the shot-noise-limited sensitivity cannot be achieved due to other larger noise factors.

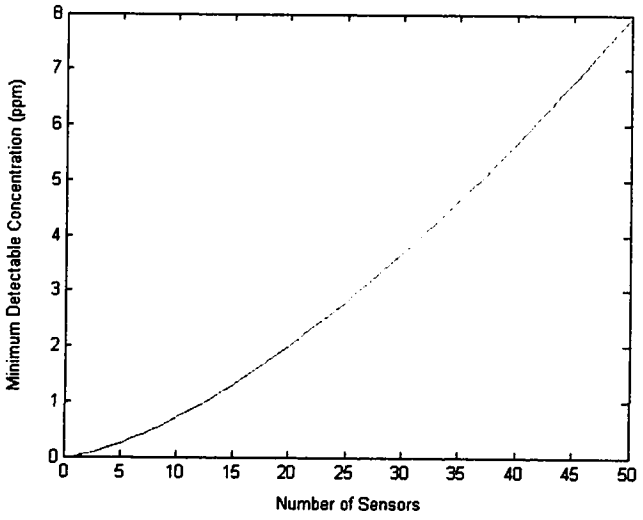

Fig.4.3 The shot-noise-limited performance of the TDM system as a function of sensor number.

4.4 Crosstalk and Noise Analysis

In practice, other noises may well exceed the shot noise level and set a limit to the system performance. A major limiting factor for the system shown in Fig.4.1 is the crosstalk between different sensors caused by the non-ideal optical switch (intensity modulator) used for input pulse generation. A practical optical switch has limited extinction ratio, this is, when the switch is in the OFF state, there is still a small amount of light passing through the optical switch (see Fig.4.2). The extinction ratio [5], which is defined as thc ratio of the low power level (P_L when the switch is OFF) and the high power level (P_H, when the switch is ON), i.e., $\alpha_e^2 = 10\log(P_L/P_H)$ [17], is of the order of -30 to -35 dB for a single Mach-Zehnder type switch and can reach -60dB for a cascaded switch consisting of two Mach-Zehnder interferometers [6]. In this section, we analyze the effect of this limited extinction ratio on the performance of the multiplexed system.

Assuming that the wavelength of the laser is modulated sinusoidally at low modulation

frequencies (e.g., less than 100 kHz), the laser light output electric field will be [7]:

$$E(t) = [I_o(1+\eta \sin \omega t)]^{1/2} \exp\left[j2\pi\left(\nu_{LO} t + \nu_{Lm} \int_0^t \sin \omega u du \right)\right] \tag{4.7}$$

where I_o and ν_{LO} represent, respectively, the average laser output power and the average laser frequency. ν_{Lm} is the amplitude of the frequency modulation and η is an intensity modulation index. ω is the angular frequency of the modulation.

Assuming a square pulse amplitude modulation with an extinction ratio α_e^2, the electric field after the optical intensity modulator may be expressed as

$$E(t) = [I_o(1+\eta \sin \omega t)]^{1/2} \exp\left[j2\pi\left(\nu_{LO} t + \nu_{Lm} \int_0^t \sin \omega u du \right)\right] \tag{4.8}$$

$$\times \begin{bmatrix} 1 \\ \alpha_e \exp(j\phi) \end{bmatrix} \quad \begin{cases} for\ mT_p \le t \le mT_p + \Delta T, & switch\ ON \\ for\ mT_p + \Delta T \le t \le (m+1)T_p, & switch\ OFF \end{cases}$$

where m=0,1,2,.... and ϕ is a phase difference between the ON and the OFF states that is caused by the optical switching [5]. The insertion loss of the switch has been omitted in the analysis as it can be regarded as a reduction in the input power.

The output electric field from the sensor array will be a summation of electric fields from all the individual sensors, i.e.,

$$E_o(t) = \sum_{i=1}^{N} E_{io}(t) \tag{4.9}$$

with $E_{io}(t)$ given by

$$E_{io}(t) = \frac{\alpha_I}{N}[I_o(1+\eta\sin\omega(t-i\tau))]^{1/2} \times \exp[-\alpha(\nu_{LO}+\nu_{Lm}\sin\omega(t-i\tau))C_iL] \times \exp\left[j2\pi\left(\nu_{LO}(t-i\tau)+\nu_{Lm}\int_0^{(t-i\tau)}\sin\omega u du\right)\right]\times\exp[j\varphi_i(t)] \times\begin{bmatrix}1\\ \alpha_e\exp(j\phi)\end{bmatrix} \quad \begin{cases} for\ mT_p+i\tau \le t \le mT_p+i\tau+\Delta T,\ \ switch\ ON \\ for\ mT_p+i\tau+\Delta T \le t \le (m+1)T_p+i\tau,\ \ switch\ OFF \end{cases} \tag{4.10}$$

where $\alpha(\nu)$ is an amplitude absorption coefficient of the gas and $\varphi_i(t)$ is a random time varying phasor that is due to changing environment. Under atmospheric pressure, the gas absorption line is collision broadened and the line shape is given by the Lorentzian distribution. The gas absorption also induces refractive index changes and therefore phase changes of light wave when it passes through the gas cell. However, under the condition of low gas concentration such that $\alpha(\nu)CL << 1$, the phase variation caused by gas absorption can be neglected.

In the following, we look at the demultiplexer output corresponding to channel *i* and study the performance limitation of channel *i* (sensor *i*) caused by crosstalk from other sensors. To simplify the analysis, we use the following approximations:

$$\eta\sin\omega(t-i\tau) \approx \eta\sin\omega t \tag{4.11}$$

$$\alpha(\nu_{LO}+\nu_{Lm}\sin\omega(t-i\tau)) \approx \alpha(\nu_{LO}+\nu_{Lm}\sin\omega t) \tag{4.12}$$

These approximations are useful in simplifying the analysis, and will be accurate for $i\omega\tau << \pi/2$, i=1,2...N-1. This approximation will set an upper limit on the delay time (or maximum optical path length difference) allowed between individual sensors. For low frequency wavelength modulation, the optical path length difference allowed for satisfying this condition ($i\omega\tau << \pi/2$) can be very long. For example, in our experiments, the modulation frequency is less than 2kHz. Assume $(N-1)\omega\tau \le \pi/10$ (18 degree), for f=2kHz,

we have $(N\text{-}1)\tau = 1/(20f) \leq 25\mu s$, corresponding to fibre length of 5km. This is significantly larger than the maximum path length difference (between the first and the last sensing channel) occurring in our network and may be already longer than the coherence length of the light source.

Using the above approximation, Eq.(4.10) can be expressed as

$$\begin{aligned} E_{io}(t) \approx & \frac{\alpha_l}{N}[I_o(1+\eta \sin \omega t)]^{1/2} \times \exp[-\alpha(\nu_{LO}+\nu_{Lm}\sin\omega t)C_i L] \\ & \times \exp\left[j2\pi\left(\nu_{LO}(t-i\tau)+\nu_{Lm}\int_0^{(t-i\tau)}\sin\omega u du\right)\right] \times \exp[j\varphi_i(t)] \\ & \times \begin{bmatrix} 1 \\ \alpha_e \exp(j\phi) \end{bmatrix} \quad \begin{cases} for\ \ mT_p + i\tau \leq t \leq mT_p + i\tau + \Delta T, & \text{switch } ON \\ for\ \ mT_p + i\tau + \Delta T \leq t \leq (m+1)T_p + i\tau, & \text{switch } OFF \end{cases} \end{aligned} \tag{4.13}$$

The light intensity output from the sensor array can be calculated from Eqs.(4.9) and (4.13) and may be divided into four categories:

- the signal light intensity of channel i, $I_{io}(t) = \left\langle |E_{io}(t)|^2 \right\rangle$;
- the light intensities from other channels (incoherent crosstalk), $I_{i,inc}(t) = \sum \left\langle |E_{jo}(t)|^2 \right\rangle$ where $j = 1,2,\cdots N\ (j \neq i)$;
- terms of mixing between the electric field of channel i and the other channels (first order coherent crosstalk), $I_{i,co,1}(t) = 2\sum \mathrm{Re}\left\langle E_{io}(t) \cdot E_{jo}^{*}(t) \right\rangle$ where $j = 1,2,\cdots N\ (j \neq i)$ and "Re" represents the real part;
- terms of mixing between the electric fields from channels other than channel i (second order coherent crosstalk), i.e., $I_{i,co,2}(t) = 2\sum \mathrm{Re}\left\langle E_{mo}(t) \cdot E_{no}^{*}(t) \right\rangle$ where $n = 1,2,\cdots N\ (m > n, m \neq i, n \neq i)$.

Assuming that an ideal electric switch is used and synchronised with the input optical switch, the demultiplexed output for the sensor i will consist of the light signals only within the time interval, $mT_p + i\tau \le t \le mT_p + i\tau + \Delta T$. The light signal within this time slot includes the four categories mentioned above. The signal intensity of channel i within this time interval may be expressed as

$$\begin{aligned} I_{io}(t) &= \left\langle \left| E_{io}(t) \right|^2 \right\rangle \\ &= \frac{\alpha_l^2}{N^2} I_o (1 + \eta \sin \omega t) \times \exp[-2\alpha(\nu_{LO} + \nu_{Lm} \sin \omega t) C_i L] \end{aligned} \tag{4.14}$$

With the second harmonic taken as the output signal, for low gas concentration such that $\alpha(\nu)CL << 1$, the average signal intensity can be obtained from the above equation and the second-harmonic signal is expressed, using Eq.(3.9), as

$$I_{i,2\omega} = 2k\alpha_o C_i L \frac{\alpha_l^2}{N^2} I_o \tag{4.15}$$

4.4.1 Incoherent crosstalk

The incoherent crosstalk is due to the optical power leakage from other channels to the channel that is measured. The incoherent crosstalk may be expressed as

$$\begin{aligned} I_{i,inc}(t) &= \sum_{j=1, j\neq i}^{N} \left\langle \left| E_{jo}(t) \right|^2 \right\rangle \\ &\approx \alpha_e^2 \frac{\alpha_l^2}{N^2} I_o (1 + \eta \sin \omega t) \times \sum_{j=1, j\neq i}^{N} \exp[-2\alpha(\nu_{LO} + \nu_{Lm} \sin \omega t) C_j L] \end{aligned} \tag{4.16}$$

The second harmonic amplitude of the incoherent crosstalk can be obtained from Eq.(4.16) by neglecting the effect of intensity modulation and the effect of gas absorption, and can be expressed as

$$I_{i,2\omega,inc}(t) = 2k\alpha_o\left(\sum_{j=1,j\neq i}^{N} C_j\right)L\alpha_e^2\frac{\alpha_l^2}{N^2}I_o \tag{4.17}$$

By setting the signal given by Eq.(4.15) equal to that given by Eq.(4.17), we obtain the detection sensitivity in terms of minimum detectable gas concentration limited by incoherent crosstalk (signal-to-noise ratio of 1) as

$$[C_{i,\min}]_{inc} = \alpha_e^2\sum_{j=1,j\neq i}^{N} C_j \leq \alpha_e^2(N-1)C_{\max} \tag{4.18}$$

where C_{max} represents the upper limit of gas concentration. Above this limit, alarm signal will be given. For simplicity, we assume that they are the same for all the sensors. The minimum detectable gas concentration limited by incoherent crosstalk increases linearly with sensor numbers and is proportional to the extinction ratio α_e^2. Fig. 4.4 shows the sensor performance limited by the incoherent crosstalk.

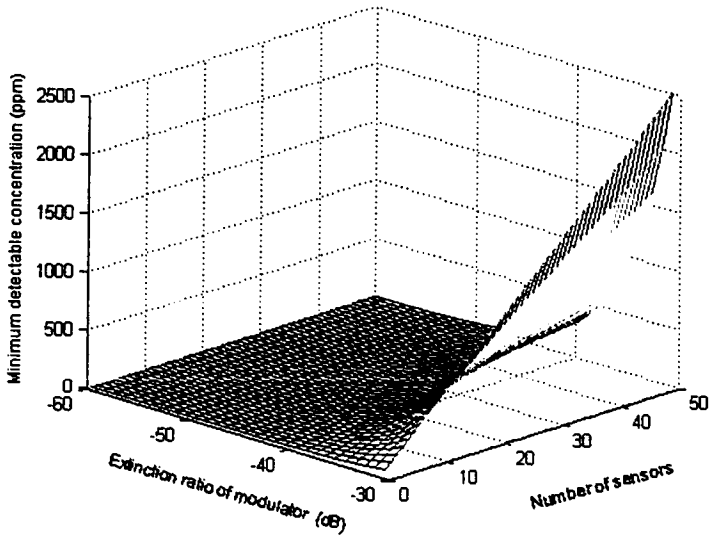

Fig. 4.4 The incoherent crosstalk level of TDM ladder sensor array.

Assuming that the maximum measurable gas concentrations for all the sensors in the array are the same and C_{max} = 5%, for a commercial available single Mach-Zhender type

intensity modulator with the extinction ratio of -30 dB ($\alpha_e^2 = 10^{-3}$), crosstalk of below 1000 ppm can be achieved with the maximum sensor number of 20. For double Mach-Zhender type intensity modulator of extinction -60 dB, the detection limit can be as small as 2 ppm.

It should be mentioned that the measurement error due to incoherent crosstalk is not random and in fact has a fixed relation (Eq.(4.17)) with the gas concentrations from other channels. It may therefore be corrected by using the measured gas concentrations.

4.4.2 First order coherent crosstalk

The first order coherent crosstalk is due to the coherent mixing between the signal wave and the leakage from other channels and may be expressed as

$$\begin{aligned} I_{i,co,1}(t) &= 2\sum \mathrm{Re}\left\langle E_{io}(t)\cdot E_{jo}^{*}(t)\right\rangle \\ &= 2\alpha_e \frac{\alpha_l^2}{N^2} I_o\left(1+\eta\sin\omega t\right)\times \sum_{j=1,j\neq i}^{N}\exp\left[-\alpha\left(\nu_{LO}+\nu_{Lm}\sin\omega t\right)\left(C_i+C_j\right)L\right] \\ &\quad \times\cos\left[2\pi\left(\nu_{LO}(i-j)\tau+\nu_{Lm}\int_{-i\tau}^{-j\tau}\sin\omega u du\right)+\phi\right] \\ &\approx 2\alpha_e \frac{\alpha_l^2}{N^2} I_o\left(1+\eta\sin\omega t\right)\times \sum_{j=1,j\neq i}^{N}\exp\left[-\alpha\left(\nu_{LO}+\nu_{Lm}\sin\omega t\right)\left(C_i+C_j\right)L\right] \\ &\quad \times\cos\left[\phi_{i,j}+\zeta_{i,j}\sin\omega t+\phi\right] \end{aligned} \tag{4.19}$$

where

$$\phi_{i,j} = 2\pi\nu_{LO}(i-j)\tau+\varphi_i(t)-\varphi_j(t), \tag{4.20}$$

$$\zeta_{i,j} = \frac{4\pi\nu_{LM}}{\omega}\sin\frac{\omega(i-j)\tau}{2} \tag{4.21}$$

The second harmonic of $I_{i,co,1}$ can be derived from Eq.(4.19) and expressed as

$$I_{i,2\omega,co,1}(t) = 2\alpha_e \frac{\alpha_i^2}{N^2} I_o \times \sum_{j=1,j\neq i}^{N} \begin{Bmatrix} 2\cos(\phi_{i,j}+\phi) J_2(\zeta_{i,j}) \sin 2\omega \\ +\eta \sin(\phi_{i,j}+\phi)\left[J_1(\zeta_{i,j}) - J_3(\zeta_{i,j})\right]\cos 2\omega t t \\ -2k\alpha_o(C_i+C_j)L\left[J_0(\zeta_{i,j}) - J_4(\zeta_{i,j})\right]\cos(\phi_{i,j}+\phi)\sin 2\omega t \end{Bmatrix} \quad (4.22)$$

where J_o, J_1, ..., J_4 are Bessel functions of the first kind. The three terms in the brackets in Eq.(4.22) may be regarded as having different origins. The first term is directly caused by the interferometric effect, the second term is proportional to the intensity modulation, and the third term is proportional to gas concentrations. All these three terms are functions of $\phi_{i,j}$, that vary randomly with environment, and therefore set a limit to the detection sensitivity of the system.

By setting the signal given by Eq.(4.15) to the noise amplitude given by first term in Eq.(4.22), we can calculate the detection sensitivity set by the first order direct interferometric effect:

$$[C_{i,\min}]_{co,1} = \frac{2\alpha_e}{k\alpha_o L} \sum_{j=1,j\neq i}^{N} J_2(\zeta_{i,j}) \cos(\phi_{i,j}+\phi) \quad (4.23)$$

As $\phi_{i,j}$ includes a random time-varying phasor $\varphi_i(t) - \varphi_j(t)$, it is logical to take the rms value of the $[C_{i,\min}]_{co,1}$, i.e.,

$$[C_{i,\min}]_{co,1,rms} = \frac{\sqrt{2}\alpha_e}{k\alpha_o L} \sqrt{\sum_{j=1,j\neq i}^{N} J_2^2(\zeta_{i,j})} \quad (4.24)$$

The detection sensitivity limited by the intensity-modulation factor can be obtained in a

similar way by the use of Eq.(4.15) and the second term in brackets in Eq.(4.22) and is expressed as

$$[C_{i,\min}]_{co,1,rms} = \frac{\alpha_e \eta}{\sqrt{2} k \alpha_o L} \sqrt{\sum_{j=1, j\neq i}^{N} [J_1(\zeta_{i,j}) - J_3(\zeta_{i,j})]^2} \tag{4.25}$$

The detection sensitivity set by the gas-concentration-related crosstalk can be obtained by use of Eq.(4.15) and the third term in brackets in Eq.(4.22) and expressed as

$$[C_{i,\min}]_{co,1,rms} \leq \sqrt{2} \alpha_e C_{\max} \sqrt{\sum_{j=1, j\neq i}^{N} [J_0(\zeta_{i,j}) - J_4(\zeta_{i,j})]^2} \tag{4.26}$$

where C_i tend to zero for the system performing low gas concentration measurement.

Now, the Eqs. (4.24), (4.25) and (4.26) can be used to evaluate the sensitivity limits as set by the first order coherent crosstalk. Fig. 4.5 shows the system sensitivity limited by the direct interferometric effect as a function of the time-delay difference between adjacent channels (calculated from Eq.(4.24)) with α_o=0.252, L=2.5cm, k=0.34, ω=400π, ν_{Lm}=14.3 GHz and α_e=0.031 which corresponds to an extinction ratio of -30dB. The upper, middle and lower curves in the figure correspond to the results for the sensor numbers, N, of 100, 20 and 3 respectively. Obviously, the performance can be greatly improved by increasing the delay between sensors. These results are expected because, the modulation index $\zeta_{i,j}$ as defined in Eq.(4.21) can be approximated as $\zeta_{i,j} \approx 2\pi\nu_{Lm}(i-j)\tau$. An increase in τ will increase the value of $\zeta_{i,j}$ and would in general result in a decrease in $J_2(\zeta_{i,j})$. When the high frequency modulation is used (e.g. 100 MHz), the above approximation may not hold and $\zeta_{i,j}$ may vary periodically with increasing time delay because of the sinusoidal function

in Eq.(4.21). From the simulation, for α_e^2 = -30dB and N =100, the minimum detectable gas concentration is around 1800 ppm with the time delay of 300ns. It can be further reduced to 60 ppm by using a double Mach-Zhender intensity modulator (α_e^2 = -60dB).

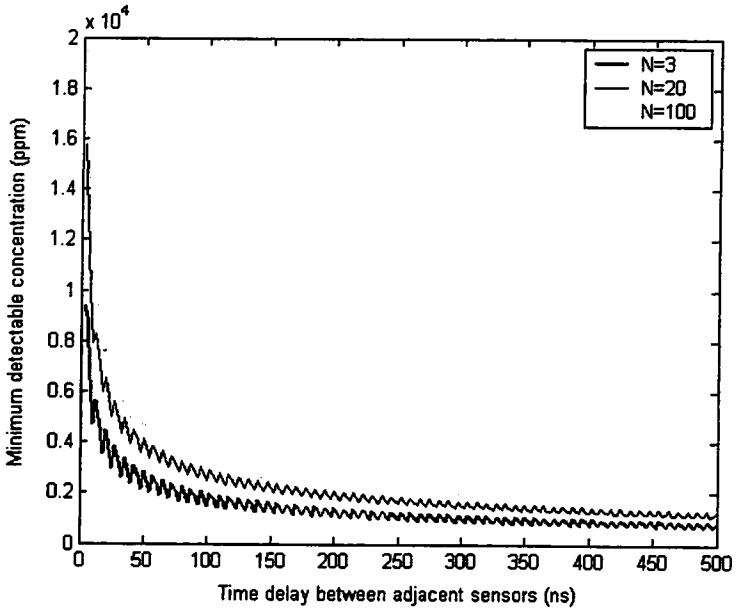

Fig. 4.5 Minimum detectable gas concentration calculated from Eq.(4.24) versus the time delay between sensor channels for N= 3, 20 and 100 respectively.

Apart from the direct interferometric effect, the system performance may be limited by the other two factors, the amplitude-modulation-effect and the gas-absorption-related effect, as stated in Eqs. (4.25) and (4.26). The simulation results are shown in Fig. 4.6 and Fig. 4.7 respectively. Similar characteristics as that for the direct interferometric effect are obtained, except the magnitude is much smaller. They also can be reduced by increasing the time delay between the sensors.

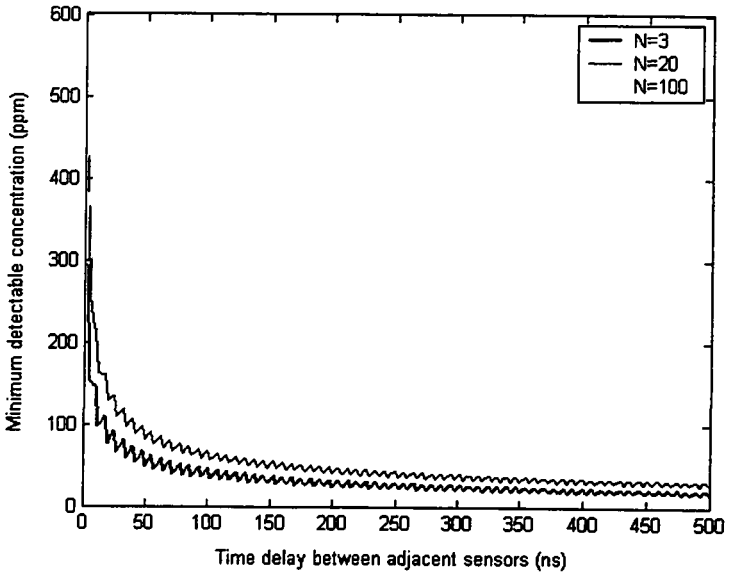

Fig. 4.6 Minimum detectable gas concentration limited by amplitude-modulation effect and calculated from Eq.(4.25) versus the time delay between sensor channels for N = 3, 20 and 100 respectively.

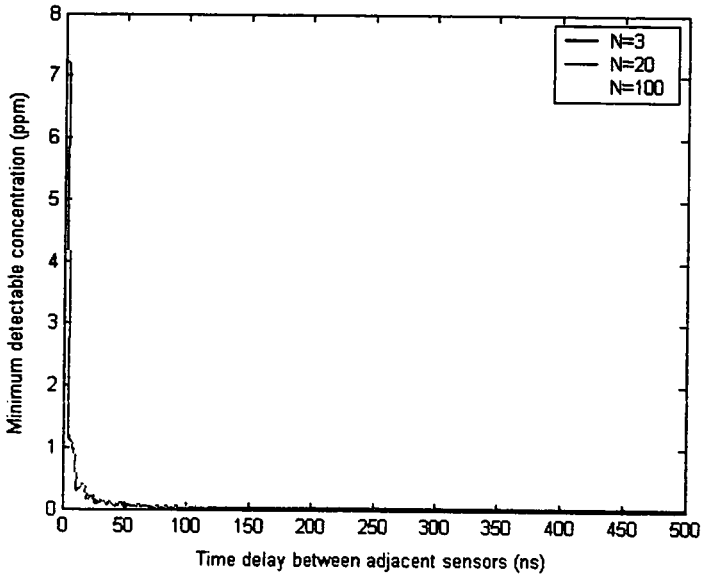

Fig. 4.7 Minimum detectable gas concentration limited by gas-absorption effect and calculated from Eq.(4.26) versus the time delay between sensor channels for N = 3, 20 and 100 respectively.

4.4.3 Second order coherent crosstalk

Second order coherent crosstalk is caused by the mixing of signals from the channels other than that we wish to measure. It can be expressed as

$$\begin{aligned} I_{i,co,2}(t) &= 2\sum \mathrm{Re}\left\langle E_{mo}(t)\cdot E_{no}^{*}(t)\right\rangle \\ &\approx 2\alpha_e^{\,2}\frac{\alpha_l^2}{N^2}I_o(1+\eta\sin\omega t)\times\sum_{m=1,m\neq i}^{N}\sum_{n>m,n\neq i}^{N}\exp[-\alpha(\nu_{LO}+\nu_{Lm}\sin\omega t)(C_m+C_n)L] \\ &\quad\times\cos\left[2\pi\left(\nu_{LO}(m-n)\tau+\nu_{Lm}\int_{-m\tau}^{-n\tau}\sin\omega u\,du\right)+\varphi_m(t)-\varphi_n(t)\right] \\ &\approx 2\alpha_e^{\,2}\frac{\alpha_l^2}{N^2}I_o\times\sum_{m=1,m\neq i}^{N}\sum_{n>m,n\neq i}^{N}\cos\left[\phi_{m,n}+\zeta_{m,n}\sin\omega t\right] \end{aligned} \tag{4.27}$$

In the above equation, we have neglected the effect of intensity modulation and the effect of gas absorption, as they are much smaller compared with the direct interferometric effect. The second harmonic of the crosstalk may be written as

$$I_{i,2\omega,co,2}=4\alpha_e^{\,2}\frac{\alpha_l^2}{N^2}I_o\times\sum_{m=1,m\neq i}^{N}\sum_{n>m,n\neq i}^{N}\cos\phi_{m,n}J_2(\zeta_{m,n})\cos 2\omega t \tag{4.28}$$

The detection sensitivity limited by the second order coherent crosstalk can be obtained by use of Eqs. (4.15) and (4.28),

$$\left[C_{i,\min}\right]_{co,2,rms}=\frac{\sqrt{2}\alpha_e^{\,2}}{\alpha_o kL}\times\sqrt{\sum_{m=1,m\neq i}^{N}\sum_{n>m,n\neq i}^{N}J_2^2(\zeta_{i,j})} \tag{4.29}$$

Comparing the second-order with the first-order coherent crosstalk, the second-order crosstalk effect is proportional to $\alpha_e^{\,2}$ instead of α_e; however, there are $(N^2-3N+2)/2$ terms for the second-order effect instead of N terms for the first-order effect. Fig. 4.8 shows the minimum detectable gas concentration limited by the second-order effect as a function of

time-delay differences between adjacent channels. The minimum detectable gas concentration for N = 100 is about 540 ppm with τ = 300ns, ν_{Lm} = 14.3 GHz, $\alpha_e^2 = 1\times10^{-3}$, k = 0.34 and L = 2.5 cm. It is about 3.4 times smaller than the first-order crosstalk.

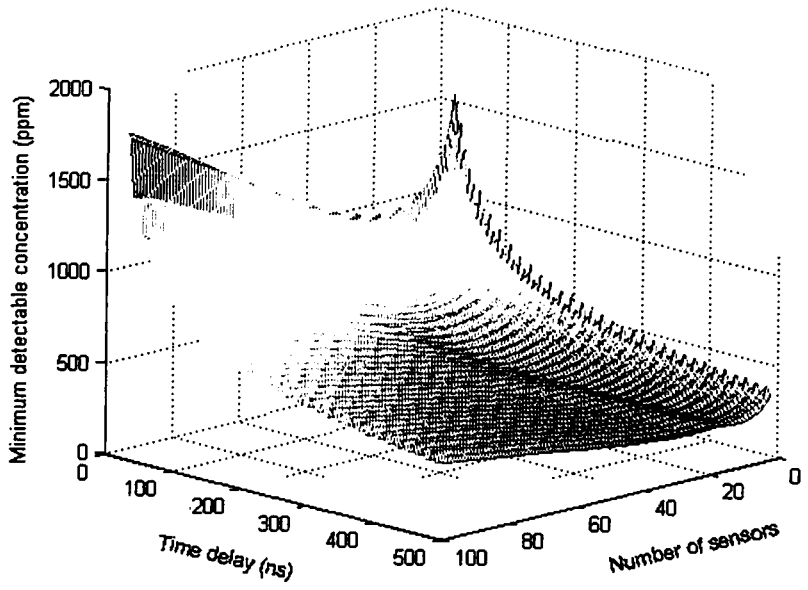

Fig. 4.8 Minimum detectable gas concentration limited by second-order coherent crosstalk as stated in Eq.(4.29)) versus time-delay difference and number of sensors.

4.5 Other Considerations on System Performance

In section 4.4, the mathematical model of signal transmission within the sensor network was developed. Predictions on the system sensitivity in terms of inter-channel crosstalk and the crosstalk-induced noises were given. The simulation results show that the system performance is severely limited by the extinction ratio of the optical intensity modulator (switch) used for pulse amplitude modulation. In practice, the system performance could be much better than the theoretical prediction using the above model. The reasons are as follows.

4.5.1 Low-pass filtering

From the equations in Section.4.4, it can be seen that the minimum detectable gas concentration is always proportional to $\cos(\phi_{i,j}+\phi)$ where $\phi_{i,j}$ consists of the phase difference between the light signals from channel *i* and channel *j* and a random phase change. After taking the *rms* value of the equations, such as Eq.(4.23), $\left|\cos(\phi_{i,j}+\phi)\right|_{rms}$ would be equal to $1/\sqrt{2}$. In practice, if the laser wavelength (frequency ν_{L0}) is scanned linearly across the gas absorption line, $\cos(\phi_{i,j}+\phi)$ would vary periodically with time. If the time delay $\tau_{i,j}$ is sufficiently large that variation of phase in the cosine term is over many times of π, $\cos(\phi_{i,j}+\phi)$ would vary much faster than the absorption signal and can therefore be removed by using a low pass filter. This indicates that sensitivity could be enhanced by combining the wavelength scanning with the use of a low pass filter. With harmonic detection, the lock-in amplifier may be regarded as a narrow band-pass filter. Hence, the sensitivity-limited factor related to the cosine term may be much smaller than $1/\sqrt{2}$. Simulations show that the value of$\cos(\phi_{i,j}+\phi)$ may be reduced 30dB for a 1Hz detection bandwidth[8], giving a minimum detectable gas concentration due to unwanted interferometric effect of 1800ppm/1000=1.8ppm/$\sqrt{}$Hz for a 100 sensor network with a pulse modulation of 30dB extinction ratio.

4.5.2 Polarization effect

In section 4.4, we have actually assumed that the polarisation states of different sensor channels are the same. In practical systems using single mode optical fibers, the polarisation states in different channels may be different and may change randomly with environmental disturbances. The effect of the different polarisation states is to reduce the magnitude of the

mixing terms as given by Eqs. (4.24) and (4.29), which in turn reduces the magnitude of the coherent crosstalk. A factor $\cos\theta_{i,j}$ $(i,j=1,2,\cdots N, i\neq j)$ may be inserted into the equations, to account for the polarisation effect. Here $\theta_{i,j}$ represents an angle between the polarisation vectors of channel i and channel j. If we assume $\theta_{i,j}$ varies randomly and independently with one another, the RMS value of the lower detection limit given by Eqs. (4.24), (4.25), (4.26) and (4.29) should be multiplied by a factor of $1/\sqrt{2}$.

4.5.3 Coherence of light source

In the mathematical derivations, we have also assumed that the source coherence length is very long, longer than the optical path difference between the first sensing channel and the last sensing channel. In practice, the source coherence is limited. However, the external cavity laser diode used in our experiment has a linewidth of 300 kHz corresponding to a coherence length of 666 m. Coherence control [9] may be implemented in order to degrade the coherence of the laser source. For the case of limited coherence length, not all the signals from other channels can induce the coherent related crosstalk. Thus, the coherent crosstalk should be reduced compared with the case of infinitely long coherence length.

4.6 Chapter Summary

The performance of a TDM addressed gas sensor array of forward ladder topology has been theoretically examined. It has been found that the system performance strongly depends on the extinction ratio of the optical intensity modulator used. From the simulation results, it can be seen that the minimum detectable gas concentration is mainly limited by the direct interferometric effect of the first order coherent crosstalk. It sets the limit of around 1800ppm with the time delay of 300ns for α_e^2= -30 dB and N = 100. The minimum detectable gas concentration of 50 ppm may be achieved by using a double Mach-Zhender

intensity modulator (α_e^2= -60 dB). By using proper filtering techniques, the unwanted interferometric signals can be further reduced to 1.8 ppm for α_e^2= -30 dB and N = 100. This value is even smaller than that of a single-sensor system in which the performance is limited by the coherent reflections occurring within the gas cells as discussed in Section 3.4.3. In fact, some practical considerations listed in Section 4.5 were not accounted for in our simulations. The predicted performance of the system would thus be the worst case and further enhancement is possible.

REFERENCES

1. G. Winzer, "Wavelength multiplexing coomponents- a review of single-mode devices and their applications," *J. Lightwave Technol.*, Vol. LT-2, pp.369-378, 1984.
2. A.D. Kersey, A.D. Dandridge, et al., "64-element time-division multiplexed interferometric sensor array with EDFA telemetry," *OFC '96 Technical Digest*, pp.270-271, 1996.
3. J.L. Brooks, B. Moslehi, B.Y. Kim and H.J. Shaw, "Time-domain addressing of remote fiber optic interferometric sensors arrays," *J. Lightwave Technol.*, Vol. LT-5, pp.1014-1023, 1987.
4. W. Jin, Y.Z. Xu, M.S. Demokan and G. Stewart, "Investigation of interferometic noise in fiber-optic gas sensors with the use of wavelength modulation spectroscopy," *Applied Optics*, Vol.36, No.28, pp.7239-7246, 1997.
5. J.C. Cartledge, "Comparsion of effective α-parameters for semiconductor Mach-Zehnder optic modulator," *J. Lightwave Technol.*, Vol. 16, pp.372-378, 1998.
6. C.K. Kirkendall, A.R. Davis, and A.Dandridge, "High extinction ratio optical switch and bias control," in *Optical Fiber Sensors*, Vol. 16, *OSA Technical Digest Series*, pp.560-563, 1997.
7. S.C. Huang, W.W. Lin and M.H. Chen, "Cross-talk analysis of time-division multiplexing of polarization-insensitive fibe-optic Michelson interferometric sensors

with a 3x3 directional coupler," Appl. Opt., Vol. 36, No. 4, pp.921-933, 1997.

8. C. C. Chan, "Interrogation of fiber Bragg grating sensors with a tunable laser," Ph.D thesis, The Hong Kong Polytechnic University, July 2000.

9. M.C. Amann and J. Buus, "Tunable Laser Diodes," Chapter 6, Artech House Publishers, 1998.

CHAPTER 5 EXPERIMENTAL IMPLEMENTATION OF TDM GAS SENSOR SYSTEM

5.1 Introduction

In Chapter 4, we reported the results of our theoretical investigation on the TDM gas detection system using a forward-coupled ladder array topology. It was found that the system performance is limited by the extinction ratio of the optical intensity modulator. The measurement error caused by the induced (or leakage) signals from other channels can be classified into two categories: incoherent crosstalk and coherent crosstalk. The measurement error due to incoherent crosstalk is the sum of the light intensity leaked from other channels where, for a particular channel, fractions of the gas concentration signals from other sensors are detected. This type of crosstalk does not vary with the environment and the portion of signal leakage between the channels is determined by the extinction ratio of the optical switch. In contrast, the coherent crosstalk would cause fluctuation of signal power which is named as "unwanted interferometric signal" in Chapter 4. The fluctuation is nearly random in nature with unpredictable environmental variations. It may contribute noise to the system. The influence of coherent crosstalk on system performance strongly depends on the signal-extraction (demodulation) method used after photodetection. These two categories of measurement errors, i.e., crosstalk and signal fluctuation are experimentally investigated with a three-sensor TDM array. The maximum number of sensors that could be multiplexed is determined by the power budget analysis and is also reported.

5.2 Experimental Setup

Fig. 5.1 shows the three-gas-sensor system using time division addressing with a forward-coupled ladder array. This system is the same as the system proposed in Chapter 4

but with $N = 3$. An external cavity tunable laser (New Focus Model 6262) was used as the source of the system. The laser wavelength was coarsely tuned to an absorption line around 1530.37 nm and modulated sinusoidally to apply the WMS technique with second harmonic detection. The *rms* value of the second harmonic (*2f*) signal current for an individual sensor is expressed as $2k\alpha_o CLI_o$ where α_o is the absorption coefficient for pure gas at the center of the absorption line, C is gas concentration, L is the length of gas cell and I_o is the average optical power corresponding to each sensor. The k value is defined as Eq.(3.10) in Chapter 3 which is a function of x where x is the modulation index and is equal to the ratio of the wavelength modulation amplitude over the linewidth of the absorption line. The $2f$ signal was found to be maximized when the wavelength modulation signal was set to an amplitude of $0.85V_{r.m.s}$ which corresponds to about 2.2 times the linewidth of the absorption line.

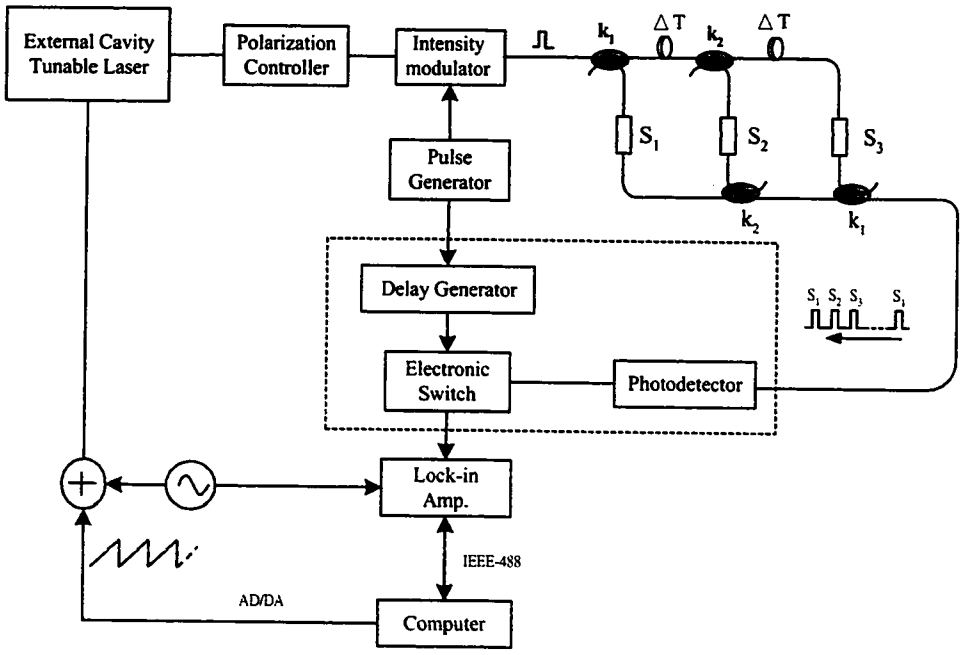

Fig. 5.1 Experimental setup of the three-sensor system using time division addressing

The light from the tunable laser source was pulsed by using a single-polarization intensity modulator. A polarization controller was used before the intensity modulator for

optimizing the launched power. The pulse width was fixed at 200 ns and the repetition rate was set as 500 kHz. The pulse width and the repetition rate can be adjusted by changing the pulse generator settings. The optical path difference between sensors is 60m long which gives a 300 ns delay. The splitting ratios, k_1 and k_2, of the couplers are chosen to be 66:33 and 50:50 respectively (according to Eq. 4.1) in order to balance the power level from the three sensors.

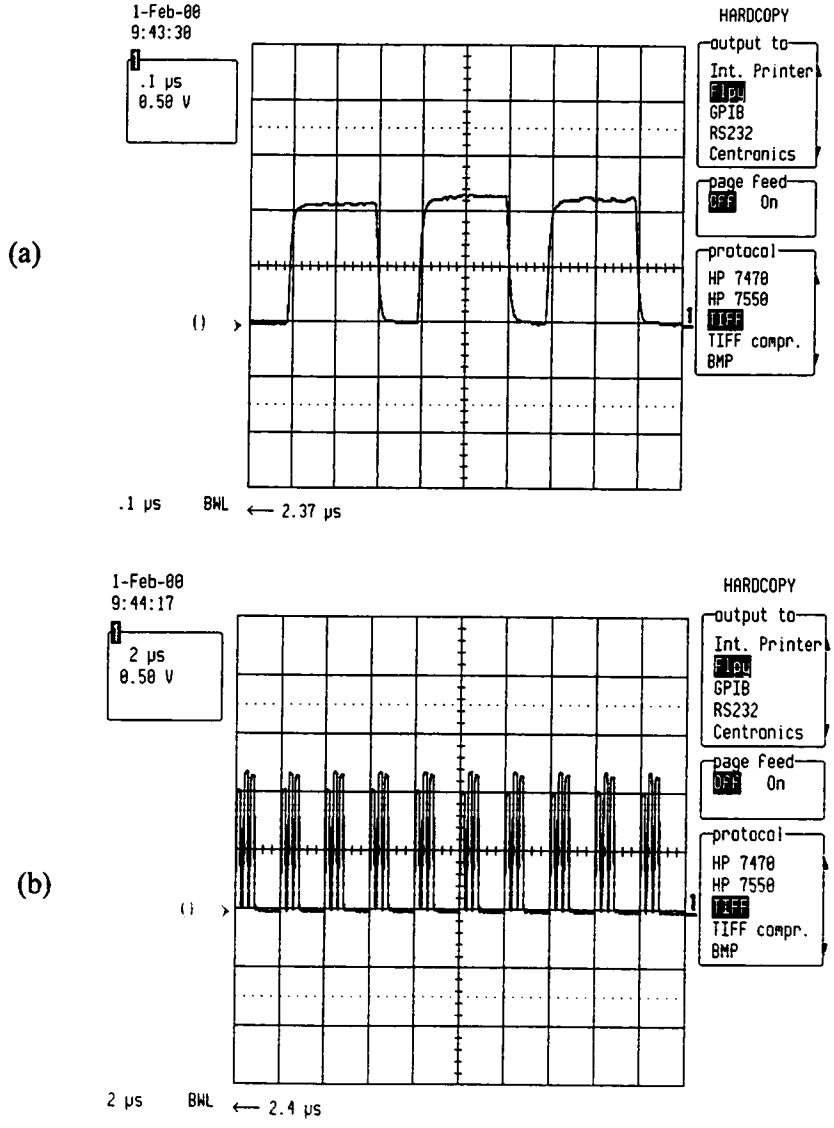

Fig. 5.2 Pulses from the three channels after photodetection. (a) within one period, (b) within ten periods

Fig. 5.2 (a) and (b) shows the pulses from the three channels after photodetection in one period and multiple periods respectively. An electronic switch is then used to separate the pulses from the three sensors after a DC-coupled photodetector. The switch is controlled by the synchronized pulses from the pulse generator with proper delay which is adjustable and depends on which channel would be measured. An AC-coupled detector used before the switch would cause large crosstalk between the sensors [1] and will be discussed in the next section. The pulse train from a selected channel at the detector output was then lock-in detected at $2f$ with a DSP lock-in amplifier (Standford Research System SR830) which was connected to a personal computer through the IEEE-488 interface [2] for data acquisition. The computer user interface for the TDM system is shown below (Fig.5.3).

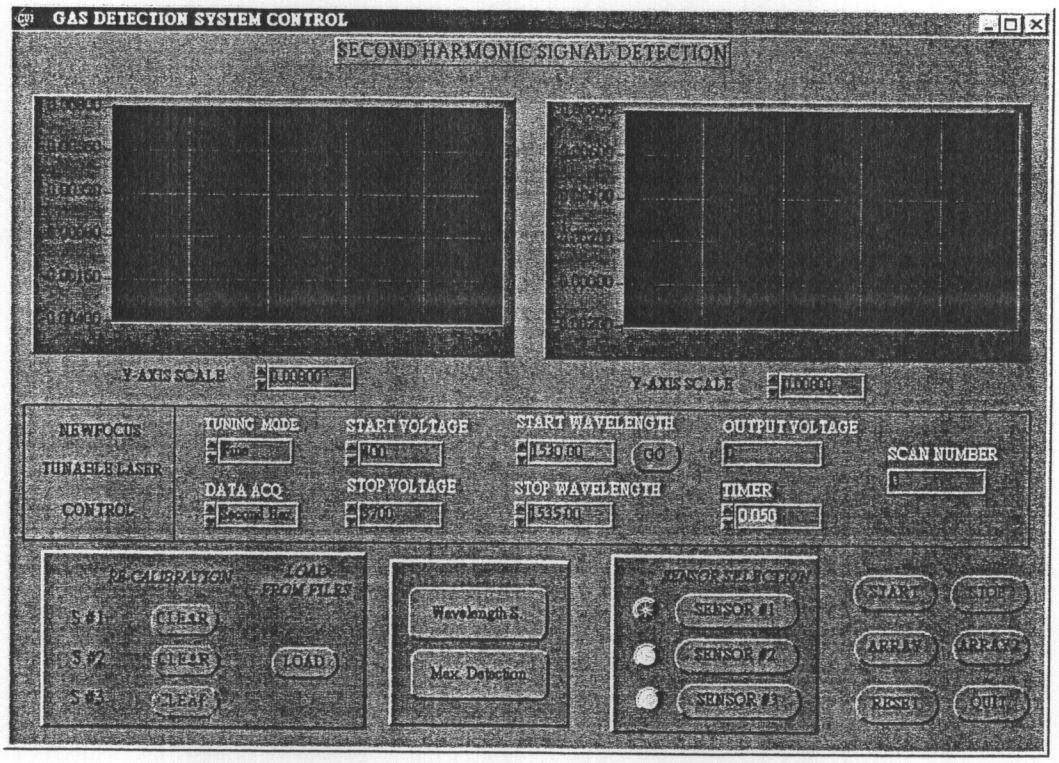

Fig. 5.3 User interface of the computer control program for the TDM gas sensor system.

The time constant and the filter slope of the lock-in amplifier were set to 300ms and 18dB/oct respectively. As for the single-sensor system, unwanted background signal

(baseline) exists in the measured spectrum due to the output power variation of the external cavity tunable laser with wavelength tuning. Again, the background signal (baseline) can be suppressed by using off-line data subtraction.

5.2.1 Problem found with the use of AC-coupled photodetector

In fact, we did our first time-division multiplexing experiment with the experimental setup shown in Fig. 5.1 but with an AC-coupled photodetector. It has been found that the configuration using an electronic switch after the AC-coupled photodetector is not suitable for our system. Fig. 5.4 shows second harmonic output of the lock-in amplifier corresponding to gas sensor 2 when the laser wavelength was tuned from 1530.15 nm to 1530.65 nm. A two-sensor system has been assumed to make the case understood.

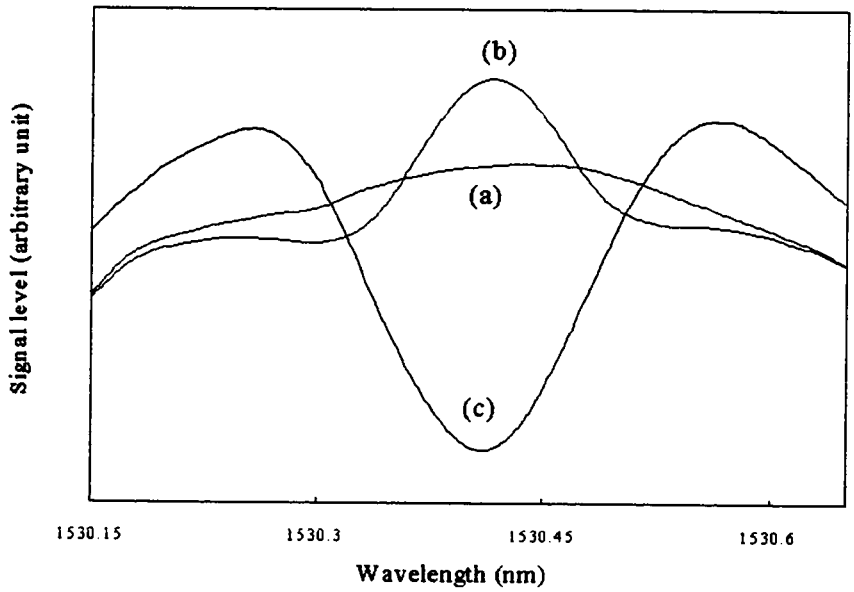

Fig.5.4 Second harmonic signals from sensor 2 obtained with the configuration of using an electronic switch after the ac-coupled photodetector.

Trace (a) shows the second harmonic background signal detected when there is no acetylene in all the two sensors. Trace (b) shows the second harmonic signal when sensor 2

was filled with 9344 ppm acetylene and no acetylene in sensor 1. Trace (c) shows the second harmonic signal when gas sensor 2 was filled with the same concentration of acetylene (9344 ppm) and sensor 1 filled with 95% (950000 ppm) acetylene. Clearly, the signal corresponding to sensor 2 is significantly affected by the crosstalk from sensor 1. This is because that the AC-coupled photodetector filters out the DC-component and the original non-negative pulse waveform as shown in Fig. 5.2 will be down shifted resulting in a 'negative' offset. The magnitude of the "negative" offset is directly proportional to the average power received by the photodetector. The change of the gas concentration in sensor 1 affects the pulse amplitude and thus the average power level at the detector and therefore affects the offset at the detector output. As the amplitude of the pulses from sensor 1 was modulated due to the wavelength modulation applied, the average power at the photodetector and therefore the "negative" bias after the AC-coupled photodetector were also modulated. The second harmonic of the offset signal is of the same characteristics as the signal from sensor 1 but 180° out of phase due to the "negative" nature of the offset. The results shown in Fig. 5.4 agrees with the previous theory that the AC-coupled photodetector is not suitable for TDM system if an electrical switch is used after photodetection [1].

With the use of AC-coupled photodetector, an alternative technique to minimize the offset-related crosstalk from other channels is to use an optical switch before the AC-coupled photodetector. This scheme is shown in Fig. 5.5. For this configuration, the sensor demultiplexing was achieved by applying the delayed pulses directly on the optical switch. The optical switch allows only the pulses from a selected sensing channel to reach the detector thus minimizing the offset-related crosstalk caused by the AC-coupled photodetector.

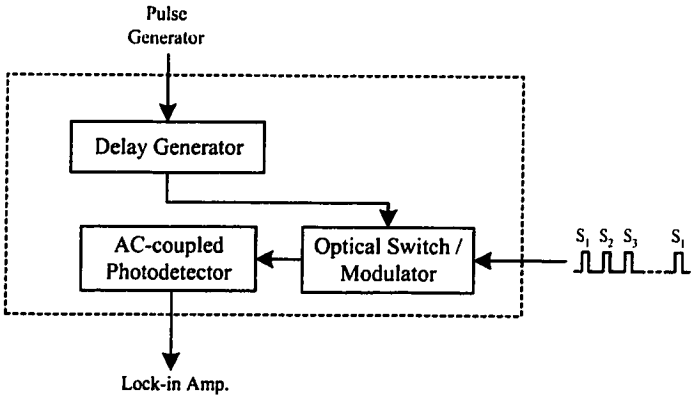

Fig. 5.5 Demultiplexing configuration with an optical switch before the AC-coupled photodetector

An experiment was conducted with this configuration and the best sensitivity obtained is similar to that obtained from using the electric switch and DC-detector configuration. The stability of the system is however poor due to random variation of the polarization state within different channels. The polarization dependence of the power transfer characteristic of the Mach-Zehnder modulators (switch) would cause varied insertion losses for the light pulses reaching the photodetector from different sensing channels. It is anticipated that this problem can be solved by the use of polarizations-preserving fiber [3,4] or polarization masking [5].

5.2.2 Drift of transfer function of the intensity modulator

The function of an electro-optical intensity modulator is to convert an electrical signal to an optical intensity variation. Lithium niobate-based [6] intensity modulators are the most common devices for this purpose. However, the working point of lithium niobate modulator can drift with time. Fig. 5.6 shows the transfer functions of the modulator which is used in our system.

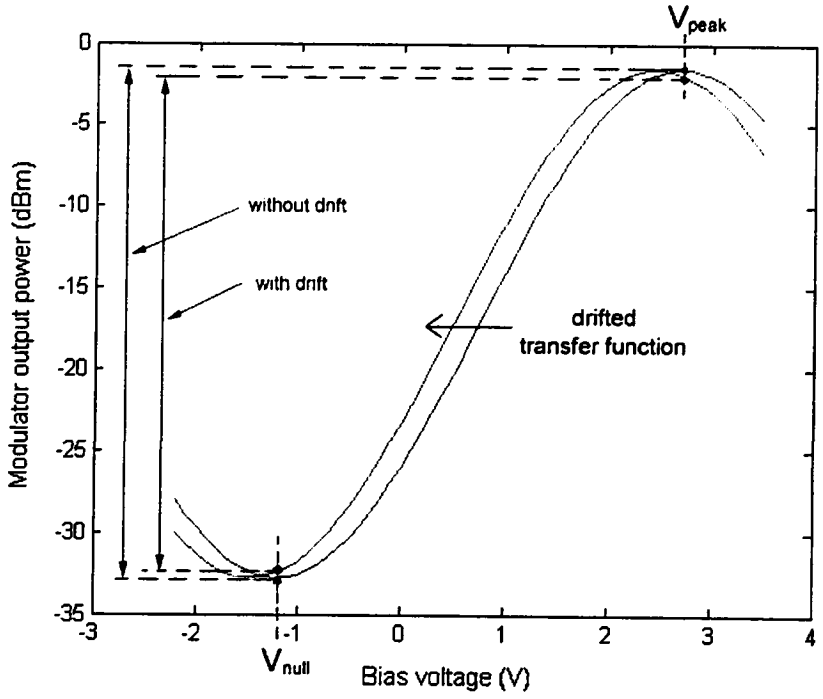

Fig. 5.6 Modulator transfer functions

The x-axis represents the bias voltage (modulation voltage), and the y-axis shows the optical output power in dBm. The transfer function is a sine function. The DC bias voltage, at which the modulator is working, determines the attenuation and the linearity of the modulator's optical output signal. The voltage difference from V_{peak} (~ 2.7 V) to V_{null} (~ -1.2 V) is called V_{π} of the modulator. This is the voltage required to switch the optical output from the maximum to the minimum intensity. When the modulator works as a switch, the modulator is operating at Peak or Null point, as a result, the modulator will switch the optical signal on or off.

As shown in Fig. 5.6, the drift of the transfer function causes the extinction-ratio degradation of the modulator when it is used as a switch. A modulator bias controller, therefore, may be needed to lock the operating point to a desired point on the transfer function if long term stabilization is required.

5.3 Performance of the Experimental TDM System

The system performance of the three-sensors system is determined by considering the sensitivity of an individual sensor and the crosstalk between the sensors. The sensitivity of the system is limited by various kinds of noise such as the power fluctuation of the tunable laser, shot noise, thermal noise and environmental noise. Unwanted interferometric signals (noise) is also cited as a key performance-limiting factor especially for a multiplexing optical network. To measure the sensitivity of the system, the $2f$ signal for a particular sensor was recorded when the laser wavelength is scanned across the gas absorption line repeatedly.

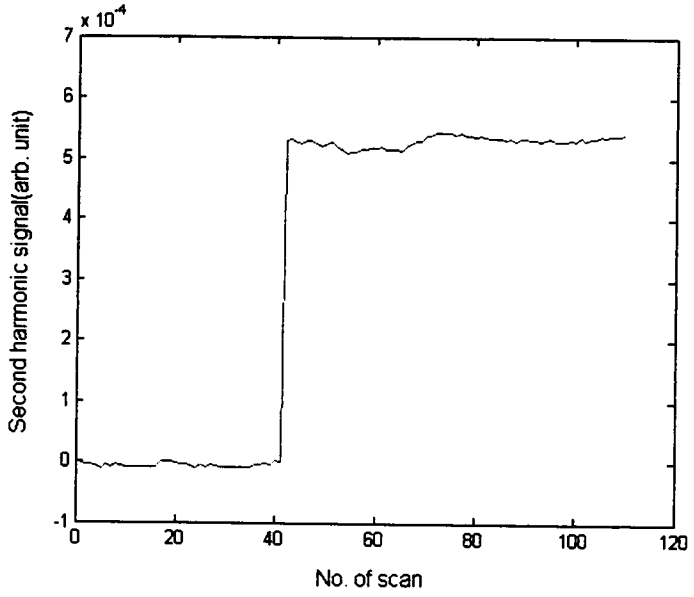

Fig. 5.7 Maximum second harmonic signal with 9344 ppm acetylene for sensor 1.

Fig.5.7 shows the maximum second harmonic signal of sensor 1 detected for each scan when the gas concentration in sensor 1 varied from 0 to 9344 ppm. The signal-to-noise ratio was calculated by using the second harmonic signal and its standard deviation corresponding to 9344 ppm acetylene and was found to be about 62. The minimum detectable concentration was calculated to be 81 ppm/$\sqrt{Hz}$ with the 25mm-long gas cell which corresponds to a

minimum detectable absorbance of $4.436\times10^{-5}/\sqrt{Hz}$. It is very close to the result obtained from the single-sensor system. Hence, we may conclude that the system sensitivity or minimum detectable concentration is not limited by the inter-channel crosstalk where the noise due to coherent crosstalk may be suppressed by combining the wavelength scanning with the lock-in detection in which the low-pass filtering technique would greatly reduce the unwanted interferometric signals.

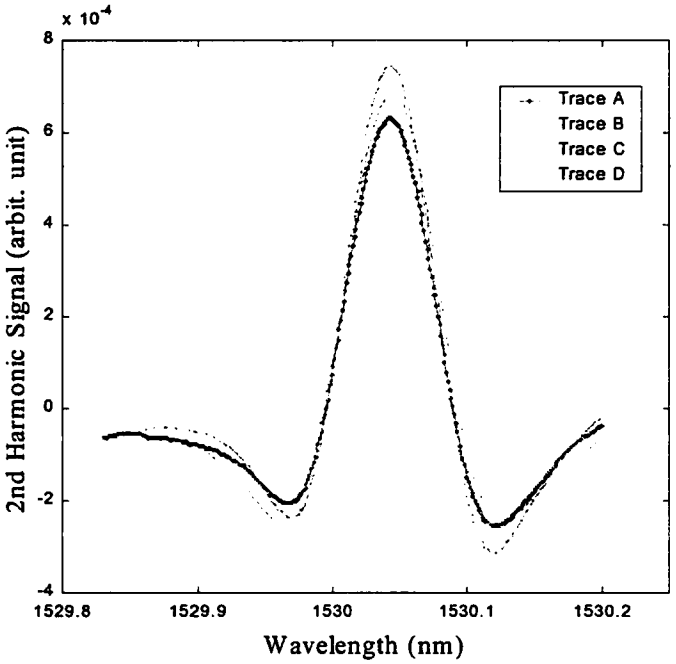

Fig. 5.8 The second harmonic signal of sensor 3 measured with the lock-in amplifier.

The crosstalk performance of the system was evaluated by filling gases of different concentrations and monitoring the output from a particular sensor. Fig. 5.8 shows the results of the 2*f*-detected signal corresponding to gas sensor 3 where the gas cell 3 is filled with 9344 ppm acetylene under 4 different conditions. Trace (a) no acetylene filled in sensor 1 and sensor 2; Trace (b) sensor 1 is filled with 95% acetylene and no acetylene is in sensor 2; Trace (c) sensor 2 is filled with 95% acetylene and no acetylene in sensor 1; Trace (d) 95% acetylene is filled in both sensor 1 and sensor 2. From the results, the gas concentration

measured with sensor 3 increased about 940 ppm due to either sensor 1 or sensor 2 being filled with 95% acetylene. Thus, the crosstalk level between the sensors is estimated to be -30dB. It is consistent with the extinction ratio (~ 32 dB) of the Mach-Zehnder switch used in our experiment and agrees with the theoretical predication as given in Eq. (4.18). The use of an intensity modulator with a higher extinction ratio such as an AOM [7,8] or a double Mach-Zehnder type modulator should reduce the crosstalk level.

5.4 Multiplexing Capacity

The motivation of sensor multiplexing is to address a large number of passive sensors from a single transceiver unit in order to reduce the cost per sensor. Higher multiplexing capacity of an optical sensing system can improve the competitiveness compared with conventional technologies. Power budget is always used for determining the maximum number of sensors which can be multiplexed. The power budget analysis for our system is presented below. The maximum input power (the peak power of the pulse, P_o) launched into the sensor array after the intensity modulator with the tunable laser is about 0 dBm. The minimum noise-equivalent power (NEP) of the photodetector used is specified as $2.5\text{pW}/\sqrt{Hz}$. As the time constant of the lock-in amplifier is set at 300 ms which is defined as $\frac{1}{2\pi f}$, the detection bandwidth, f, may be regarded as 0.53 Hz which gives a minimum detectable power of -87.4 dBm. Assuming that the repetition rate of the pulses is adjusted to maximize the average power level at the photodetector ($N\tau=T_p$) and a dynamic range of 20 dB is reserved to account for the absorption process, the maximum power loss allowed for the sensor array should then be -67.4 dB. The peak power of each received pulse after passing through the sensor array is equal to P_o / N^2 where N is the total number of sensors, in which only power splitting reduction due to the coupling ratio of the couplers is accounted. Hence, the loss may be regarded as 10 log (N^2) dB. In practice, additional loss should be

included to account for the coupler and splice excess losses and the insertion loss of the gas cell. In our system, the gas cell insertion loss is 1 dB and an additional 0.3 dB loss per sensing channel due to the excess losses of the couplers and splices. Hence, at the worst case, the total loss of the pulse power can be expressed as [-10 log (N^2) - (0. 3×N) -1] dB. Fig. 5.9 shows the relationship between the minimum power requirement and the theoretical peak power of the pulses after passing through the sensor array as a function of sensor number, N. According to the analysis, using a light source of 1mW, a maximum number of 90 sensors could be multiplexed with time division addressing and the forward-coupled ladder array topology.

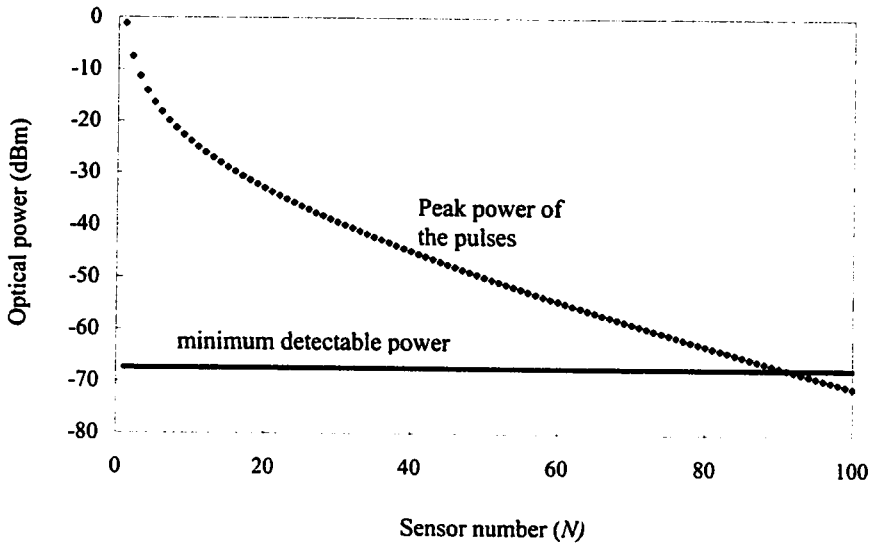

Fig. 5.9 The relationship between the minimum power requirement of the photodetector and the theoretical peak power of the pulses as a function of sensor number, N.

5.5 Chapter Summary

We have reported the experimental performance of the time-division multiplexed three-sensor system with a forward-coupled ladder topology where quantitative measurement of gas concentration based on wavelength modulation spectroscopy (WMS) is demonstrated

by applying low-frequency wavelength modulation to the external-cavity tunable diode laser. The tunable laser operating at 1530nm region is used to detect acetylene (C_2H_2). The system uses single pass absorption cells of 2.5cm long and have demonstrated sensitivity of 81 ppm/$\sqrt{Hz}$ corresponding to the minimum detectable absorbance of $4.44\times10^{-5}/\sqrt{Hz}$. The crosstalk between the sensors was found to be -30 dB by use of a single Mach-Zehnder intensity modulator. Power budget analysis shows that a sensor network consisting of 90 sensors could be realized with the same multiplexing topology. It can be used to realize low-cost, multi-point gas detection.

REFERENCES

1. J. L. Brooks, B. Moslehi, B. Y. Kim and H. J. Shaw, "Time-domain addressing of remote fiber-optic interferometric sensor arrays," *Journal of Lightwave Technology*, Vol. LT-5, No. 7, pp.1014-1023, 1987.
2. M. Colloms, *Computer controlled testing and instrumentation : an introduction to the IEC-625: IEEE-488 bus*, New York: Wiley, 1983.
3. Y. Katsuyama, H. Matsumura and T. Suganuma, "Low-loss single polarization fibers," *Electronics Letters*, Vol. 17, pp.473-474, 1981.
4. J. Noda, K. Okamoto and Y. Sasaki, "Polarization-maintaining fibers and their applications," *J. Lightwave Technol.*, Vol. LT.4, pp.1071-1089, 1986.
5. N.J. Frigo, A. Dandridge and A.B. Tveton, "Technique for elimination of polarization fading in fiber interferometers," *Electronics Letters*, Vol. 20, No. 8, pp.319-320, 1984.
6. P.G. Suchoski, et. al., "Commercialization of Lithium Niobate Modulators," *Integrated Optical Circuits and Components: Design and Applications*, edit. By B. J. Thompson, New York: Marcel Dekker, 1999.
7. T.V. Higgins, "There is a lot more to an A-O modulator than meets the eye," *Laser Focus World*, pp.133, July 1991.
8. A. Korpel, *Acousto-Optics*. 2nd ed., New York: Marcel Dekker, Inc., 1997.

CHAPTER 6 FMCW MULTIPLEXING OF GAS SENSORS

6.1 Introduction

This chapter studies the use of Frequency Modulated Continuous Wave (FMCW) technique for multiplexing fiber-optic gas sensors. FMCW technique has a very long history, but in the past its use has been limited to certain specialized applications, such as radio altimeters [1] and radar ranging [2-4]. With the development of the optical waveguide, this technique has been employed in fiber-optic systems for different applications. The FMCW systems are mainly characterized by their way of signal detection, i.e. coherent or incoherent. The basis of coherent FMCW systems is the interferometric mixing of two optical signals originating from the same source for which modulation of light frequency is performed. This scheme is commonly used in optical reflectometry [5,6] and interferometric sensor addressing [7]. In our system, the incoherent detection scheme is chosen since it performs with better immunity to external disturbances especially for the case of remote sensing where long optical paths may be involved. In this scheme, the light intensity is modulated in radio frequency and the two signals from the same source, one of them delayed, are electrically mixed. The operation principle of incoherent FMCW for sensor multiplexing and the mathematical formulation of the beat note will be presented in Section 6.2. Gas sensors multiplexed with FMCW technique and using wavelength modulation spectroscopy (WMS) will be introduced in Section 6.3. Although, FMCW technique gives the advantage of better power utilization, poor channel isolation may cause large unwanted interferometric signals (noise) and hence reduce the system sensitivity. The modulation characteristics of the unwanted interferometric signals are critically important and they are investigated in Section 6.4. Methods for minimizing the effect of the unwanted interferometric signals are presented in Section 6.5. The effect of non-zero sidelines of the FMCW technique on the system

performance is investigated in Section 6.6. Finally, a chapter summary will be given in Section 6.7.

6.2 FMCW Principle

The principle of FMCW technique is well known [2]. The frequency modulation for FMCW can take many forms. Linear and sinusoidal modulations have both been used in the past. For sensor multiplexing, FMCW using triangular (linear) frequency sweeping modulation is chosen because of its better side-line suppression as compared with sinusoidal or sawtooth modulations where finite flyback time and ramp overshoot may occur. Fig. 6.1(a) shows the basic operation of FMCW technique where two signals originating from the same linearly chirped source are electrically mixed or made to 'beat' together by the use of an electrical mixer. The solid line represents the instantaneous reference frequency, varying with time in a triangular function. The broken line represents the same waveform which have been subjected to a delay τ caused by propagation along an optical fiber. The instantaneous difference, or beat frequency, f_b, is shown in Fig.6.1(b).

It is clear from the illustrations that the value of the beat frequency f_b depends on the delay τ for a given frequency deviation, Δf, and a modulation period T_s, as follows

$$f_b = 2 \cdot \tau \cdot \frac{\Delta f}{T_s} \tag{6.1}$$

Hence, if the sensors in a network are assigned with different delays, they can be distinguished in the frequency domain. The information corresponding to each sensor is placed on the signal carrier (output of the mixer at corresponding beat frequency).

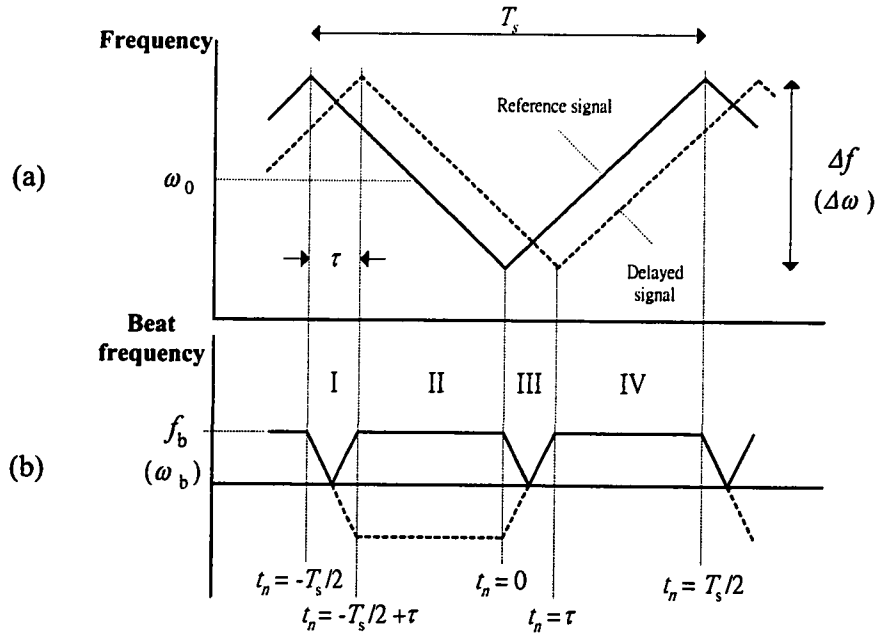

Fig 6.1 Basic principle of FMCW technique

6.2.1 Mathematical formulation of the beat note

In general, to study the characteristic of the output signal from the mixer, signal inputs represented in terms of amplitude and phase will be used in the following derivation. The instantaneous angular frequency (as shown in Fig. 6.1), ω_i, is given by the following set of expressions:

$$\omega_i = \begin{cases} \omega_0 - \dfrac{\Delta\omega}{2} - 2t_n \dfrac{\Delta\omega}{T_s}, & \dfrac{-T_s}{2} \le t_n \le 0 \\ \omega_0 - \dfrac{\Delta\omega}{2} + 2t_n \dfrac{\Delta\omega}{T_s}, & 0 < t_n \le \dfrac{T_s}{2} \end{cases} \tag{6.2}$$

where $t_n = t - nT_s$ and $n = 1, 2, 3, \ldots$; $\Delta\omega$ (= $2\pi\cdot\Delta f$) is angular frequency excursion. The phase of the chirped signal is expressed as

$$\varphi(t) = \int_0^t \omega_i(t)\, dt \tag{6.3}$$

If two signals $V_r \sin\varphi_r$ and $V_s \sin\varphi_s$ are considered, where 'r' refers to reference wave and 's' refers to signal wave with propagation delay, the resulting signal due to the mixing of V_s and V_r will contain a d.c. term, and a product term $G \cdot V_r \sin\varphi_r \cdot V_s \sin\varphi_s$, where G is the conversion factor of the mixer. The d.c. term is not related to the time delays between the signals and will therefore not be considered here. The product term may be rewritten as

$$\frac{1}{2} G V_r V_s [\cos(\varphi_r - \varphi_s) - \cos(\varphi_r + \varphi_s)] \tag{6.4}$$

The phase-sum term is an oscillation in high frequency and can be removed by using a low pass filter. We are interested here in the phase-difference term, $\cos(\varphi_r - \varphi_s)$ from which the beat note arises. It will be seen that the phase-difference term can be divided into four parts corresponding to four different regions (I – IV) as shown in Fig.6.1 and may be obtained by using Eq. (6.2) and Eq. (6.3). In practice, under the condition of $\tau << T_s$, the contribution of the beat signal by the first and third region (I and III) to the overall frequency spectrum may be neglected. Ref. [8] shows that the error caused by neglecting these regions is less than -60 dB.

During time $-\frac{T_s}{2} + \tau \le t_n \le 0$ (region II),

$$\varphi_r = n\omega_0 T_s + (\omega_0 - \frac{\Delta\omega}{2}) t_n - \frac{\Delta\omega}{T_s} t_n^2;$$

$$\varphi_s = n\omega_0 T_s + (\omega_0 - \frac{\Delta\omega}{2})(t_n - \tau) - \frac{\Delta\omega}{T_s}(t_n - \tau)^2;$$

Thus, $\varphi_r - \varphi_s = (\omega_0 - \frac{\Delta\omega}{2})\tau + \frac{\Delta\omega}{T_s}\tau^2 - 2\frac{\Delta\omega}{T_s}\tau \cdot t_n$ (6.5)

During time $\tau \le t_n \le \frac{T_s}{2}$ (region IV),

$$\varphi_r = n\omega_0 T_s + (\omega_0 - \frac{\Delta\omega}{2})t_n + \frac{\Delta\omega}{T_s}t_n^2;$$

$$\varphi_s = n\omega_0 T_s + (\omega_0 - \frac{\Delta\omega}{2})(t_n - \tau) + \frac{\Delta\omega}{T_s}(t_n - \tau)^2;$$

Thus, $\varphi_r - \varphi_s = (\omega_0 - \frac{\Delta\omega}{2})\tau - \frac{\Delta\omega}{T_s}\tau^2 + 2\frac{\Delta\omega}{T_s}\tau \cdot t_n$ (6.6)

The oscillation $\frac{1}{2}GV_rV_s\cos(\varphi_r - \varphi_s)$ is the beat note between the reference signal and the sensing (delayed) signal. This oscillation is not a pure sinusoid and can be seperated into separate harmonic components by the use of the Fourier transform. If ω is the general variable in the transform, it is defined as

$$\begin{aligned} F(\omega) &= \int_{-\infty}^{+\infty}\frac{1}{2}GV_rV_s\cos(\varphi_r - \varphi_s)\exp(-j\omega t)dt \\ &= \frac{1}{2}GV_rV_s\sum_{-\infty}^{+\infty}\int_{(n-\frac{1}{2})T_s}^{(n+\frac{1}{2})T_s}\cos(\varphi_r - \varphi_s)\exp(-j\omega t)dt \end{aligned} \quad (6.7)$$

With the use of $t_n = t - nT_s$ and the neglecting of regions I and III,

$$\begin{aligned} F(\omega) &= \frac{1}{2}GV_rV_s\sum_{-\infty}^{+\infty}\exp(-jn\omega T_s)\int_{-\frac{T_s}{2}}^{\frac{T_s}{2}}\cos(\varphi_r - \varphi_s)\exp(-j\omega t_n)dt_n \\ &= \frac{1}{2}GV_rV_s\sum_{-\infty}^{+\infty}\exp(-jn\omega T_s)\cdot\left[\int_{-\frac{T_s}{2}+\tau}^{0}\cos(\varphi_r - \varphi_s)\exp(-j\omega t_n)dt_n\right. \\ &\qquad \left. + \int_{0}^{\frac{T_s}{2}}\cos(\varphi_r - \varphi_s)\exp(-j\omega t_n)dt_n\right] \end{aligned} \quad (6.8)$$

The integral can be simplified as

$$F(\omega) = \frac{1}{2}GV_rV_s\sum_{-\infty}^{+\infty}\exp(-jn\omega T_s)\times[F_1(\omega) + F_2(\omega) + F_3(\omega) + F_4(\omega)] \quad (6.9)$$

where

$$F_1(\omega) = \frac{\sin\left[\frac{1}{2}\left(\omega + \frac{2\Delta\omega}{T_s}\tau\right)\left(\frac{T_s}{2} - \tau\right)\right]}{\omega + \frac{2\Delta\omega}{T_s}\tau} \exp j\left[\omega_0\tau + \frac{\omega}{2}\left(\frac{T_s}{2} - \tau\right)\right] \tag{6.10}$$

$$F_2(\omega) = \frac{\sin\left[\frac{1}{2}\left(\omega - \frac{2\Delta\omega}{T_s}\tau\right)\left(\frac{T_s}{2} - \tau\right)\right]}{\omega - \frac{2\Delta\omega}{T_s}\tau} \exp -j\left[\omega_0\tau - \frac{\omega}{2}\left(\frac{T_s}{2} - \tau\right)\right] \tag{6.11}$$

$$F_3(\omega) = \frac{\sin\left[\frac{1}{2}\left(\omega - \frac{2\Delta\omega}{T_s}\tau\right)\left(\frac{T_s}{2} - \tau\right)\right]}{\omega - \frac{2\Delta\omega}{T_s}\tau} \exp j\left[\omega_0\tau - \frac{\omega}{2}\left(\frac{T_s}{2} + \tau\right)\right] \tag{6.12}$$

$$F_4(\omega) = \frac{\sin\left[\frac{1}{2}\left(\omega + \frac{2\Delta\omega}{T_s}\tau\right)\left(\frac{T_s}{2} - \tau\right)\right]}{\omega + \frac{2\Delta\omega}{T_s}\tau} \exp -j\left[\omega_0\tau + \frac{\omega}{2}\left(\frac{T_s}{2} + \tau\right)\right] \tag{6.13}$$

The remaining factor in $F(\omega)$ is a delta function,

$$\sum_{-\infty}^{+\infty} \exp(-jn\omega T_s) = \omega_s \delta(\omega - k\omega_0) \tag{6.14}$$

where k is an integer and $\omega_s = 2\pi / T_s$. Thus the full expression of the Fourier transform of the beat note becomes,

$$F(\omega) = \frac{1}{2} G V_r V_s \omega_s \sum_{k}^{+\infty} \delta(\omega - k\omega_s) \times [F_1(\omega) + F_2(\omega) + F_3(\omega) + F_4(\omega)] \tag{6.15}$$

From an inspection of Eq. (6.10) to Eq. (6.13), it can be seen that $F(\omega) = F^*(-\omega)$ where $F^*(\omega)$ is the complex conjugate of $F(\omega)$. To obtain the phases and amplitudes of the real components, one must combine the positive- and negative-frequency terms in pairs (i.e. F_1 and F_4, F_2 and F_3) so that the real parts reinforce and the imaginary parts cancel. $F(\omega)$ can be rewritten as

$$F(\omega) = 2GV_r V_s \omega_s \sum_k^{+\infty} \delta(\omega - k\omega_s) \times \frac{1}{2}(\frac{T_s}{2} - \tau) \frac{\sin[\frac{1}{2}(k\omega_s - \frac{2\Delta\omega}{T_s}\tau)(\frac{T_s}{2} - \tau)]}{\frac{1}{2}(k\omega_s - \frac{2\Delta\omega}{T_s}\tau)(\frac{T_s}{2} - \tau)} \times \cos(\omega_0 \tau - \frac{k\pi}{2}) \quad (6.16)$$

The equation shows that the general form of the spectrum is a set of lines spaced with an interval ω_s, because $F(\omega)$ only takes non-zero values when $\omega = k\omega_s$. The amplitude of these lines has a $\frac{\sin x}{x}$ (where $x = \frac{1}{2}(k\omega_s - \frac{2\Delta\omega}{T_s}\tau)(\frac{T_s}{2} - \tau)$) envelope. Under the conditions that the time delay difference (τ) between the sensor and the reference channels and the parameters of triangular chirped carrier, i.e., the angular frequency excursion $\Delta\omega$ and the average angular frequency of ω_0, are adjusted to satisfy

$$\Delta\omega\tau = k\pi \quad (6.17)$$

$$\omega_0\tau = \frac{k\pi}{2} + l\pi \quad (6.18)$$

where k and l are integers, one of the harmonics of ω_s, the $k\omega_s$ component will be maximized ($\frac{\sin x}{x}$=1) and other harmonics components would be near the minima of $\frac{\sin x}{x}$ function. This means that the spectrum of the beat note may be regarded approximately a single line at $\omega = k\omega_s$ if the aforementioned conditions are satisfied.

6.2.2 Simulated beat note spectrum

According to the analysis in Section 6.2.1, the spectrum of the beat note consists of a group of discrete lines at ω_s interval. Under the conditions as stated in Eq. (6.17) and Eq. (6.18), the beat frequency coincides with one of the harmonics of ω_s, the suppression ratio between the $k\omega_s$ (or $k f_s$) component and the other harmonic components would be

maximized. The predicted output spectrum from the mixer can be determined with the substitution of the system parameters, such as f_s, k, τ, ω_0 and $\Delta\omega$ into Eq. (6.16). Fig. 6.2 shows the simulation results for the beat note spectrum for f_s = 10 kHz, $\omega_0 \approx 2\pi\cdot(60\text{ MHz})$ and $\Delta\omega \approx 2\pi\cdot(6.3\text{ MHz})$. These are the values used in our experiment which will be reported in the next chapter.

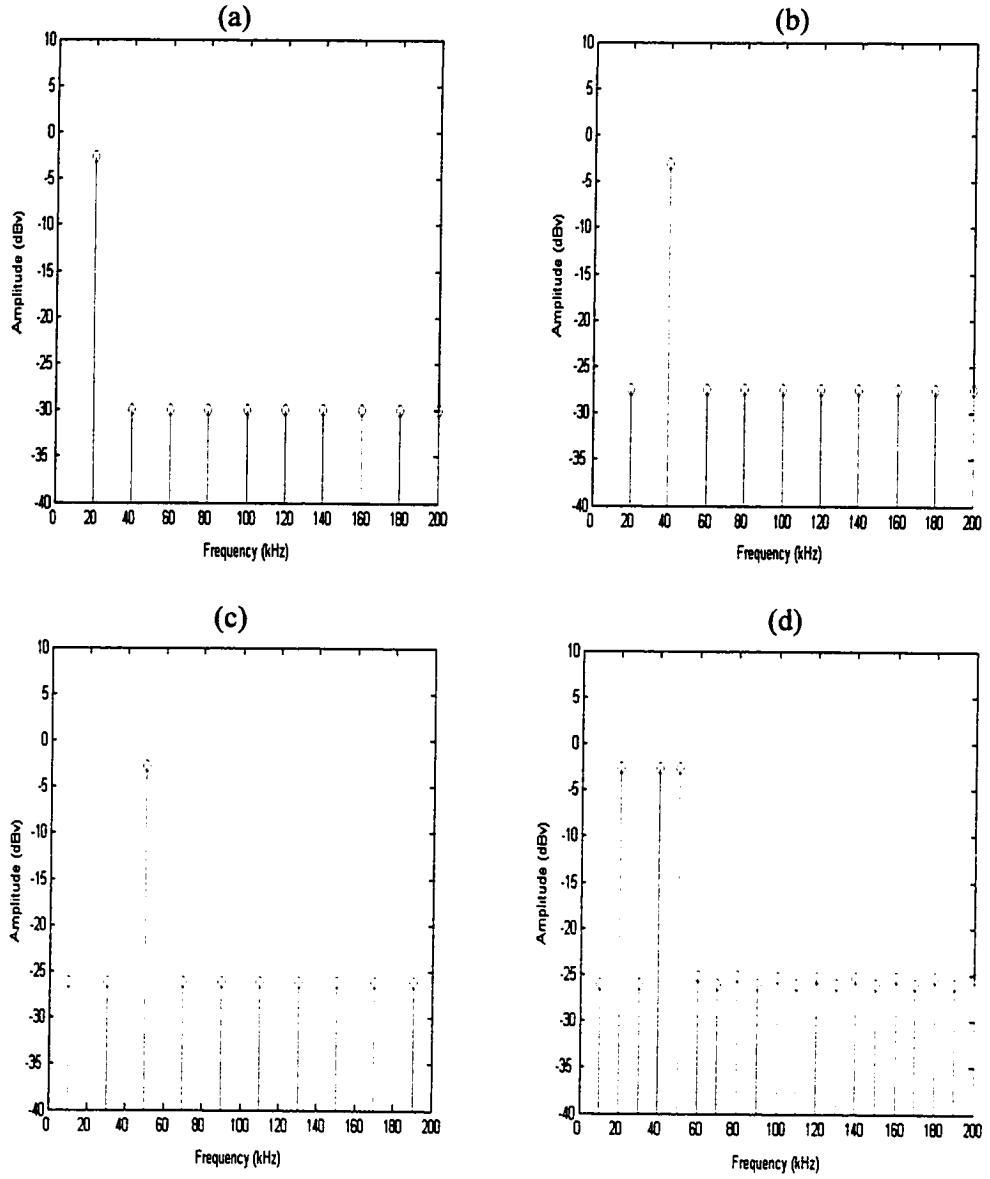

Fig. 6.2 Line spectra for the beat note of (a) k=2, (b) k=4, (c) k=6, (d) combined spectrum.

In Fig. 6.2(a) to 6.2(c), the delay differences, τ_1, τ_2, τ_3, were chosen to be around 158.7 ns, 317.5 ns and 396.8 ns respectively. They correspond to the beat frequency at 20 kHz (k = 2), 40 kHz (k = 4) and 50 kHz (k = 5). In addition, Fig. 6.2(d) shows the combined spectrum with a superposition of the individual sensor signals in the frequency domain. Fig. 6.3 shows the sideline suppression ratio as a function of τ (with Eqs.(6.17) and (6.18) still valid). The magnitudes of the sidelines increases with the value of k. This means that the crosstalk due the non-zero sidelines would increase as the time delay increases. Hence, a larger frequency deviation (Δf) operating with a smaller time delay is preferred for which the sideline suppression ratio can be enhanced.

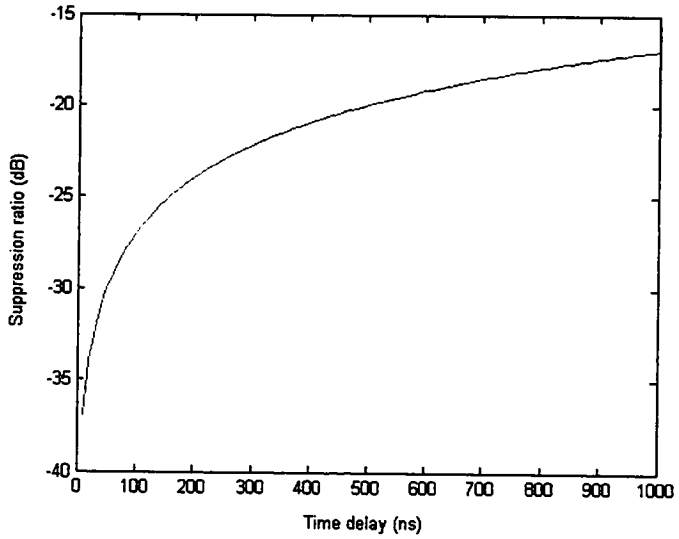

Fig. 6.3 Sideline suppression ratio with varying time delay.

6.3 FMCW Multiplexed Gas Sensor System

Fig. 6.4 shows the FMCW multiplexed gas sensor array. The system consists of N-transmission type gas cells connected in a forward-coupled ladder topology. Light from the tunable laser source is modulated in intensity, through the use of an external intensity modulator, with a triangular chirped frequency carrier generated from a voltage-controlled

oscillator (VCO) and coupled into the gas sensor array. When light passes through the gas cells, gas concentration information is encoded on to the light intensity. The return light signals from different sensors are coupled into a common output fiber and then converted to electric signals by a high-speed photodetector and mixed with a reference signal from the VCO subsequently. The output from the mixer will consists of N-beat notes (corresponding to N sensors) with their respective beat frequencies determined by the time delay differences between the sensor and the reference signals.

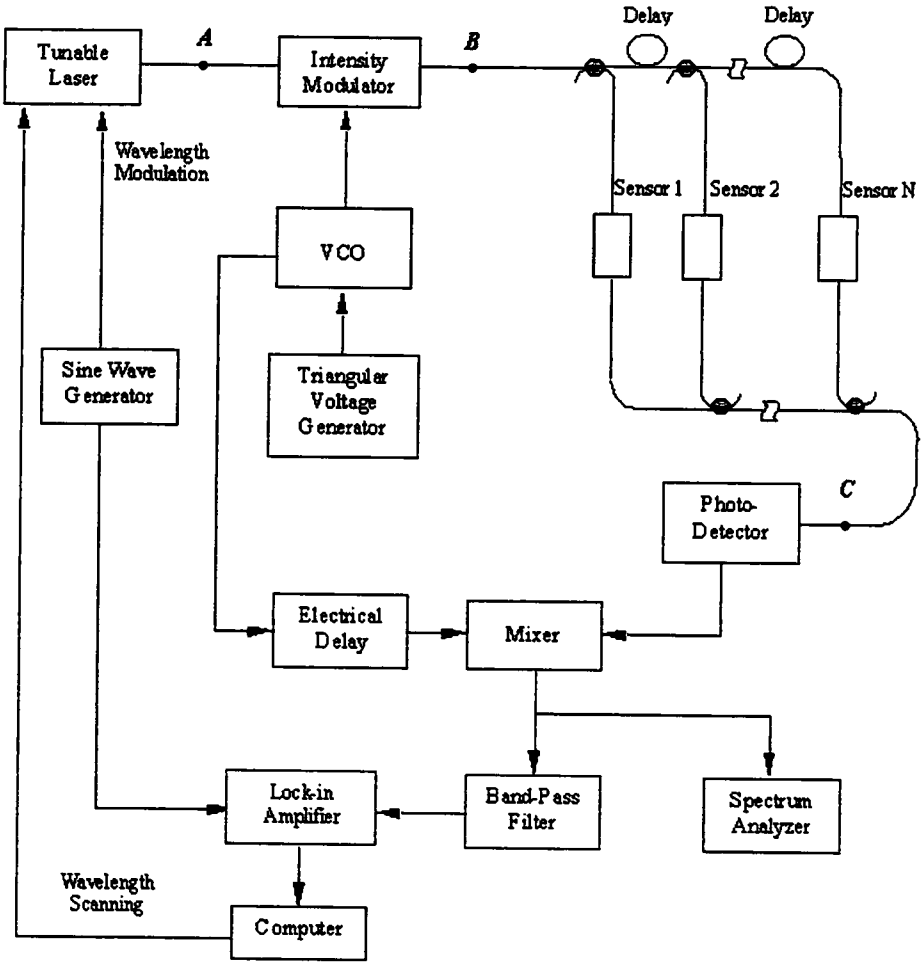

Fig. 6.4 FMCW multiplexed ladder gas-sensor array.

Assume that the light intensity from the laser at point A as indicated in Fig.6.4 is I_A.

The electric field of the optical signal at point B may be expressed as

$$E_B(t) = [I_A(1 + m\cos\varphi(t))]^{1/2} \exp[j2\pi \int_0^t \nu(t)dt] \tag{6.19}$$

where m is the intensity modulation index and $\varphi(t)$ is the phase angle of the intensity modulation applied through the external intensity modulator which is defined in Eq. (6.2) and Eq. (6.3).

After passing through the N-sensor network, the electric field of the optical signal at the point C in Fig. 6.4 may be written as:

$$E_c = \sum_{i=1}^{N} E_{ci} \tag{6.20}$$

where E_{ci} (i=1,2,...N) represents the electric field at point C after passing through the i^{th} sensor channel and may be expressed as

$$\begin{aligned} E_{ci}(t) = [k' I_A]^{1/2}[1 + m\cos\varphi(t_i)]^{1/2} \exp[-\alpha(\nu(t_i))C_i L] \\ \exp[j2\pi \int_0^{t_i} \nu\ (t_i)dt + \phi(\nu(t_i))] \end{aligned} \tag{6.21}$$

In Eq. (6.21), I_A is the light intensity from the laser at point A, $\alpha(\nu)$ is the amplitude absorption coefficient of the gas, ν represents the laser frequency and is related to wavelength by $\nu = c/\lambda$, C_i is the gas concentration at the i-th sensor, and L is the length of the gas cells. For simplicity, we have assumed that all the gas cells are of the same length. k' is a loss factor that depends on the coupling ratio of the couplers used in the network. For simplicity, we have assumed that that loss is the same for all the channels. $\phi(\nu(t_i))$ is the phase modulation resulting from gas absorption. It may be neglected for small gas concentration and/or short length gas cell.

The total light intensity at point C may be written as:

$$I_c = < E_c \cdot E_c^* > = \sum_{i=1}^{N} | E_{ci} |^2 + 2 \sum_{j=1, j>i}^{N} \mathrm{Re} < E_i E_j^* > \tag{6.22}$$

where the first term on the right hand side is the summation of the light intensities from all the sensors. The second term is the summation of the coherent mixing terms between signals from different channels. Assume first that the signals from different channels are incoherent. The second term would then vanish (in practice, this term may be significant and this will be discussed in section 6.4). The output light intensity I_c(t) at point C may be obtained by substituting (6.21) into the first term in (6.22):

$$I_c = \sum_{i=1}^{N} | E_{ci} |^2 = k' I_A \sum_{i=1}^{N} \exp[-2\alpha(\nu) C_i L][1 + m \cos\varphi(t_i)] \tag{6.23}$$

The electric signal V_s from the photodetector will then be equal to KI_c, with K representing a conversion coefficient of the photodetector.

The reference signal directly from the VCO may be written as

$$V_r = V_0 \cos(\varphi(t_r)) \tag{6.24}$$

where $\varphi(t_r)$ is the phase angle of the reference signal. Again, with the mixing of V_s and V_r at the mixer produces both phase-sum and phase-difference terms. We are interested here in the phase-difference terms that may be written as

$$V(t) = \frac{1}{2} K k' m G V_0 \sum_{i=1}^{N} I_A(t_i) \exp(-2\alpha(\nu) C_i L) \cos[\varphi(t_i) - \varphi(t_r)] \tag{6.25}$$

where G is the conversion loss of the mixer. There are N terms in Eq.(6.25), each corresponding to a different sensing channel. $V_F(\omega)$, the spectrum of $V(t)$, may be obtained by taking the Fourier transform of $V(t)$ and written as

$$V_F(\omega) = \sum_{i=1}^{N} V_i'(\omega) \tag{6.26}$$

where $V_i'(\omega)$ represents the signal spectrum of the i^{th} sensor channel. For a triangular frequency sweeping of angular frequency excursion Δf and period T_s, and with small delay difference τ_i, i.e., $\tau_i/T_s<<1$, $V_i'(\omega)$ may be expressed as

$$V_i'(\omega) \approx 2k'KGmV_0I_A \exp(-2\alpha(\nu)C_iL) \times \sum_{k}^{+\infty} \delta(\omega - k\omega_s) \times \frac{1}{2}(\frac{T_s}{2} - \tau_i) \frac{\sin[\frac{1}{2}(k\omega_s - \frac{2\Delta\omega}{T_s}\tau)(\frac{T_s}{2} - \tau)]}{\frac{1}{2}(k\omega_s - \frac{2\Delta\omega}{T_s}\tau_i)(\frac{T_s}{2} - \tau_i)}$$
$$\times \cos(\omega_0\tau_i - \frac{k\pi}{2}) \tag{6.27}$$

where τ_i represents a delay time difference between the signals from the i^{th} sensor and the reference. When Eqs. (6.17) and (6.18) are satisfied, the amplitude of the spectrum $V_i'(\omega)$ is approximately a single line at $k\omega_s$ and can be written as:

$$\begin{aligned} V_i(k\omega_s) &= k'KGmV_0I_A \exp(-2\alpha(\nu)C_iL)(\frac{T_s}{2} - \tau_i) \\ &\approx \frac{1}{2}k'KGmV_0T_sI_A \exp(-2\alpha(\nu)C_iL) \\ &\approx \chi I_A \exp(-2\alpha(\nu)C_iL) \end{aligned} \tag{6.28}$$

where we have used approximation $T_s/2\text{-}\tau_i \approx T_s/2$ because we have assumed that the value of τ_i is small ($\tau_i / T_s <<1$) and χ is a constant depending on a number of parameters ($\chi=k'KmGV_0T_s/2$). If we can design the delay difference τ_i so that each sensor corresponds to a different value of k, we may be able to multiplex a number of sensors in the frequency domain. The sensor signals may be separated (de-multiplexed) by using electronic band pass filters of appropriate pass bands.

The gas concentration C_i can be recovered from Eq.(6.28) by further processing the

signal $V_i(k\omega_s)$ after de-multiplexing. Similar to the TDM system, we examine the use of WMS technique where the laser wavelength is modulated sinusoidally at a relatively higher frequency while the average wavelength is locked to or scanned across a gas absorption line. The second harmonic of the wavelength modulation is detected by using a lock-in amplifier and used as a measure of gas concentration.

Assume that the laser frequency (wavelength) is sinusoidally modulated, i.e.,

$$\nu(t) = \nu_{L0} + \nu_{Lm} \sin \omega_m t \tag{6.29}$$

where ν_{L0} and ν_{Lm} are respectively the laser average frequency and the amplitude of wavelength modulation. $\omega_m = 2\pi f_m$, f_m is the frequency of the wavelength modulation. As the laser wavelength modulation is usually accompanied by residual intensity modulation, the light intensity from the laser (at point A as indicated in Fig. 6.4) will be time-varying and may be written as

$$I_A(t) = I_0(1 + \eta \sin \omega_m t) \tag{6.30}$$

where η is the residual intensity modulation index, I_0 is the average light intensity from the source. Substituting Eqs.(6.29) and (6.30) into Eq.(6.28), we obtain

$$V_i(\omega_i = k\omega_s) = \chi I_0[1 + \eta \sin(\omega_m t)] \exp[-2\alpha(\nu_{L0} + \nu_{Lm} \sin \omega_m t) C_i L] \tag{6.31}$$

The second harmonic of the modulation signal can be obtained by expanding Eq. (6.31) into a Fourier series of ω_m. The second harmonic is maximized when the average wavelength of laser is at the center of the gas line ($\nu_{L0} = \nu_g$) and may be expressed as:

$$V_{i,2\omega_m} \approx -2\chi I_0 k_0 \alpha_0 C_i L \tag{6.32}$$

Eq.(6.32) is the output corresponding to sensor i and is similar to the formula for the single

gas sensor system (see Section 3.2.1).

6.4 Shot-noise-limited Sensitivity for the FMCW System

Since the FMCW system and the TDM system have the same optical configuration, the shot-noise-limited sensitivity of the FMCW system can be simply determined from the result of the TDM system obtained in Section 4.3. The FMCW system seems to have an advantage from its higher duty cycle compared with the TDM system. It provides a higher average power at the photodetector and thus provides a better signal-to-noise ratio. Here, with the purpose of comparison, the conversion coefficients after the photodetection and the system parameters are assumed to be the same for the two systems. As stated in Section 4.3, the shot noise current at the detector output is proportional to the square root of the total average optical power at the photodetector. For the FMCW system, with the frequency-varying sinusoidal modulation at the intensity modulator, the duty cycle would be equal to 1/2. Hence, the term, $\frac{\Delta T}{T_p}$, in Eq.(4.3) and Eq.(4.4) will be replaced by the constant, 1/2. The shot-noise-limited sensitivity for the FMCW system can then be rewritten as:

$$\frac{\alpha_o CL}{\sqrt{B}} = \frac{1}{k}\sqrt{\frac{q}{R}\frac{2N^2}{\alpha_l^2 P_o}} \tag{6.33}$$

It is found that, with a higher duty cycle, the signal enhancement would be superior to the increase in the shot noise. Fig. 6.5 shows the simulation result for Eq.(6.33) where the shot-noise-limited performance is plotted against the number of sensors. The same parameters, P_o=1 mW, α_l^2=0.8, q=1.6×10^{-19}C, R=1 A/W, α_o=0.252, L=2.5cm, used in the TDM system are substituted. The detection limit is around 1.6 ppm/$\sqrt{Hz}$ for a sensor array of 50 sensors which is 5 times smaller than that of the TDM system.

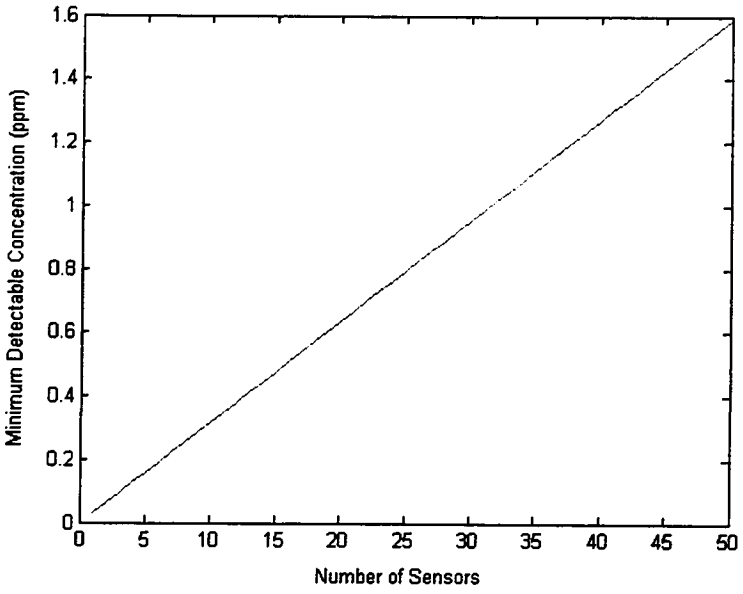

Fig. 6.5 The shot-noise-limited performance of the FMCW system as a function of sensor number.

6.5 Unwanted Interferometric Signals in FMCW System

In practice, there would be coherent mixing of light waves from different channels and would result in an additional term in the output of sensor i (at $\omega_i=k\omega_s$). The interferometric term is the second term in Eq.(6.22) and may be re-written as

$$\begin{aligned} I_{c,n}(t) &= 2\sum_{i=1,j>i}^{N} \mathrm{Re} < E_{ci}E_{cj}^{*} > \\ &= 2\sum_{i=1,j>i}^{N} (I_i I_j)^{1/2}[1+m\cos\varphi(t_i)]^{1/2}[1+m\cos\varphi(t_j)]^{1/2}\cos(\Delta\psi_{ij}) \end{aligned} \tag{6.34}$$

with I_l (l= i,j =1,2,..N) and $\Delta\psi_{ij}$ given by

$$I_l = [k' I_A]^{1/2}\exp[-\alpha(\nu(t_l)C_l L] \tag{6.35}$$

$$\Delta\psi_{ij} = 2\pi\int_{t_1}^{t_l}\nu\ (t)dt + \Delta\phi_{ij} \tag{6.36}$$

where $\Delta\psi_{ij}$ represents a phase difference between the light signals from channel i and channel j in which $\Delta\phi_{ij}$ is randomly varying due to environmental disturbances. $I_{c,n}(t)$ depends on the signals from all the channels and varies randomly with environment. The mixing of $V_{c,n}(t)=KI_{c,n}(t)$ with $V_r(t)$ would produce additional signals at the beat frequency of the sensor and therefore introduce errors in the measurement of gas concentration. For small modulation index $m<<1$, $I_{c,n}(t)$ may be approximated by

$$I_{c,n}(t)=2\sum_{i=1,j>i}^{N}(I_iI_j)^{1/2}\left[1+\frac{1}{2}m\left(\cos\varphi(t_i)+\cos\varphi(t_j)\right)\right]\times\cos(\Delta\psi_{ij}) \tag{6.37}$$

where we have used approximation

$$[1+m\cos\varphi(t)]^{1/2}\approx 1+\frac{1}{2}m\cos\varphi(t) \tag{6.38}$$

and have neglected the higher order term $m^2\cos\varphi(t_i)\cos\varphi(t_j)/4$. The mixing of $V_{c,n}(t)=KI_{c,n}(t)$ with $V_r(t)$ will produce both sum and difference frequency terms. The difference frequency terms of interest here may be written as

$$V_n(t)=\frac{1}{2}KmGV_0\sum_{i=1,j>i}^{N}(I_iI_j)^{1/2}\cos(\Delta\psi_{lm})\left(\sum_{l=i,j}\cos[\varphi(t_l)-\varphi(t_r)]\right) \tag{6.39}$$

By following the same process in deriving Eq.(6.25) to Eq.(6.28), we obtain the additional signal at $\omega_i=k\omega_s$, due to the unwanted interferometric signals, as

$$V_{i,n}(\omega_i=k\omega_s)=\frac{1}{2}k'KmGV_0T_sI_A\sum_{j=1,j\neq i}^{N}\exp[-\alpha(\nu)(C_i+C_j)L](\cos\Delta\psi_{i,j})_B \tag{6.40}$$

With $\chi=k'KmGV_0T_s/2$, Eq.(6.39) can be written as,

$$V_{i,n}(\omega_i=k\omega_s)=\chi I_A\sum_{j=1,j\neq i}^{N}\exp[-\alpha(\nu)(C_i+C_j)L](\cos\Delta\psi_{ij})_B \tag{6.41}$$

where $(\cos\Delta\psi_{ij})_B$ represents the frequency component of $\cos\Delta\psi_{ij}$ that passes through the

band-pass filter with centre at $k\omega_s$. To see the effect of this unwanted interferometric term on the system performance, we consider a simple case where no wavelength modulation or tuning is applied. The phase difference $\Delta\psi_{ij}$ can now be expressed as $\Delta\psi_{ij}=2\pi\nu_{L0}(\tau_j-\tau_i)+\Delta\phi_{ij}$, where ν_{L0} is the laser frequency. This phase difference varies randomly at relatively low frequency due to environmental disturbance $\Delta\phi_{ij}$ and causes $(\cos\Delta\psi_{ij})_B$ to vary from 1 to −1 if the change in $\Delta\psi_{ij}$ is beyond 2π. The unwanted signal given in Eq.(6.40) would then vary significantly compared with the sensor signal as given in Eq.(6.28), making detection of small gas concentration difficult, if not impossible.

Apart from the unwanted interferometric signals, the performance of the gas sensor array is also affected by various kinds of noise such as source and shot noise and the effect of time-varying polarization state. All these have been analyzed in previous chapters for a TDM system. For the FMCW system reported here, the effect of polarization variation and the source noise would be more or less the same as that for the TDM system. The shot noise limited performance should be better than the TDM system because of the relatively high average power level associated with the FMCW system. The effect of the shot and the source noise is however much smaller than that of the unwanted interferometric signals.

When the wavelength modulation as given in Eq.(6.29) is applied, the phase term $\Delta\psi_{ij}$ as given in Eq.(6.36) may be rewritten as

$$\Delta\psi_{ij}=2\pi\int_{t_1}^{t_1}\nu_{L0}(t)dt+2\pi\nu_{Lm}\int_{t_1}^{t_1}\sin\omega_m t\cdot dt+\Delta\phi=\xi_{ij}+\zeta_{ij}\sin\omega_m(t-\tau_{ji}/2) \tag{6.42}$$

with ξ_{ij} and ζ_{ij} defined as,

$$\xi_{ij}=2\pi\int_{t-\tau_{ji}}^{t}\nu_{L0}(t)dt+\Delta\phi_{ij} \tag{6.43}$$

and

$$\zeta_{ij} = \frac{4\pi v_{Lm}}{\omega_m}\sin(\omega_m \tau_{ji}/2) \approx 2\pi v_{Lm}\tau_{ji} \tag{6.44}$$

where $\tau_{ji}=\tau_j-\tau_i$ represents a delay time difference between the signals from the sensor j and sensor i. Substituting Eqs.(6.42), (6.29) and (6.30) into (6.41), we obtain

$$\begin{aligned} V_{i,n}(k\omega_s) = \chi I_0 \sum_{j=1,j\neq i}^{N} &[(1+\eta\sin\omega_m t_i)(1+\eta\sin\omega_m t_j)]^{1/2} \\ &\times\exp[-\sum_{l=i,j}\alpha(\nu(t_l))C_l L](\cos[\xi_{ij}+\zeta_{ij}\sin\omega_m(t-\tau_{ji}/2)])_B\} \end{aligned} \tag{6.45}$$

The second harmonic of $V_{i,n}(k\omega_s)$ can be obtained by expanding Eq.(6.45) into a Fourier series. Under the conditions that $\alpha(\nu)C_i L \ll 1$, $\eta \ll 1$ and $\omega_m \tau_{ji} \ll 1$, the magnitude of the second harmonic, when the average laser wavelength is at the center of the gas line, is given as below.

$$V_{i,n,2\omega_m}(\omega_i = k\omega_s) = \chi I_0 \times \sum_{j=1,j\neq i}^{N}\begin{bmatrix}(\cos\xi_{ij}\times M_{s,ij} + \eta\sin\xi_{ij}\times M_{0,ij}) \\ +\cos\xi_{ij}\times\alpha_0 C_i L\times M_{c,ij} \\ +\cos\xi_{ij}\times\alpha_0 C_j L\times M_{c,ij}\end{bmatrix} \tag{6.46}$$

with

$$\begin{aligned} M_{c,ij} = &\frac{-x^2 J_2(\zeta_{ij})}{(1-\sqrt{1+x^2})^2} - (J_0(\zeta_{ij})+J_4(\zeta_{ij})) - (J_2(\zeta_{ij})+J_6(\zeta_{ij})) \\ &\times\left(\frac{2}{x^2} - \frac{1}{2(1-\sqrt{1+x^2})^2}\right) \end{aligned} \tag{6.47}$$

$$M_{0,ij} = -[J_1(\zeta_{ij}) - J_3(\zeta_{ij})]\frac{x^2\sqrt{1+x^2}}{(1-\sqrt{1+x^2})^2} \tag{6.48}$$

$$M_{s,ij} = -J_2(\zeta_{ij})\frac{x^2\sqrt{1+x^2}}{(1-\sqrt{1+x^2})^2} \tag{6.49}$$

6.6 Minimization of the Unwanted Interferometric Signals

It is found that the unwanted interferometric signals in a fiber network can be effectively suppressed by using the wavelength modulation technique [9] and low-pass filtering. In this section, we study the effects of the two techniques on reducing errors in gas measurement.

6.6.1 Wavelength modulation technique

Eq.(6.46) gives the second harmonics $V_{i,n,2\omega_m}(\omega_i = k\omega_s)$ of the unwanted interferometric signals. We now look at how these signals affect the sensor performance in terms of minimum detectable gas concentration. $V_{i,n,2\omega_m}(\omega_i = k\omega_s)$ includes three terms. The second term is proportional to C_i and will vanish when C_i tends to zero and therefore will not set a limit to the detection sensitivity of sensor i. The first term is independent of gas concentration and will set a limit to the detection sensitivity. By setting this term to be equal to the signal given in Eq.(6.32), we obtain the detection sensitivity of sensor i in terms of minimum detectable gas concentration as

$$C_{i,\min 1} = \frac{\sum_{j=1,j\neq i}^{N}\left(M_{s,ij}\cos\xi_{ij} + M_{0,ij}\eta\sin\xi_{ij}\right)}{2\alpha_0 Lk_0} \approx \frac{\sum_{j=1,j\neq i}^{N} M_{s,ij}\cos\xi_{ij}}{2\alpha_0 Lk_0} \tag{6.50}$$

where we have neglected the $M_{0,ij}\eta\sin\xi_{ij}$ term because it is very small (η is very small). The rms value of $C_{i,\min 1}$ is

$$[C_{i,\min 1}]_{rms} \approx \frac{\sqrt{2\sum_{j=1,j\neq i}^{N}\left(M_{s,ij}\right)^2}}{4\alpha_0 Lk_0} \leq \frac{\sqrt{2(N-1)}M_{s,\max}}{4\alpha_0 Lk_0} \tag{6.51}$$

where the rms value of $\cos\xi_{ij}$ has been taken as $1/\sqrt{2}$. $M_{s,\max}$ represents the maximum value of $M_{s,ij}$. The third term is proportional to C_j and will cause crosstalk to sensor i. By setting this term to be equal to the right hand side term in Eq.(6.32), we obtain the crosstalk performance of sensor i as

$$C_{i,\min 2} \approx \frac{\sum_{i=1, j\neq i}^{N} C_j M_{c,ij} \cos\xi_{ij}}{2k_0} \tag{6.52}$$

with a corresponding rms value of

$$[C_{i,\min 2}]_{rms} \approx \frac{\sqrt{2\sum_{i=1, i\neq j}^{N} C_j^2 M_{c,ij}^2}}{4k_0} \leq \frac{\sqrt{2(N-1)}M_{c,\max} C_{\max}}{4k_0} \tag{6.53}$$

where $C_{\max}$ is the upper limit of the gas concentration, $M_{c,\max}$ represent the maximum values of $M_{c,ij}$.

As ζ_{ij} is a function of ν_{Lm}, hence $M_{c,ij}$, $M_{0,ij}$ and $M_{s,ij}$ are also functions of ν_{Lm}. We take the case of i =1, j =2 as an example. $M_{c,12}/k_0$ $M_{0,12}/k_0$, and $M_{s,12}/k_0$ as functions of ν_{Lm} were calculated using Eqs.(6.47)-(6.49) and are shown in Fig.6.6.

For the calculation, we assumed $f_m = 500Hz$, $\tau_{21} = 100ns$. As shown in Fig.6.6, all the three parameters are rapidly oscillating when ζ_{ij} or ν_{Lm} is varied. Any small variation in wavelength or path length would therefore significantly affect the values of these parameters. It is therefore only meaningful to look at the envelope of these oscillations. The (envelope) value of $M_{0,12}/k_0$, and $M_{s,12}/k_0$ are of the same order and reduces with the increase of ν_{Lm}. $M_{c,12}/k_0$ follows a similar trend but decreases much faster and to a much smaller value compared with $M_{0,12}/k_0$ and $M_{s,12}/k_0$. At around ν_{Lm} = 28GHz, the maximum value of the

envelope of $M_{c,12}/k_0$ is about 4×10^{-3}, while the values of $M_{0,12}/k_0$ and $M_{s,12}/k_0$ are about 0.08.

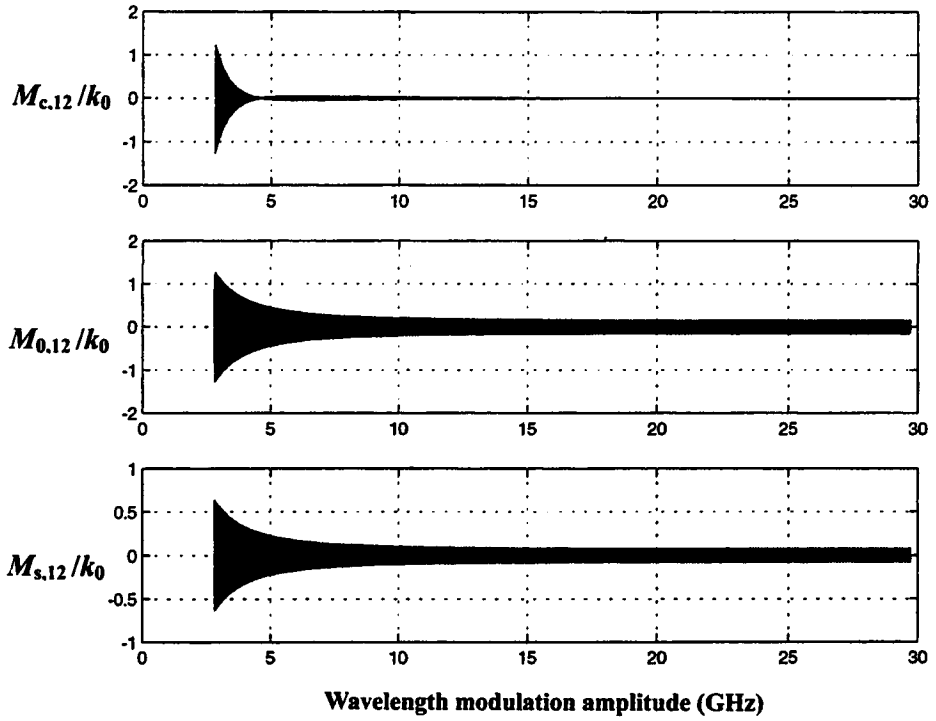

Fig. 6.6 $M_{s,12}/k_0$, $M_{0,12}/k_0$ and $M_{c,12}/k_0$ as functions of v_{Lm}

Eqs.(6.51) and (6.53) can be used to estimate the performance of the gas measurement system where the average wavelength of the laser is locked at the center of the gas absorption line. The value of ξ_{ij} under this condition may be written as:

$$\xi_{ij} = 2\pi \int_{t-\tau_{ji}}^{t} v_{L0}(t)dt + \Delta\phi_{ij} = 2\pi v_{L0}\tau_{ji} + \Delta\phi_{ij} \tag{6.54}$$

ξ_{ij} varies randomly within a low frequency range due to environmental induced phase change $\Delta\phi_{ij}$. For gas sensors with wavelength tuned across the gas absorption, the measurement accuracy may be further enhanced by using a proper low pass filter. This will be discussed in section 6.5.2.

6.6.2 Low-pass filtering technique

It can be seen from Eqs.(6.50) and (6.52) that the measurement errors are proportional to $\cos\xi_{ij}$. If the laser wavelength (frequency ν_{L0}) is scanned linearly across the gas absorption line, $\cos\xi_{ij}$ would vary periodically with time. If the time delay τ_{ji} is sufficiently large that variation of ξ_{ij} ($=2\pi\nu_{L0}\tau_{ji}+\Delta\phi_{ij}$) is over many times of π, $\cos\xi_{ij}$ would vary much faster than the absorption signal and can therefore be removed by using a low pass filter. This indicates that much higher sensitivity could be achieved by combining the wavelength scanning with the use of a low pass filter. This technique has actually been applied in gas absorption spectroscopy to minimize unwanted etalon effects [10].

When the laser is scanned, the laser average frequency $\nu_{L0}(t)$ may be expressed as

$$\nu_{L0}(t) = \nu_{La} + B_{Lb}t, \qquad t \in (0,T) \tag{6.55}$$

where T is the period of the wavelength scanning and is typically of the order of a second or tens of seconds. ν_{La} is the lowest average frequency and B_{Lb} is the slope of the wavelength scanning.

Eq.(6.42) may be rewritten as:

$$\xi_{ij} = 2\pi \int_{t-\tau_{ji}}^{t} \nu_{L0}(t)dt + \Delta\phi_{ij} = 2\pi B_{Lb}\tau_{ji}t + 2\pi(\nu_{La} - \frac{1}{2}B_{Lb}\tau_{ji})\tau_{ji} + \Delta\phi_{ij} \tag{6.56}$$

and

$$\cos\xi_{ij} = \cos(2\pi B_{Lb}\tau_{ji}t + \phi_0 + \Delta\phi_{ij}) \tag{6.57}$$

where $\phi_0 = 2\pi(\nu_{La} - \frac{1}{2}B_{Lb}\tau_{ji})\tau_{ji}$ is a constant.

Assume that a lock-in amplifier is used to detect the second harmonic signal. As the lock-in may be regarded as a narrow band-pass filter, only signals with frequencies around

$2f_m(\pm$ several Hz) can pass through. Therefore only the DC component of $\cos\xi_{ij}$ can appear at the output of the lock-in and Eqs.(6.50) and (6.52) may then be rewritten as:

$$C_{i,\min 1} \approx \frac{\sum_{j=1,j\neq i}^{N} M_{s,ij}(\cos\xi_{ij})_{DC}}{2\alpha_0 Lk_0} \leq \frac{(N-1)M_{s,\max}(\cos\xi_{ij})_{DC,\max}}{2\alpha_0 Lk_0} \tag{6.58}$$

$$C_{i,\min 2} \approx \frac{\sum_{j=1,j\neq i}^{N} C_j M_{c,ij}(\cos\xi_{ij})_{DC}}{2k_0} \leq \frac{(N-1)C_{\max}M_{c,\max}(\cos\xi_{ij})_{DC,\max}}{2k_0} \tag{6.59}$$

where $(\cos\xi_{ij})_{DC}$ represents the DC component of $\cos\xi_{ij}$. Computer simulation has been conducted to calculate the value of $(\cos\xi_{ij})_{DC}$ as a function of delay time τ_{ij} for an arbitrary set of parameters: ν_{La} =19608GHz(1530nm), B_{Lb} =2.7GHz/s, T=15s, ϕ_0=0 and $\Delta\phi$=0. The values of $(\cos\xi_{ij})_{DC}$ as a function of time delay difference τ_{ij} between sensors are shown in Fig. 6.7.

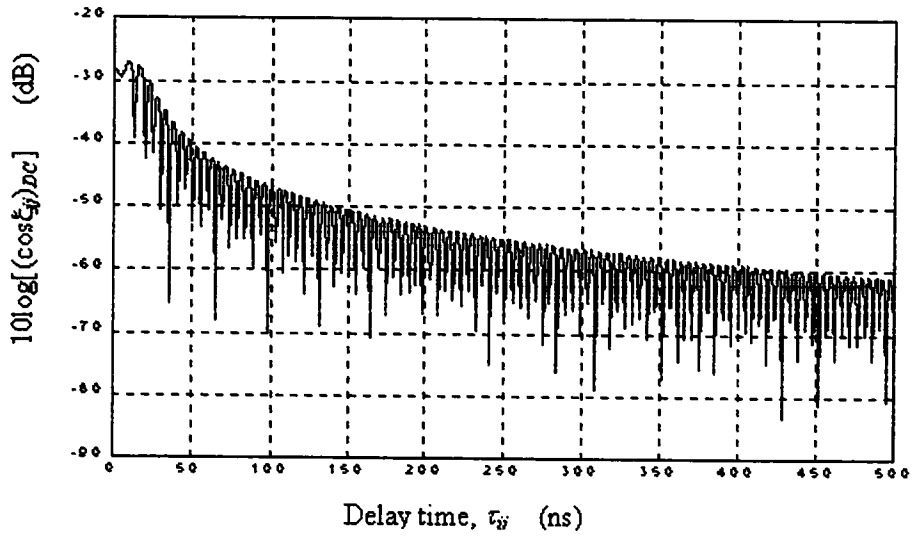

Fig. 6.7 DC component of $\cos\xi_{ij}$ as a function of time delay difference τ_{ji} between sensors.

The vertical axis $10\log\left|(\cos\xi_{ij})_{DC}\right|$ expresses the value of the DC component of $\cos\xi_{ij}$ with the unit of dB. For 20m delay between sensors, corresponding to $\tau_{ji} \approx 100ns$, the maximum value of $(\cos\xi_{ij})_{DC}$ is found to be 47dB smaller than that of the value of $\cos\xi_{ij}=1$, indicating that the detection sensitivity can be improved by 47dB by wavelength scanning and lock-in detection. However, as we are dealing with a fiber optic system, environmental variation may affect the fiber length and the refractive index and therefore results in random variation of the phase $\Delta\phi_{ij}$. This phase variation would affect the efficiency of noise reduction using the lock-in detection and would limit the improvement factor to about 30dB [11] instead of 47dB as mentioned above.

The maximum possible value of the detection sensitivity if sensor i ($C_{i,\min 1}$) as a function of sensor number was calculated by using Eq.(6.58) and in Fig. 6.8. It can be seen that, the minimum detectable gas concentration ($C_{i,\min 1}$) for a three-sensor system is about 0.008% (80 ppm). $C_{i,\min 1}$ is below 0.2% (2000 ppm) for sensor number up to 50.

For the calculation, the value of $10\log\left|(\cos\xi_{ij})_{DC,\max}\right|$, α_0 and L were taken as -30dB, 0.252cm^{-1} and 2.5cm, respectively. The crosstalk effect $C_{i,\min 2}$ calculated by using Eq.(6.59) was found to be much smaller than $C_{i,\min 1}$ and is not shown. It should be mentioned that detection limit is an estimation of the upper limit of $C_{i,\min 1}$ based on Eq. (6.58). The actual value of $C_{i,\min 1}$ could be smaller than that given in Fig. 6.8. This is because that we have taken the value of $(\cos\xi_{ij})_{DC}$ (j=1, 2, ... N and, $j \neq i$) $(\cos\xi_{ij})_{DC,\max} = -30dB$. The

detection sensitivity in terms of minimum detectable gas concentration $C_{i,\min 1}$ as limited by the unwanted interferometric signals (Eq.(6.58) and Fig. 6.8) is inversely proportional to α_0 and L. It can also be expressed in terms of minimum detectable absorbance, by simply multiplying $C_{i,\min 1}$ by $\alpha_0 L$=0.25×2.5=0.625.

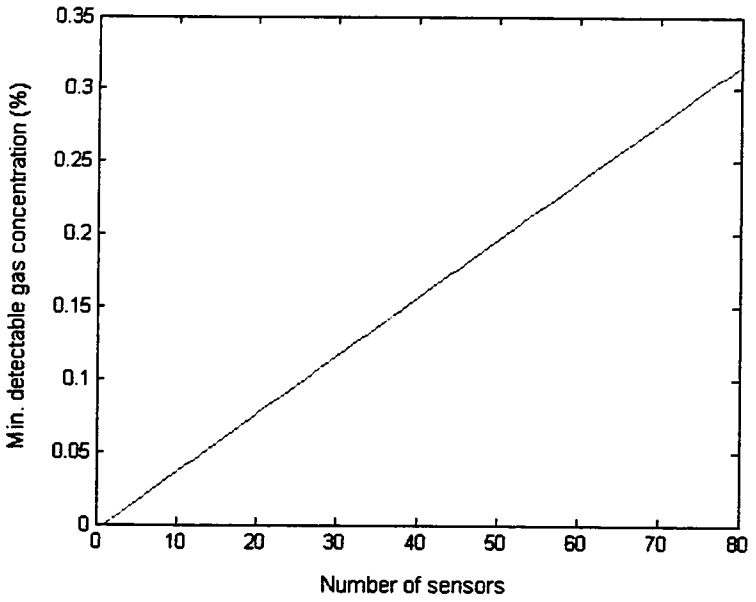

Fig. 6.8 The minimum detectable gas concentration due to the interferometric effect versus the number of sensors.

6.7 Crosstalk resulting from the sidelines

As discussed in section 6.2, signal from each sensor would consist of a set of discrete lines in the frequency domain with frequency interval ω_s. If the modulation and the system parameters are selected carefully according to Eq.(6.17) and Eq.(6.18), the signal from any particular sensor would have an approximately single line spectrum. For a single sensor system, this can easily be achieved by adjusting ω_0, $\Delta\omega$ and τ. For a multiple sensor system, ω_0 and $\Delta\omega$ are usually fixed and Eq.(6.17) and Eq.(6.18) may not be satisfied accurately due to the error in controlling the length of the fiber delay lines. If Eq.(6.17) and Eq.(6.18) can

not be realized, this would increase the magnitude of the sidelines. This implies that the signal at a particular frequency would not only include the beat signal from the sensor of interest but also the sidelines from other neighboring sensors. These non-zero sidelines would cause crosstalk between sensors and affect measurement accuracy [8, 12].

The second harmonic signal of sensor i (at $\omega_i = k\omega_s$) is given by Eq.(6.32). The second harmonic of the sideline signal at ω_i from the j^{th} channel may be obtained from Eqs.(6.27) and (6.32) and written as:

$$V_{2\omega_m}(\omega_i = k\omega_s)_j = -2k_0 k' KGmV_0 I_0 \frac{\sin[(\frac{\Delta\omega}{T_s}(\tau_i - \tau_j)(\frac{1}{2}T_s - \tau_j)]}{\frac{\Delta\omega}{T_s}(\tau_i - \tau_j)} \times \cos(\omega_0\tau_j - \frac{1}{2}\Delta\omega\tau_i)\alpha_0 C_j L \tag{6.60}$$

The total second harmonic at $\omega_i = k\omega_s$ for an N-sensor system may be expressed as

$$V_{2\omega_m}^N(\omega_i)_j = \sum_{j=1, j\neq i}^{N} V_{2\omega_m}(\omega_i)_j = 2k_0 k' KGmV_0 I_0 \alpha_0 L \sum_{j=1, j\neq i}^{N} M_j C_j \tag{6.61}$$

with M_j is the side line amplitude relative to the major line at $\omega_i = k\omega_s$ and is defined as

$$M_j = -\frac{\sin[(\frac{\Delta\omega}{T_s}(\tau_i - \tau_j)(\frac{1}{2}T_s - \tau_j)]}{\frac{\Delta\omega}{T_s}(\tau_i - \tau_j)} \cos(\omega_0\tau_j - \frac{1}{2}\Delta\omega\tau_i) \tag{6.62}$$

The value of the sideline amplitude M_j determines the crosstalk level between sensors. By setting the signal given by Eq.(6.61) equal to that given by Eq.(6.32), the detection accuracy of sensor i as limited by the FMCW sidelines is obtained as

$$[C^{N}_{i,cross}]_{\min} = \frac{2\sum_{j=1,j\neq i}^{N} M_j C_j}{T_s} \leq \frac{2}{T_s} \times Max\{\sum_{j=1,j\neq i}^{N} M_j C_j\} \tag{6.63}$$

where C_j is in the range from 0 to $C_{\max}$. The sensor performance in terms of minimum detectable gas concentration due to crosstalk from the non-zero sidelines as a function of the number of sensors are evaluated using Eq.(6.63) and shown in Fig.6.9 as curves *a,b,c,d*. The maximum gas concentrations for all the sensors are assumed to be the same and equal to $C_{\max} = 5\%$. The curve *a* is obtained under the ideal condition where Eqs. (6.17) and (6.18) are satisfied. Curves *b*, *c* and *d* are for the cases when the time delay bias from Eqs. (6.17) and (6.18) equal to 0.025 ns, 0.05 ns and 0.1 ns, corresponding to fiber lengths of 0.5 cm, 1 cm and 2 cm respectively.

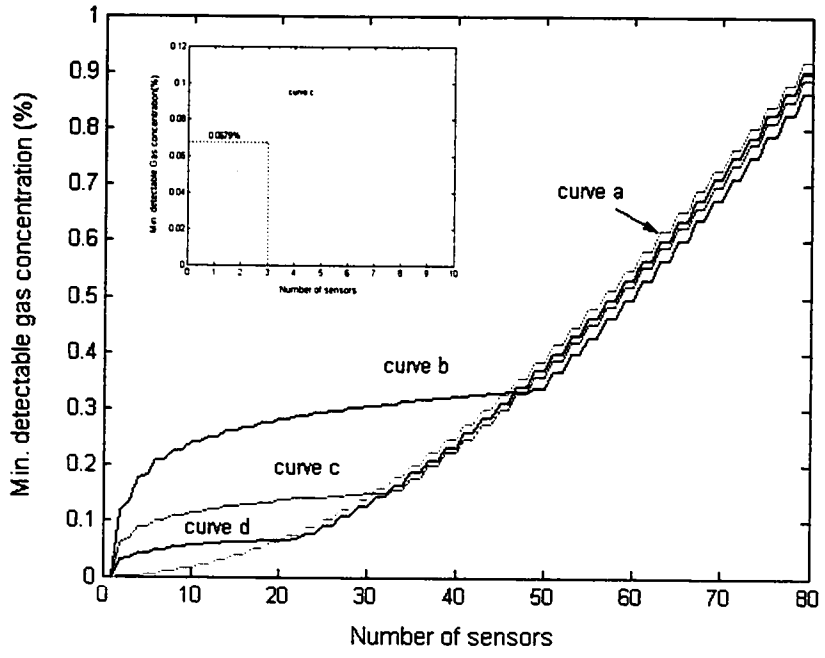

Fig. 6.9 The minimum detectable gas concentration due to the effect of the sideline versus the number of sensors.

Summing up, the interferometric effect is dominant and will set a limit to the system performance when Eqs. (6.17) and (6.18) are satisfied and the number of sensor is less than 23. However, for a small number of sensors (up to 17 for 0.5 cm bias, curve *b*), if Eqs. (6.17) and (6.18) are not satisfied, the sideline effect associated with the FMCW technique may exceed the interferometric effect. From Fig. 6.9, we can see that it should be possible to achieve 2000 ppm (0.2%) accuracy for a sensor number of up to 37 when the bias of the delay fiber length is less than 1 cm (curve *c*).

It should be mentioned that the detection accuracy limited by the sideline-related crosstalk as stated in Eq.(6.63) is independent of $\alpha_0 L$ and therefore should remain unchanged for different gas types (different α_0) and different cell length L.

6.8 Chapter Summary

We have investigated the performance of a multi-point fiber gas sensor array based on a FMCW technique and wavelength modulation of a tunable external-cavity semiconductor laser. We investigated the limitation imposed on the sensitivity of the fiber gas sensor array by the unwanted interferometric signals and the crosstalk effect due to the non-zero sidelines of the FMCW. We show how the interferometric effects may be reduced by using a combination of wavelength modulation/scanning and proper electronic filtering. It is theoretically possible to realize a 37-sensor array with detection accuracy of better than 2000 ppm.

REFERENCES

1. M.I. Skolnik, "Introduction to radar systems," New York : McGraw-Hill, pp.84-86, 1980

2. A.J. Hymans and J. Lait, "Analysis of a frequency-modulated continuous-wave ranging system," *Proc. IEE*, Vol. 107B, pp.365-372, 1960.

3. B.R. Mahafza, "Introduction to radar analysis," CRC Press, pp.119-132, 1998.

4. H.D. Griffiths, "New ideas in FM radar," *Electronics & Communication Eng. Journal*, pp.185-194, Oct., 1990.

5. D. Uttam and B. Culshaw, "Precision time domain reflectometry in optical fiber systems using a frequency modulated continuous wave ranging technique," *Journal of Lightwave Technology*, Vol. LT-3, No.5, pp.971-977, 1985.

6. W.V. Sorin, D.K. Donald, S.A. Newton and M. Nazarathy, "Coherent FMCW reflectometry using a temperature tuned Nd:YAG ring laser," *IEEE Photonic Technology Letters*, Vol.2, No.12, pp.902-904, 1990.

7. I. Sakai, "Frequency-division multiplexing of optical-fibre sensors using a frequency-modulated source," *Optical and Quant. Electron.*, Vol. 18, pp.279-289, 1986.

8. Peter K. C. Chan, "Multiplexing of fiber optic bragg grating sensors," Ph. D Thesis, HK PolyU, EE Department, 2000.

9. P.K. Pepelijugoski and K.Y. Lau, "Interferometric noise reduction in fiber-optic links by superposition of high frequency modulation," *Journal of Lightwave Technology*, Vol. 10, No.7, pp.957-963, 1992.

10. H. Riris, C. B. Carlisle, R. E. Warren and D. E. Cooper, "Signal-to-noise ratio enhancement in frequency-modulation spectrometers by digital signal processing," Optics Letters, Vol.19, 144-146, 1994.

11. C. C. Chan, "Interrogation of fiber Bragg grating sensors with a tunable laser," Ph.D thesis, The Hong Kong Polytechnic University, July 2000.

12. Peter K. C. Chan, W. Jin, J. M. Gong, and M. S. Demokan, "Multiplexing of fiber Bragg grating sensors using an FMCW technique," IEEE Photonics Technology letter, Vol. 11, No. 11, pp.1470-1472, 1999.

CHAPTER 7 EXPERIMENTAL STUDIES ON FMCW SYSTEM

7.1 Introduction

The principle and performance of the FMCW-multiplexed gas sensor system have been theoretically studied in Chapter 6 in which the sensitivity limitation due to the unwanted interferometric signals and the crosstalk due to the non-zero sidelines were investigated. It was found that the unwanted interferometric signals may be reduced by using a combination of wavelength modulation- scanning and proper low-pass filtering. In this chapter, we report the experimental results for the system with a three-sensor array. Experiments with varying parameters were conducted in order to verify the consistency between the theoretical analysis and the experimental results. The configuration of the FMCW system is given in Section 7.2. In Section 7.3, the characteristics of the beat note spectrum with varying wavelength modulation amplitudes are discussed. Determination of the system performance in terms of sensitivity and crosstalk are presented in Section 7.4. A chapter summary is given in the Section 7.5.

7.2 System Configuration and Output Signals

A three-sensor system as shown in Fig. 7.1 was constructed and experimentally tested. The sensors were addressed by the FMCW technique coupled with WMS to achieve high sensitivity gas detection. Light from a New Focus external cavity tunable laser was modulated in intensity by the use of a UTP single-polarization intensity modulator on which a triangular swept-frequency carrier generated from a voltage controlled oscillator (VCO) was applied. The sweep rate (f_s) and the frequency deviation (Δf) of the carrier were 10 kHz and 6.3 MHz respectively. A polarization controller was used before the intensity modulator for optimizing the launched power. The splitting ratios of the couplers k_1, k_2 were chosen to be 66:33 and

50:50, respectively, in order to balance the power level from each sensor. When light passes through the gas cells, gas concentration information is encoded on to the light intensity. The return light signals from different sensors are coupled into a common output fiber and then converted to an electric signal by a high speed photo-detector and mixed with a reference signal from the VCO subsequently.

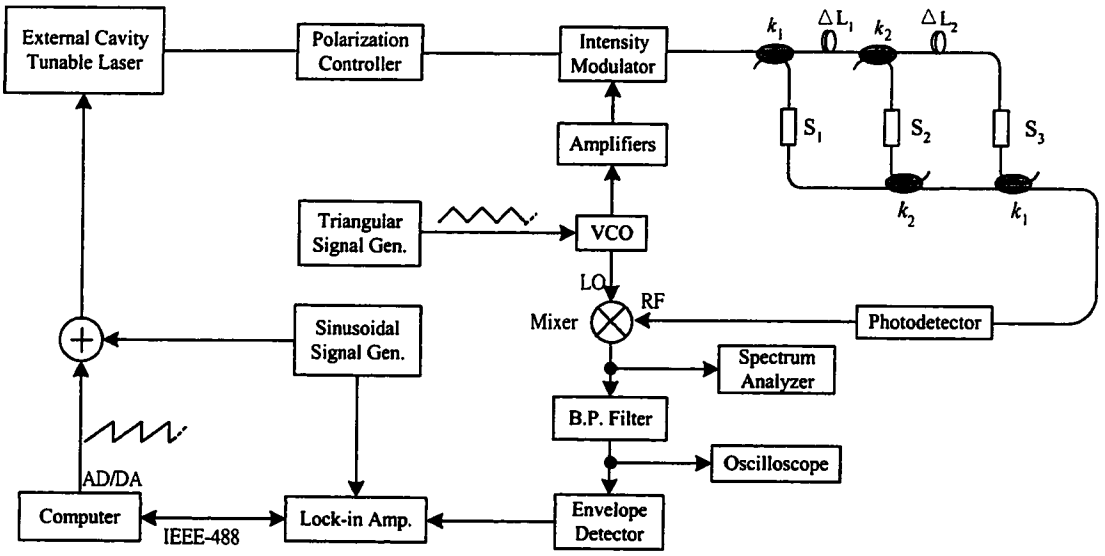

Fig. 7.1 FMCW addressed fiber-optic gas sensor network.

The output from the mixer consists of N-beat notes (here, N=3) with their respective beat frequencies ($f_{beat,i}$) determined by the time delay differences (τ_i, i=*1,2,3*, corresponding to the 3 sensors) between the sensor signals and the reference:

$$f_{beat,i} = 2\,\Delta f \cdot f_s \cdot \tau_i \qquad (7.1)$$

In our system, the optical path differences between the sensing channels and the electric delay of the reference were adjusted in order to make the beat frequencies coinciding with integer multiples, k, of the sweep rate (i.e., $f_{beat,i} = kf_s$). Under such conditions, the beat note spectra of the three sensors with k = 2, 4 and 5 are approximately of single-line spectra with their beat

frequencies corresponding to 20kHz, 40kHz and 50kHz respectively. The corresponding values of τ_i are 158.7 ns, 317.4 ns and 396.8 ns respectively. The length of the delay lines between S_1 and S_2, S_2 and S_3 are approximately 32m and 16m. During experiments, the lengths of the delay lines were cut 1 cm by 1 cm and the output beat frequency spectrum for each sensor was being monitored until the suppression ratio of the sidelines reached the maximum. The beat note spectra of each of the three sensors are shown in Fig. 7.2(a) to Fig. 7.2(c) respectively, when the light from the other two sensors were blocked.

(a)

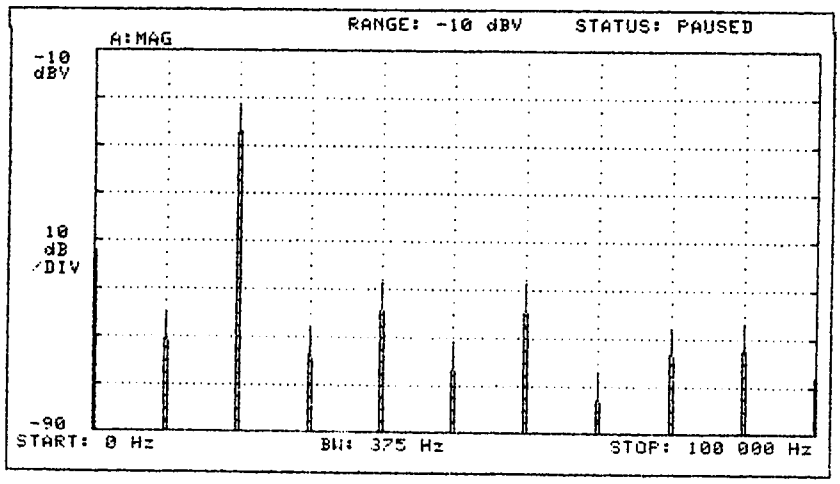

(b)

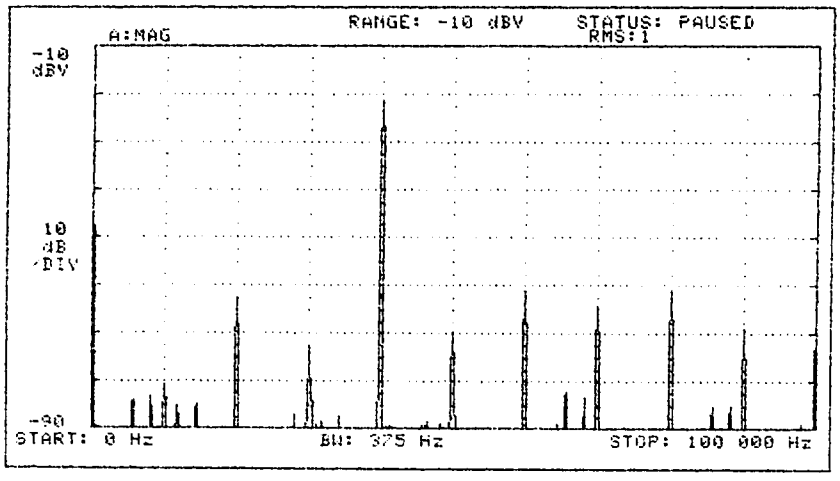

(c)

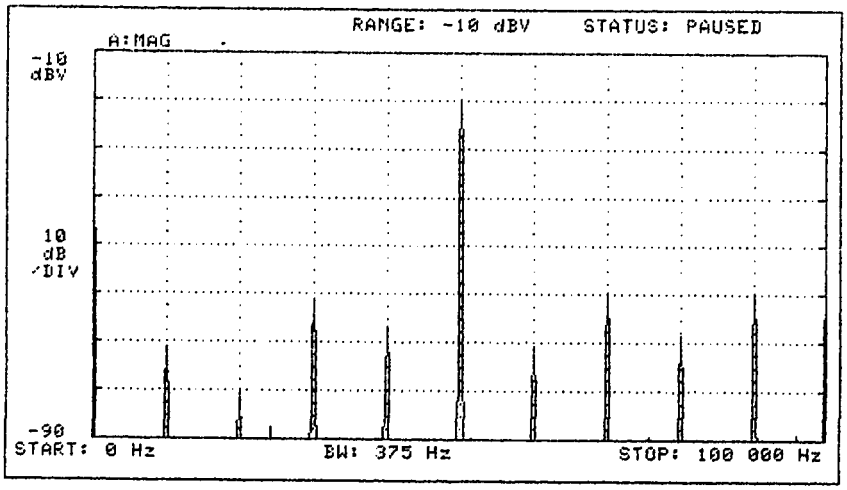

Fig. 7.2 The beat note spectra of the three sensors. (a) sensor 1, (b) sensor 2, (c) sensor 3.

Although, ideally, the spectrum of the beat-note for a particular sensor is approaching a single line at the beat frequency, there are however sidelines associated with the FMCW technique (as discussed in Sections 6.2 and 6.7). The overlapping of these sidelines and the beat frequencies would cause crosstalk between sensors. The magnitude of the sidelines (and thus crosstalk) was evaluated by blocking the light signal from say S_1 and looking at the signal magnitude at 20kHz when one of the other gas cells (#2 and #3) was blocked. For example, the crosstalk in terms of power spectrum amplitude was found to be about -42dB from S_2 to S_1 and -60dB from S_3 to S_1.

A band-pass filter was then employed to separate a selected beat frequency component from the mixer output for extracting information from a selected sensor. With the use of WMS technique, the $2f_m$ signal and hence the gas concentration information is carried by the envelope of the associated beat frequencies. The wavelength modulation frequency, f_m, used in this system is 400 Hz. Like in the TDM system in Chapter 5, the laser wavelength was scanned slowly across the gas absorption line of acetylene around 1530.37 nm. The wavelength modulation amplitude is about 14.3 GHz which corresponds to 2.2 times the

half-width of the absorption line.

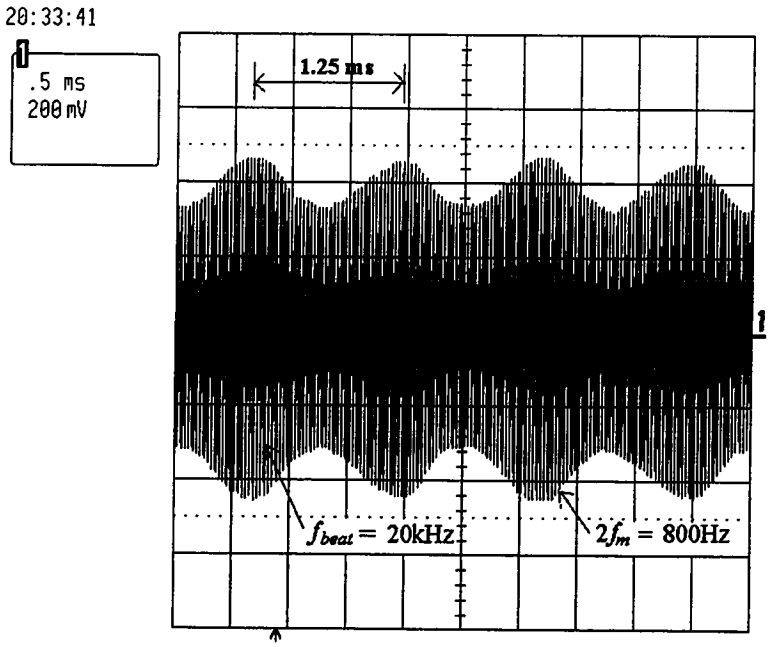

Fig. 7.3 Time domain signal of sensor #1 before envelope detection

Fig. 7.3 shows an oscilloscope display of the signal from a band pass filter centred at 20kHz (corrsponding to sensor #1) when gas cell #1 was filled with acetylene gas of 50% concentration and the laser wavelength was tuned to the centre of the gas absorption line. The envelope of the selected beat signal was then restored by use of an envelope detector and lock-in detected with the lock-in amplifier which is connected to a personal computer through the IEEE-488 (GPIB) interface for data acquisition. Fig.7.4 shows the second harmonic signal for the sensor 1 obtained by filling the gas cell with 9415 ppm acetylene.

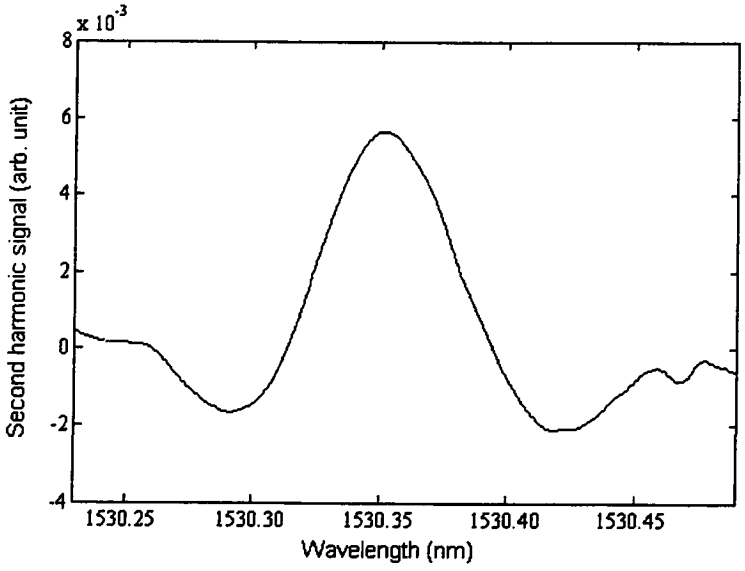

Fig. 7.4 Second harmonic signal for gas sensor 1 when the gas cell was filled with 9415ppm acetylene.

7.3 SNR Enhancement by Using Wavelength Modulation

In Fig. 7.2, the beat note spectra for the three sensors were shown individually where the light from the other two channels were blocked. In a real multiplexed system, light signals from all the channels would be combined together before the mixer. Three stable peaks in the beat note spectrum were expected. But, in practice, a large fluctuation of the beat note spectrum was observed. The spectrum of the signal from the mixer was found dependent on the amplitude of the frequency modulation applied. The SNR around the beat frequencies was improved from about 20dB to better than 45dB (with a bandwidth of 375Hz) when the modulation amplitude was varied from 67 MHz to 14.3 GHz (as shown in Fig. 7.5).

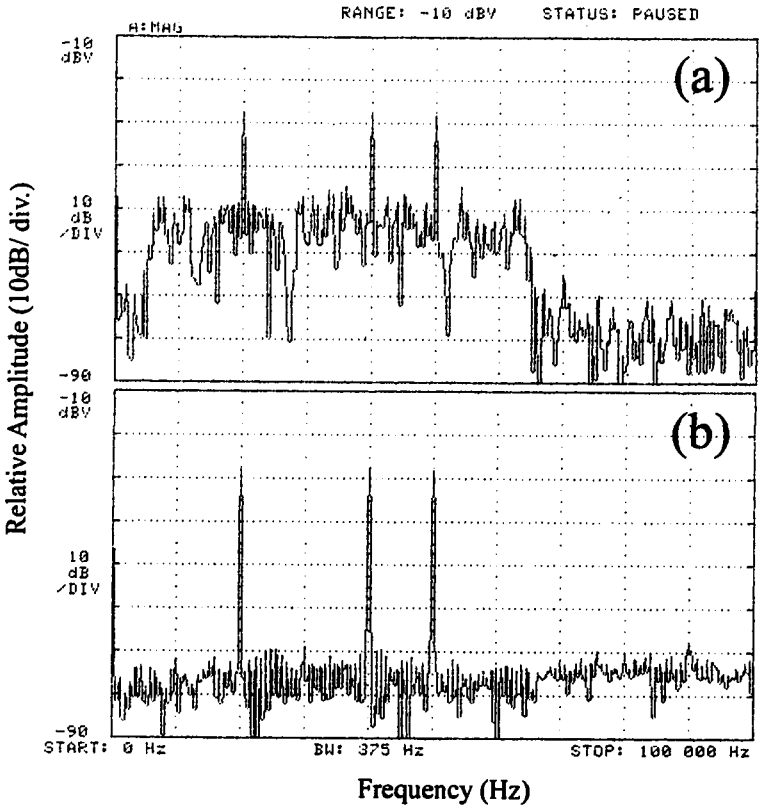

Fig. 7.5 Spectra of signal from the mixer (a) small modulation amplitude, i.e., 67MHz; (b) large modulation amplitude, i.e., 14.3GHz.

The poor SNR at low modulation amplitude was due to coherent interference between the signals from different sensor channels. The coherence length of the tunable laser is typically of the order of several hundred meters, and the coherent interferometric effect would definitely exist in our system and affect the performance of the sensor network. Fig. 7.6 shows the relationship between the SNR and the wavelength modulation amplitude obtained from the experiment. The use of large modulation amplitude shifts the (unwanted) interferometric signals to higher frequency band (beyond 100kHz range as shown in Fig. 7.5) and thus results in better SNR around the beat frequencies [1].

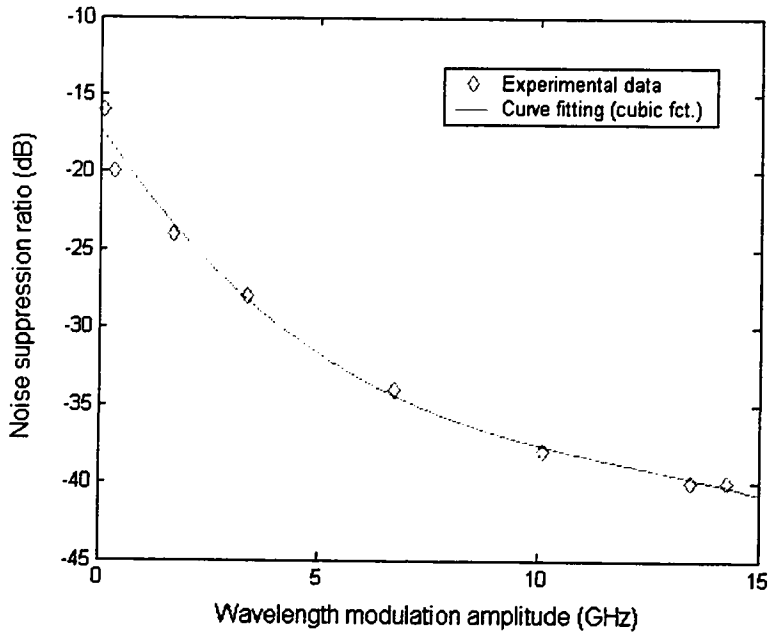

Fig. 7.5 The relationship between the SNR and the wavelength modulation amplitude.

7.4 Performance Evaluation

In this section, the performance of the system is evaluated in terms of the sensitivity and the inter-channel crosstalk. The factors which reduce the suppression ratios of the sidelines, thus the crosstalk performance of the system, will be discussed.

7.4.1 System sensitivity

The sensitivity of the system was determined by filling gas cell #1 with 9415ppm acetylene gas when gas cells #2 and #3 were filled with no acetylene. With a wavelength modulation amplitude of about 14.3 GHz, the maximum $2f_m$ signal obtained from the lock-in amplifier with repeated scans is shown in Fig.7.7. The SNR was estimated to be about 20 and the minimum detectable concentration was calculated to be 270 ppm/$\sqrt{Hz}$ for the 2.5 cm gas cell or 6.75 ppm·m which corresponds to a minimum detectable absorbance of 1.48×10^{-4}. Similar results were obtained for the other two gas sensors. This detection sensitivity is similar

to that measured from a single sensor (sensor #1) when the light signals from the other two channels were completely blocked, indicating that the system performance is not limited by the interferometric signals due to coherent mixing between the light waves from different sensor channels and is believed to be limited by the residual etalon interference effect from the gas cells. A better value of sensitivity would be expected if averaging were performed over a number of scans.

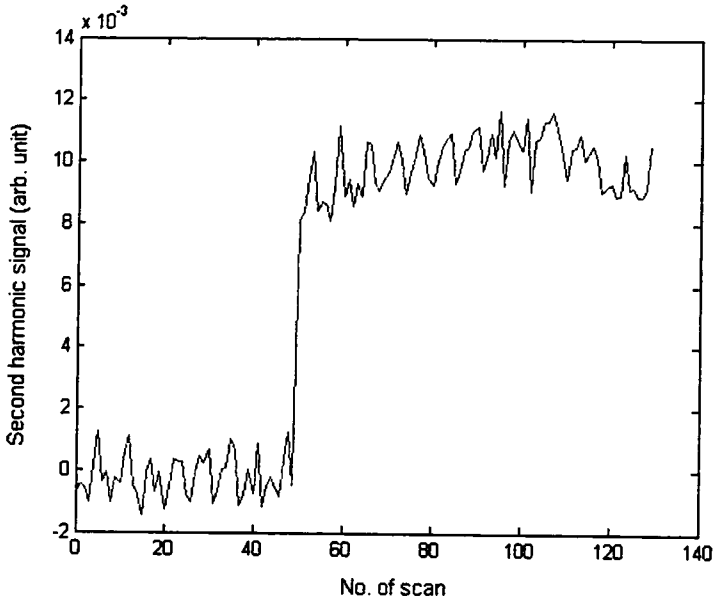

Fig. 7.7 Second harmonic signal when the acetylene concentration was changed from 0 ppm to 9344 ppm.

7.4.2 Inter-channel crosstalk

From Fig. 7.7, it is seen that the variation is too large if only one scan is conducted for determining the gas concentration in the gas cells. When the sensor #1 was selected, the crosstalk performance of the system was evaluated by repeating measurements (50 scans for each combination as stated below) of the second harmonic signals when the gas cells #1, #2 and #3 were filled by the following combination of gas concentrations: (1%, 0%, 0%), (1%, 95%, 0%) and (1%, 0%,95%). The inter-channel crosstalk from S_2 to S_1 and from S_3 to S_1 can

be determined from the deviations of the signal measured from S_1 with these three combinations. They were found to be about -22dB and -31 dB respectively. This corresponds to crosstalk levels of -44dB and -62dB, respectively, in terms of signal power that agrees well with the measured results of the sideline amplitudes of the FMCW. Similar procedures are carried out for the other two sensors, S_2 and S_3. Table 7.1 shows the crosstalk levels between the sensors obtained in our experiment.

	S_1	S_2	S_3
Crosstalk from S_1	-	-20 dB	-24 dB
Crosstalk from S_2	-22 dB	-	-23 dB
Crosstalk from S_3	-31 dB	-22 dB	-

Table. 7.1 Crosstalk levels between the sensors.

As we have discussed in Section 6.7, the crosstalk level is determined by the relative magnitude of the sidelines, i.e., the value of M_j. From Table 7.1, the worse case measurement accuracy limited by the crosstalk effect may be estimated from the crosstalk from sensors 1 and 3 to sensor 2 as *5%* [(-20dB)+(-22dB)]=815*ppm* or 0.08%. This value agrees with the theoretical prediction with the fiber length bias of 1 cm (curve c in Fig.6.9).

It is obvious that the crosstalk performance of the system critically depends on the suppression ratios of the non-zero sidelines. The factors which caused the reduction in the suppression ratios may include the non-linear characteristics of the devices in the system such as the voltage-controlled oscillator and the bias from the optimized delays. For the non-linear effect of the VCO, different techniques for lowering the non-linearity have been proposed [2,3]. For the delay bias, it may be minimized by the fine adjustment of the length of the delay lines by using a translation stage

It should also be pointed out that the crosstalk induced measurement error is not randomly changing with environment and may therefore be corrected by using the measured values of gas concentrations from different channels using Eq.(6.63).

7.4.3 Multiplexing capacity

Power budget analysis is commonly used for estimating the multiplexing capacity of optical systems. The number of sensor that can be interrogated will depend on the optical network configuration, power of the optical source and the performance of the detector. Since the FMCW and TDM systems have the same optical configuration and use the same transceiver units, the multiplexing capacity of the FMCW system would be the same as that of the TDM. Detailed analysis and results were presented in Section 5.4.

7.5 Chapter Summary

In conclusion, we have examined the use of FMCW coupled with WMS for addressing a multipoint gas sensor network. The unwanted interferometric signals due to coherent mixing between signals from different channels were found to be reduced significantly by using proper wavelength modulation coupled with slow wavelength scanning and lock-in detection. The experimental results agree with the analysis and the predictions in Chapter 6. For the experimental demonstration of the system with a three sensors network, a minimum detectable concentration of 270 ppm/$\sqrt{Hz}$ and the crosstalk between the sensors of better than -20 dB were achieved.

REFERENCES

1. F.W. Willems and W. Muys, "Suppression of interferometric noise in externally modulated lightwave AM-CATV systems by phase modulation," *Electronics Letters*,

Vol. 29, No. 23, pp.2062-2063, 1993.

2. X. Wang, J. Feng and J. Xiang, "Linearity correction for linear FM sweep signals," *Acta Electronica Sinica*, Vol. 24, No. 10, pp.120-122, 1996.

3. V.I. Orlyanskii, "Lowering of the nonlinearity of the modulation response in voltage-controlled oscillators," *Radioelectronics and Communications Systems*, Vol.33, No.1, pp.90-91, 1990.

CHAPTER 8 RESEARCH SUMMARY AND FUTURE WORK

8.1 Research Summary

In this thesis, we have reported the results of our research study on the multi-point fiber optic gas sensor systems. Two different multiplexing systems for high sensitivity, multi point gas detection, one named time-division-multiplexed (TDM) system, the other frequency modulated continuous wave (FMCW) system, were investigated theoretically and experimentally. The basic principles of operation, multiplexing schemes, and performance analysis of the systems were presented. Wavelength modulation spectroscopy (WMS) with second-harmonic detection was implemented by applying low-frequency wavelength modulation to an external-cavity tunable diode laser and a large improvement of the signal-to-noise ratio has been achieved.

The principle of operation for the TDM system is quite simple. Our investigation is mainly focused on the system performance in terms of minimum detectable gas concentration and crosstalk between different channels that are caused by the finite extinction ratio of the optical intensity modulator (switch). From the simulation results, it was seen that the minimum detectable gas concentration is mainly limited by the first order interferometric effect caused by the coherent mixing between the signal from the channel being detected and the leakage signal from other channels. By applying wavelength modulation of appropriate amplitude and by using appropriate filtering technique, detection sensitivity of 1800 ppm for a 100-Sensor network may be obtained with a commercial 30dB pulse modulator (α_e^2=-30 dB). A minimum detectable gas concentration of 50 ppm may be achieved by using a double Mach-Zhender intensity modulator (α_e^2= -60 dB). This level of sensitivity is similar to that obtained from a single sensor system and is limited by the

unwanted interferometric signals due to coherent reflection occurring within the gas cells. The experimental system using micro-optic cells of length 25mm have demonstrated a sensitivity of 81 ppm/$\sqrt{Hz}$. The crosstalk between the sensors was found to be -30 dB. Power budget analysis shows that a sensor network consisting of 90 sensors could be realized with the same multiplexing topology.

The FMCW system is comparatively complicated. The principles of operation and the performance of the FMCW system have been studied in detail where the sensitivity limitation due to the unwanted interferometric signals and the crosstalk due to the non-zero sidelines were investigated. Also, we have showed how the interferometric effects may be reduced by using a combination of wavelength modulation/scanning and proper electronic filtering. It was possible to realize a 37-sensor array with detection accuracy of better than 2000 ppm. Experiments with a three-sensor system demonstrates a minimum detectable concentration of 270 ppm/$\sqrt{Hz}$ and the crosstalk between the sensors of better than -20 dB. A better value of sensitivity would be expected if averaging were performed over a number of scans. The experimental results agreed with the theoretical analysis and predictions. It is also possible to further reduce the sideline-related crosstalk by using some proposed techniques for lowering the non-linearity of the VCO and the fine adjustment of the length of the delay lines.

Since the FMCW system and the TDM system have the same optical configuration and use the same transceiver units, the multiplexing capacity of the FMCW system would be the same as that of the TDM system. From the theoretical analysis and experimental results, the relative advantages and disadvantages of the TDM and FMCW systems can be concluded as follows. TDM system is realized with a simple concept where simple circuitries are employed for either encoding or decoding. It shows excellent system tolerance compared

with the FMCW system. The performance of the TDM system is greatly affected by the extinction ratio of the optical switch that can be simply improved by using a double M-Z type modulator or switch. In contrast, the performance of the FMCW system is heavily influenced by a number of factors such as the biases of the fiber delays, the settings of the triangular chirped carrier and the linearity of the VCO. Deviations from the optimized values of the above parameters would cause a rise in inter-channel crosstalk and unwanted interferometric signals (noise). If a highly coherent light source is used and no noise suppression techniques are implemented, the sensitivity and the crosstalk of the FMCW system are definitely worse than that of the TDM system. But the fact is, these unwanted interferometric signals can be effectively suppressed by the use of a low coherent source and specified signal processing techniques, and the FMCW system would get an advantage from its better optical power utilization where a continuous optical signal is fed into the network instead of the optical pulses used in the TDM system. Better signal-to-noise ratio would be obtained with the FMCW system since the signal enhancement would be superior to the increase of the power-related noise (shot noise). The FMCW system would have a better sensitivity under such conditions.

8.2 Future Work

During the course of this investigation, some promising directions have been identified but cannot be followed due to insufficient time and equipment unavailability. We have the following suggestions for future work:

1. For real applications, the demodulation scheme for our system is not efficient enough due to the low scanning rate. Faster electronic circuits, such as digital signal processor, may be used for reducing the sampling time and for performing automatic channel switching.

2. Differential baseline suppression techniques may be implemented. It can improve the long term stability of the system since the uncertainties due to environmental changes and power fluctuation can be eliminated.

3. By using the physical demodulator (electrical switch), only one channel or one sensor can be monitored in each scan. An all-digital data acquisition scheme may be used where the pulse train from the sensor network can be directly recorded by using an ultra-fast data acquisition board. Demultiplexing and demodulation for all sensors can be conducted in a digital way. Hence, simultaneous measurement of a number of sensors may be achieved.

4. It is believed that the non-zero sidelines of the FMCW system can be further supppressed by the use of the techniques for VCO nonlinearity correction. Hence, these techniques should be examined and could be implemented into our system for reducing the crosstalk levels between the sensors.

5. Inter-channel crosstalk in both of the systems may be eliminated by using the matrix-inversion or the artificial neural network techniques where the real gas concentration of each sensor can be determined with the crosstalk correlation of the sensors.